



UNIVERSIDADE DE BRASÍLIA
INSTITUTO DE GEOCIÊNCIAS
PROGRAMA DE PÓS GRADUAÇÃO EM GEOCIÊNCIAS APLICADAS E
GEODINÂMICA

KIMBERLY COUTINHO PAES LEME DE CASTRO

**AVALIAÇÃO DA INFLUÊNCIA DOS PARÂMETROS FÍSICOS (TEOR
DE UMIDADE E TEOR DE ARGILA) NA IDENTIFICAÇÃO DE
EVIDÊNCIAS FORENSES COM GROUND PENETRATING RADAR
(GPR)**

Orientador: Prof. Dr. Luciano Soares da Cunha

DISSERTAÇÃO DE MESTRADO EM GEOCIÊNCIAS APLICADAS
PUBLICAÇÃO N° 226

BRASÍLIA

2024

AVALIAÇÃO DA INFLUÊNCIA DOS PARÂMETROS FÍSICOS (TEOR DE UMIDADE E TEOR DE ARGILA) NA IDENTIFICAÇÃO DE EVIDÊNCIAS FORENSES COM GROUND PENETRATING RADAR (GPR)

KIMBERLY COUTINHO PAES LEME DE CASTRO

Dissertação de Mestrado apresentada ao Programa de Pós Graduação em Geociências Aplicadas e Geodinâmica do Instituto de Geociências como requisito para o título de grau de Mestre em Geociências Aplicadas e Geodinâmica.

Orientador: Prof. Dr. Luciano Soares da Cunha

BRASÍLIA

2024

AVALIAÇÃO DA INFLUÊNCIA DOS PARÂMETROS FÍSICOS (TEOR DE UMIDADE E TEOR DE ARGILA) NA IDENTIFICAÇÃO DE EVIDÊNCIAS FORENSES COM GROUND PENETRATING RADAR (GPR)

KIMBERLY COUTINHO PAES LEME DE CASTRO

Orientador: Prof. Dr. Luciano Soares da Cunha

Banca Examinadora:

Presidente: Prof. Dr. Luciano Soares da Cunha (UnB/IG)

Membro Interno: Prof. Dr. Marcelo Peres Rocha (UnB/IG)

Membro Externo: Prof. Dr. Antônio Lázaro Ferreira Santos, Universidade Estadual de Goiás (UEG).

BRASÍLIA

2024

**Ficha catalográfica elaborada automaticamente,
com os dados fornecidos pelo(a) autor(a)**

CK49aa

Coutinho Paes Leme de Castro, Kimberly
Avaliação da Influência dos Parâmetros Físicos (Teor de
Umidade e Teor de Argila) na Identificação de Evidências
Forenses com Ground Penetrating Radar (GPR). / Kimberly
Coutinho Paes Leme de Castro; orientador Luciano Soares da
Cunha. -- Brasília, 2024.
147 p.

Dissertação (Mestrado em Geociências Aplicadas) --
Universidade de Brasília, 2024.

1. Sepultamentos Clandestinos. 2. Sítios Controlados. 3.
Ciências Forenses. 4. Sepulturas Simuladas. 5. Radar de
Penetração no Solo GPR. I. Soares da Cunha, Luciano, orient.
II. Título.

Dedico este trabalho a uma vida bonita de
se viver.

AGRADECIMENTOS

Em primeiro lugar agradeço à minha mãe, Ivani da Cunha Coutinho que, por gostar muito de mim, me deu confiança para viver e me deu segurança para me exibir, não tenho medo porque sou amada.

Um agradecimento especial ao meu orientador, Professor Dr. Luciano Soares da Cunha, por apoiar desde o início o meu desejo de pesquisar o campo da geofísica forense. Obrigada por construir comigo esse projeto, etapa por etapa e por sempre me orientar no desenvolvimento de um trabalho de excelência considerando as contingências apresentadas, sem nunca perder de vista o mais importante: a nossa saúde física e emocional.

Agradeço também, ao Dr. Márcio Maciel Cavalcanti, que bem no início da minha graduação permitiu que eu o auxiliasse em aquisições de dados para o seu doutorado e dividiu comigo muito conhecimento, dentro e fora de campo, o que me proporcionou a convicção de que era essa a área de conhecimento na qual eu queria me especializar. Obrigada por aceitar a "presepada" de ir comigo a campo, para aquisição de dados GPR *quasi*-3D, com espaçamento entre as linhas de 5 centímetros, em pleno cerrado, no período de seca e em um feriado. Márcio, você é um santo, Obrigada!

Agradeço ao Professor Dr. Weliton Rodrigues Borges pelo apoio em campo, por seu tempo e por compartilhar seu conhecimento comigo.

Agradeço ao Professor Dr. Marcelo Peres Rocha pela oportunidade de ter o primeiro contato com a geofísica forense. Esse caminho que comecei a trilhar é devido a você, obrigada!

Agradeço a todos os professores que tiveram participação na minha formação, principalmente os do Instituto de Geociências, obrigada por me transmitirem o conhecimento necessário para que eu chegasse até aqui.

Agradeço imensamente a todos os funcionários da Fazenda Água Limpa (FAL) pelo suporte no projeto, em especial, ao Diretor Professor Reginaldo Pereira, ao Professor Fábio e aos funcionários Luciano e Guilherme. Agradeço pela área cedida e por todo apoio logístico.

Agradeço ao Instituto de Geociências pelo empréstimo de equipamentos e veículos para execução deste trabalho, em especial, ao técnico Péricles.

Agradeço a Hartos Agropecuária Cenci pela doação das carcaças de suíno, em especial, ao Sr. Delmo Martins e ao Sr. Dejalma que foram muito solícitos em colaborar com este projeto.

Agradeço imensamente ao Pedro Vencovsky Nogueira pelo apoio intelectual e braçal. Obrigada por várias vezes ter ido a campo comigo, às vezes só pra ser meu motorista, obrigada pelas conversas no caminho que sempre me arrancavam gargalhadas, obrigada pelas aulas de processamento de dados, sou muito grata pelo tempo que você dedicou a este projeto comigo.

Agradeço ao Danilo Portela, Celso Guerra, Douglas Carvalho e Ana Clara Araujo pelo apoio na aquisição dos dados. Vocês são maravilhosos e compusemos um ótimo grupo em campo.

Agradeço a Alexandra Elbakyan pela sua coragem e por promover um acesso mais igualitário à informação científica!

Como disse David Steindl-Rast: não é a alegria que nos torna agradecidos, é a gratidão que nos torna alegres. E devo dizer que estou muito alegre em fechar mais uma etapa do que eu considero uma trejetória de muitas conquistas.

O presente trabalho foi realizado com apoio da Coordenação de Aperfeiçoamento de Pessoal de Nível Superior - Brasil (CAPES) – Código de Financiamento 001.

“A tempestade é sol também”
(Helio Flanders)

RESUMO

Os avanços obtidos nas pesquisas de identificação de alvos forenses em diferentes cenários de sepultamento com o auxílio do Radar de Penetração do Solo (GPR) foram constatados a partir de uma Revisão Sistemática de Literatura (RSL). A linha de pesquisa identificada com potencial para ser desenvolvida é relacionada a um melhor entendimento a respeito da influência de parâmetros físicos nas respostas geofísicas. Desse modo, o objetivo desta dissertação é avaliar a influência do teor de umidade e teor de argila na identificação de alvos forenses que simulam evidências humanas com o GPR. Para cumprir o objetivo foi reservada uma área da Fazenda Água Limpa (FAL) para ampliar o Sítio Controlado de Geofísica Forense da UnB (FOREN-FAL). O sítio controlado é composto por quatro Sepulturas Experimentais (SEP's) com diferentes cenários de sepultamento. As metas estabelecidas para atingir o objetivo do projeto incluem monitorar a variação espaço-temporal da umidade do solo por meio de imagens de GPR 2D, *quasi*-3D e 4D e monitorar a influência do conteúdo de argila (15%, 20%, 30% e 70%) na detecção do alvo por meio de imagens de GPR 2D, *quasi*-3D e 4D. Os resultados mais assertivos foram obtidos em uma SEP composta por 85% de areia e 15% de material argiloso, independentemente da sazonalidade. Foi observada uma atenuação do sinal nos dados do GPR durante a estação chuvosa e após a reflexão de alvos maiores, principalmente devido ao comportamento condutor dos tecidos moles dentro dos alvos. Os melhores resultados foram observados na estação seca devido ao menor conteúdo de água no solo e ao menor tempo desde o sepultamento quando comparado à estação chuvosa. Em conclusão, solos com maior umidade e teor de argila tendem a apresentar uma atenuação significativa nos sinais do GPR, embora a mineralogia da argila também influencie a profundidade de penetração. Na estação seca, os resultados foram mais claros, especialmente na visualização dos alvos, enquanto a estação chuvosa apresentou reflexões difusas e visibilidade limitada. Os diagramas pseudo-3D destacaram a migração de fluidos de decomposição, influenciada pela composição do solo e condições climáticas.

Palavras-chave: Sepultamentos Clandestinos. Sítios Controlados. Ciências Forenses. Sepulturas Simuladas. Radar de Penetração no Solo. GPR.

ABSTRACT

Advancements in forensic target identification research across various burial scenarios with the assistance of Ground Penetrating Radar (GPR) were established through a Systematic Literature Review (SLR). A research avenue identified as having potential for further exploration is related to a deeper understanding of the influence of physical parameters on geophysical responses. Thus, the aim of this dissertation is to assess the impact of moisture content and clay content on the identification of forensic targets simulating human evidence using GPR. To achieve this goal, an area of the Água Limpa Farm (FAL) was allocated to expand the University of Brasília's Controlled Forensic Geophysics Site (FOREN-FAL). The controlled site comprises four Experimental Graves (SEPs) with distinct burial scenarios. The set objectives to accomplish the project goal include monitoring the spatiotemporal variation of soil moisture through 2D, *quasi*-3D, and 4D GPR images, and tracking the influence of clay content (15%, 20%, 30%, and 70%) on target detection through 2D, *quasi*-3D, and 4D GPR images. The most accurate results were obtained in a SEP composed of 85% sand and 15% clayey material, regardless of seasonality. Signal attenuation was observed in GPR data during the rainy season and after reflection from larger targets, primarily due to the conductive behavior of soft tissues within the targets. Superior outcomes were noted in the dry season due to lower soil water content and less time since burial compared to the rainy season. In conclusion, soils with higher moisture and clay content tend to exhibit significant attenuation in GPR signals, although clay mineralogy also influences penetration depth. In the dry season, results were clearer, especially in target visualization, whereas the rainy season featured diffuse reflections and limited visibility. Pseudo-3D diagrams highlighted the migration of decomposition fluids, influenced by soil composition and climatic conditions.

Keywords: Clandestine Grave. Controlled Research Site. Forensic Science. Burials. Ground Penetrating Radar. GPR.

LISTA DE ABREVIATURAS E SIGLAS

LISTA DE ABREVIATURAS

FOREN/FAL	Sítio Controlado de Geofísica Forense da Universidade de Brasília
SEP	Sepultura Experimental
SEP01	Sepultura Experimental 01
SEP02	Sepultura Experimental 02
SEP03	Sepultura Experimental 03
SEP04	Sepultura Experimental 04

LISTA DE SIGLAS

GPR	Radar de Penetração no Solo (Ground Penetrating Radar)
RSL	Revisão Sistemática da Literatura
FAL	Fazenda Água Limpa
SLR	Systematic Literature Review
CAFe	Federated Academic Community
CAPES/MEC	Coordenação de Aperfeiçoamento de Pessoal de Nível Superior/Ministério da Educação
Fig	Figure
ER	Electroresistivity
MS	Magnetic Susceptibility
MC	Magnetic Conductivity
MG	Magnetic Gradient
MT	Microwave Tomography
LMT	Linear Microwave Tomography
MD	Metal Detector
LS	Laser Scanning
RP	Rectified Photography
ERT	Electrical Tomography
TDR	Time Domain Reflectometry

TLS	Terrestrial Laser Scanning
UAV	Unmanned Aerial Vehicle
GIS	Geographic Information System
VRD	Victim Recovery Dogs
GSSI	Geophysical Survey System Inc.

SUMÁRIO

CAPÍTULO 1 – INTRODUÇÃO	13
CAPÍTULO 2 – ARTIGO CIENTÍFICO 1	17
GROUND PENETRATING RADAR (GPR) RESPONSES OF BURIAL MATERIAL ON FORENSIC TARGETS ON TROPICAL SOIL IN DRY SEASON	17
CAPÍTULO 3 – ARTIGO CIENTÍFICO 2	40
INFLUENCE OF THE SAND-CLAY RATIO OF THE BURIAL MATERIAL OF FORENSIC TARGETS ON GROUND PENETRATING RADAR (GPR) RESPONSES – COMPARISON OF DRY AND RAINY SEASON DATA	40
CAPÍTULO 4 – CONCLUSÕES E CONSIDERAÇÕES FINAIS	60
CAPÍTULO 5 – REFERÊNCIAS BIBLIOGRÁFICAS.....	63
ANEXOS	66
A – FUNDAMENTAÇÃO TEÓRICA	66
A1 – PRINCÍPIOS MATEMÁTICOS	68
A2 – PROCESSAMENTO.....	70
B – ARTIGO CIENTÍFICO – REVISÃO SISTEMÁTICA DA LITERATURA	75
FORENSIC INVESTIGATIONS WITH THE IDENTIFICATION OF HUMAN REMAINS WITH GROUND PENETRATING RADAR (GPR): A REVIEW.	75
C – RADARGRAMAS OBTIDOS NO PERÍODO DE SECA.....	100
C1 – RADARGRAMAS 2D OBTIDOS PARALELAMENTE NO PERÍODO DE SECA 100	
C2 – RADARGRAMAS 2D OBTIDOS TRANSVERSALMENTE NO PERÍODO DE SECA	114
D – RADARGRAMAS OBTIDOS NO PERÍODO CHUVOSO.....	120
D1 – RADARGRAMAS 2D OBTIDOS PARALELAMENTE NO PERÍODO CHUVOSO	120
D2 – RADARGRAMAS 2D OBTIDOS TRANSVERSALMENTE NO PERÍODO CHUVOSO	134
E – FOTOGRAFIAS DA ÁREA DO SÍTIO CONTROLADO	140

CAPÍTULO 1 – INTRODUÇÃO

Nos últimos anos, tem havido um aumento significativo na aplicação do conhecimento de geociências forenses em investigações criminais (Gráfico 1), acompanhado por uma crescente aceitação de ferramentas geofísicas, especialmente o Radar de Penetração no Solo (GPR), para localizar sepulturas clandestinas e evidências físicas associadas a atividades criminosas (Castro & Cunha, 2021). Este avanço reflete uma mudança paradigmática na abordagem investigativa, com a comunidade científica reconhecendo cada vez mais o potencial das técnicas geofísicas na resolução de casos criminais (Wisniewski et al., 2019; Abate et al., 2019; Büyüksaraç et al., 2013; Billinger, 2009; Novo et al., 2011).

O êxito do GPR na detecção de sepulturas não marcadas levou a numerosos estudos controlados que simulam cenários forenses (Cavalcanti et al., 2018; Schoor et al., 2017; Molina et al., 2016a; Molina et al., 2016b; Molina et al., 2015), onde diferentes aspectos do método foram avaliados em contextos controlados para entender melhor sua aplicabilidade e limitações (Schultz & Martin, 2012). Estes estudos, muitas vezes realizados em colaboração com órgãos de aplicação da lei e instituições acadêmicas, têm contribuído para o desenvolvimento de protocolos e diretrizes para a utilização do GPR em investigações criminais (Schultz & Martin, 2012).



Gráfico 1 Análise de publicações, na temática de aplicação dos conhecimentos de geociência forense no campo das investigações criminais, durante o período de 2000-2021, a primeira década teve uma média de publicação de 3,0 artigos enquanto na segunda década apresentou uma média de 6,9 artigos (Fonte: Web of Science, acesso: 15/03/2021).

O GPR tornou-se uma opção geofísica comum nas investigações forenses, pois, além de ser eficaz na localização de alvos enterrados, pode ser integrado com outros métodos como parte de um protocolo para pesquisa de alvos forenses. Uma das vantagens de se utilizar o GPR na busca de alvos sepultados é a rapidez na coleta de dados, economia de custos e tempo, além de possuir uma natureza não destrutiva (Abate et al., 2019; Rubio-Melendi et al., 2018; Aziz et al., 2016; Doolittle et al., 2010). Ademais, a tecnologia do GPR tem se mostrado versátil e capaz de fornecer informações detalhadas sobre a estrutura do solo e dos alvos enterrados, permitindo uma análise forense mais precisa e eficiente.

Esta dissertação é composta por cinco capítulos distintos, cada um abordando uma etapa específica do estudo. No Capítulo 1, a introdução é apresentada, fornecendo um contexto geral sobre o tema de pesquisa e delineando os objetivos do estudo.

No Capítulo 2 é apresentado o primeiro artigo, submetido a revista *FrontiersIn – Earth Science*, em março de 2024. O artigo apresenta a instalação do experimento em campo, os resultados do monitoramento GPR no período de seca e a influência do teor de areia e do material argiloso no sepultamento de alvos forenses em respostas de GPR no Sítio Controlado de Geofísica Forense da Universidade de Brasília – UnB.

No Capítulo 3 é apresentado o segundo artigo, publicado pela revista *FrontiersIn – Earth Science*, em março de 2024 ([artigo disponível aqui](#)). Nesta etapa da pesquisa o objetivo é avaliar o impacto do teor de umidade e de argila na detecção de alvos forenses, que mimetizam evidências humanas, utilizando o GPR, comparando dados adquiridos em período de seca e de chuva. Desta forma, foi possível destacar uma atenuação do sinal de reflexão do GPR durante a estação chuvosa e após a reflexão de alvos maiores, principalmente devido ao comportamento condutor dos tecidos moles dentro dos alvos (Castro et al., 2024).

No Capítulo 4, são apresentadas as conclusões e considerações finais do estudo, destacando os principais achados e suas implicações para a área de estudo. O Capítulo 5 inclui as referências bibliográficas utilizadas ao longo da dissertação, fornecendo uma lista completa das fontes consultadas. Por fim, no Anexo A, é

desenvolvida a fundamentação teórica, onde são explorados os principais conceitos e teorias relevantes para fundamentar a investigação.

No Anexo B é apresentado um terceiro artigo, publicado em 2021, pela revista Estados Geológicos. O artigo relata uma Revisão Sistemática da Literatura (RSL) que investiga como o GPR auxilia na identificação de corpos em diversos cenários de sepultamento (Castro & Cunha, 2021). Foi possível destacar áreas promissoras e determinar um escopo de desenvolvimento científico na geofísica forense. De forma complementar, foi possível identificar as características principais de sítios controlados, aplicabilidade e limitações do método GPR e demonstração da eficácia do método.

Esta dissertação faz parte de um projeto de pesquisa maior – "Influência de Parâmetros Físicos, Umidade e Conteúdo de Argila na Identificação de Alvos Forenses com Radar de Penetração no Solo (GPR)" – conduzido na expansão do Sítio Controlado de Geofísica Forense da UnB (FOREN-FAL) (Figura 1) (Cavalcanti, 2017). O projeto visa monitorar com GPR, Tomografia Elétrica e Potencial Espontâneo a variação espaço-temporal da umidade com imagens 2D e *quasi*-3D, analisar a influência da proporção areia-argila na detecção do alvo por meio de imagens de GPR 4D e métodos elétricos.

Esse esforço multidisciplinar visa contribuir para a compreensão e o avanço da geofísica forense, fornecendo esclarecimentos valiosos sobre como os parâmetros físicos e as condições ambientais afetam a detecção de alvos forenses com GPR. Além disso, pretende-se estabelecer diretrizes e metodologias padrão para futuras investigações forenses, com base em dados empíricos e experimentais obtidos neste estudo e em colaborações interdisciplinares.

O objetivo principal desta dissertação é avaliar a influência dos parâmetros físicos (teor de umidade e teor de argila) na identificação de evidências humanas em pesquisas forenses com o GPR. Para atingir tal objetivo, as seguintes metas foram executadas:

- Monitorar a variação espaço-temporal da umidade do solo por meio de imagens de GPR 2D, *quasi*-3D e 4D;

- Monitorar a influência do conteúdo de argila (15%, 20%, 30% e 70%) na detecção do alvo por meio de imagens de GPR 2D, *quasi*-3D e 4D.

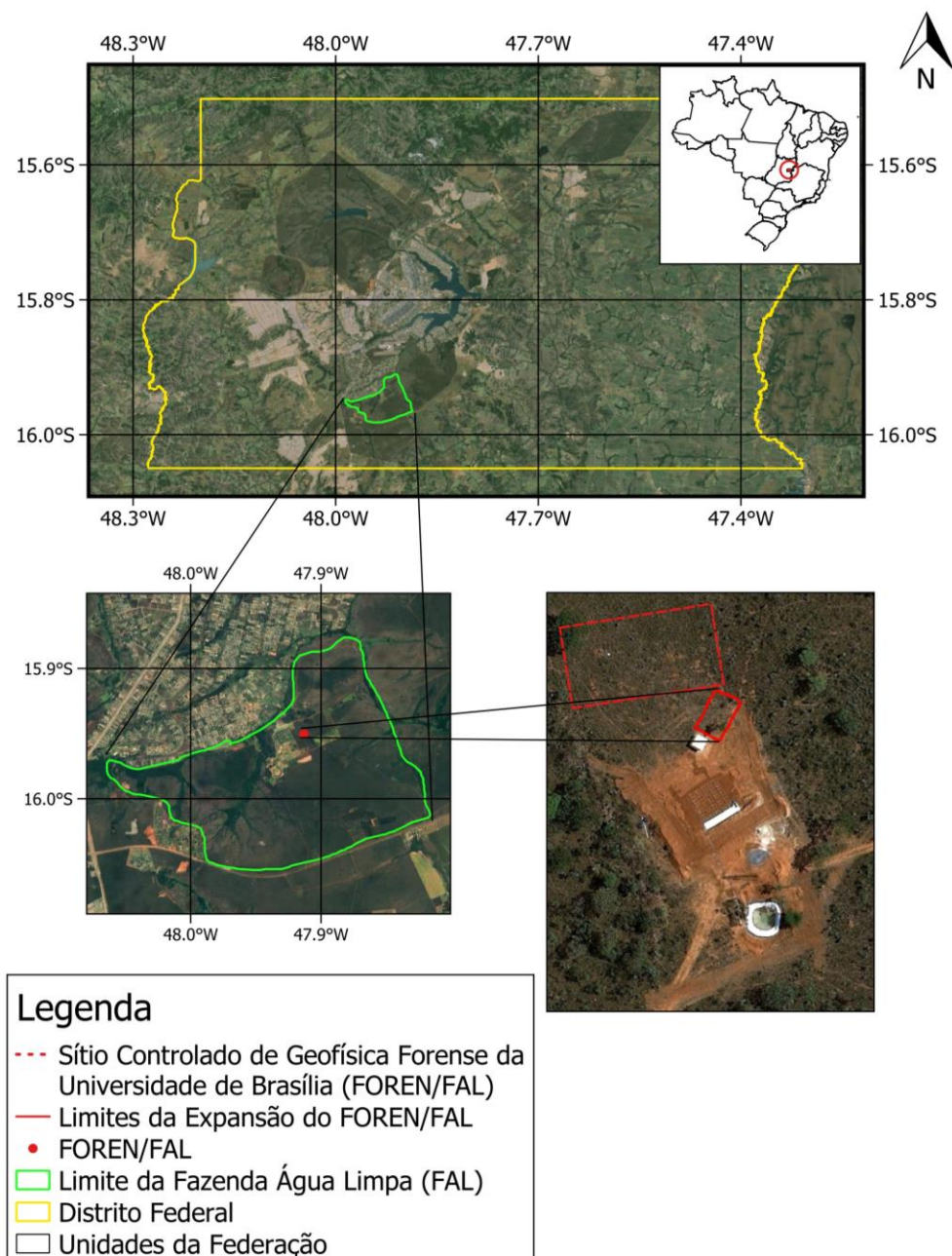


Figure 1 - Mapa de localização da área de expansão do sítio controlado (retângulo vermelho contínuo), dentro dos limites da Fazenda Água Limpa (polígono verde) na região de Brasília, Distrito Federal – DF. (Fonte: Imagem Google Earth, 2021).

CAPÍTULO 2 – ARTIGO CIENTÍFICO 1

Ground Penetrating Radar (GPR) Responses of Burial Material on Forensic Targets on Tropical Soil in Dry Season

Kimberly Coutinho Paes Leme de Castro^{1*}, Luciano Soares da Cunha¹

¹University of Brasília, Institute of Geosciences, Graduate Program in Applied Geosciences and Geodynamics

*** Correspondence:**

Kimberly Coutinho Paes Leme de Castro
kimberlycplcastro@yahoo.com

Keywords: clandestine grave, controlled research site, forensic science, burials.

Abstract

This study aims to assess the impact of sand-clay ratio on the detection of forensic targets, which mimic human evidence, using Ground Penetrating Radar (GPR). To achieve this objective, we establish a control site, comprising four Experimental Graves (SEPs) with varying burial scenarios. Fulfilment of the objectives involve examining the effect of clay soil content on the detection of swine targets, utilizing both 2D and quasi-3D GPR imaging techniques. Analysis of the results reveals a signal attenuation in GPR reflections from larger targets attributed to the conductive behavior of the soft tissues within the targets. Optimal outcomes were observed in SEPs with an 85% sand and 15% clay composition, whereas SEP03 (with a 70% sand and 30% clay composition) necessitated further refinement of the results. The study concludes that controlled sites serve as valuable resources for geophysical investigations, providing an environment which is conducive to refining parameters and enhancing the precision of the results.

1 Introduction

Forensic geophysics research, employing ground-penetrating radar (GPR), holds promise for the non-destructive detection of buried or concealed targets. Forensic investigations utilizing GPR have gained traction across various scientific domains, encompassing diverse lines of inquiry such as organic material decomposition [Pringle et al., 2020; Dick and Pringle, 2018; Schoor et al., 2017; Schultz et al., 2016], submerged areas [Parker et al., 2010; Schultz et al., 2013; Ruffel et al., 2017], and controlled environments [Pringle et al., 2020; Schultz et al., 2016; Molina et al., 2016; Pringle et al., 2016; Molina et al., 2015; Schultz, 2008; Schultz et al., 2006; Schultz et al., 2002], often in conjunction with complementary methods [Pringle et al., 2020; Abate et al., 2019; Rubio-Melendi et al., 2018; Cavalcanti et al., 2018; Molina et al., 2016; Aziz et al., 2016; Hansen and Pringle, 2013]. However, the application of GPR for subsurface human body detection encounters constraints such as site characteristics, soil

composition, and target decomposition state [Barone and Di Maggio, 2019; Lester and Bernold, 2006].

Significant progress has been made in research conducted at controlled sites. This research has been meticulously analyzed and developed under closely monitored conditions, incorporating parameters such as depth, target dimensions, soil properties, frequency, and the integration of complementary methods with rigorous controls. The research is primarily aimed at comparing different antenna frequencies and establishing foundational principles for forensic research and optimal methodologies for burial detection. One of the promising research avenues identified in the Systematic Literature Review (SLR) [Castro and Cunha, 2021] aligns with the objective of this study: to assess the impact of clay soil content and GPR frequency on the recognition of forensic targets in a controlled setting, simulating human burial evidence.

2 Materials and Methods

2.1 Study Area

A controlled site was extended for conducting experiments, covering an approximate area of 100 m² within the Experimental Farm (FAL) of the Federal University of Brasília (UnB). The vegetation at the site had already undergone partial suppression, with only shrubs, medium-sized trees, and grasses remaining. Figure 1 provides a visual representation of the specific location of the controlled site [Castro, 2021].

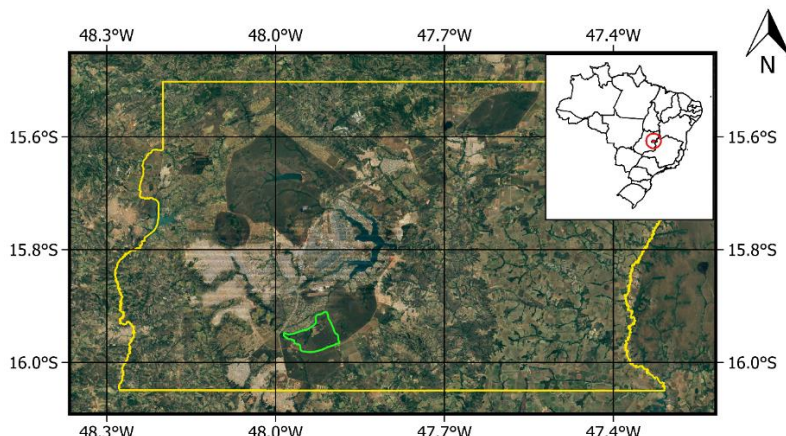


Figure 1 - Location map of the controlled site area situated within the Experimental Farm (highlighted by the green polygon) in Brasilia, Distrito Federal—DF. (Source: Google Earth image, 2021).

The controlled site within the FAL is located in an area characterized by the presence of oxisols. The climate in the Federal District follows Koppen's classification, falling into the category of a tropical savanna and a temperate region with distinct dry winters. This climate exhibits

pronounced seasonal changes: a rainy and hot period from October to April, followed by a cold and dry phase from May to September. Temperature variations are significant, with the coldest months reaching as low as 12 °C, while the hottest months can experience temperatures exceeding 28.5 °C [Cavalcanti, 2017]. The average annual precipitation in this region amounts to 1,600 mm (available at: <https://tempo.inmet.gov.br/Graficos/A001> and accessed on: November 2021).

2.2 Implementation of the Controlled Site

In July 2021, the controlled site was established, comprising four experimental inhumations of target specimens (pigs) at depths of either 0.50 m or 0.90 m, each with varying cover texture compositions (Figure 2). Detailed specifications, regarding the dimensions of the targets and the composition of the cover textures, are presented in Table 1 [Castro, 2021].

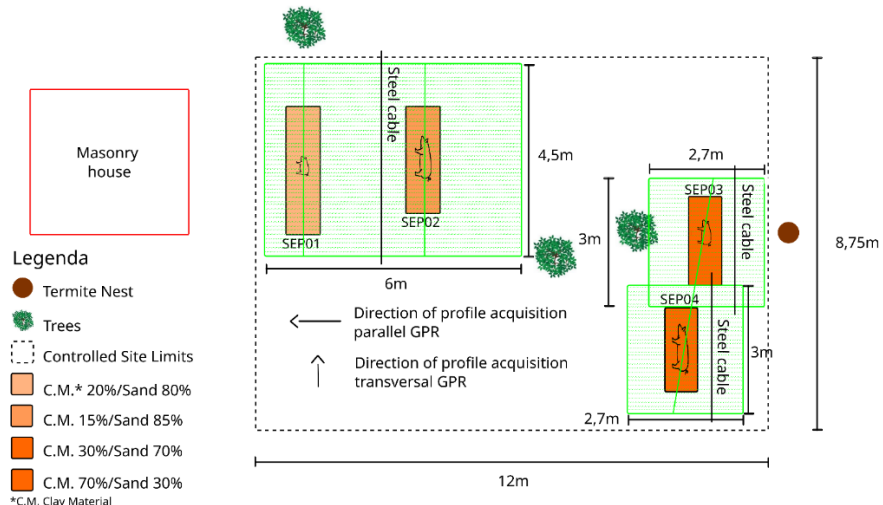


Figure 2 - Sketch of the controlled site area featuring the layout of the experimental graves, illustrating the composition of the SEP fill and outlining the GPR data acquisition scheme.

The oxisols, sourced from the excavation of the graves, were employed as the clay material constituting the cover for the targets. Laboratory analysis was conducted to assess the granulometry of the clay and sand materials and the results are presented in Table 2. The technique used to analyze the fine particles in the granulometry analysis was the sedimentology test while, for the larger particles (>0.075 mm), the sieving test was used [NBR 5734/ABNT, 1989].

Experimental Grave 01 (SEP01) had dimensions of 3.00 m in length, 0.80 m in width, and 1.50 m depth and was filled according to the following sequence (Figure 3a). Starting from the base, the sequence comprised a layer of 0.15 m of gravel, followed by a nonwoven geotextile layer, then 0.20 m of sand, 0.65 m of clay material and, finally, the pig target was placed at a depth of 0.50 m (the specific dimensions are outlined in Table 1). A mixture consisting of 20% clay

material and 80% sand was employed to bury the target and complete the filling of the grave [Castro, 2021].

Experimental Grave 02 (SEP02) measured 2.50 m in length, 0.80 m in width, and 1.30 m depth. The filling process (Figure 3b) proceeded as follows, from the bottom to top: a layer of 0.15 m of gravel, followed by a nonwoven geotextile layer, then 0.25 m of clay material. The pig target was positioned at a depth of 0.90 m, with dimensions as specified in Table 1. A mixture of 15% clay and 85% sand was utilized for both burying the target and completing the grave filling [Castro, 2021].

Experimental Grave 03 (SEP03) measured 2.10 m in length, 0.80 m in width, and 0.85 m depth. The filling process (Figure 3c) proceeded as follows, from bottom to top: a layer of 0.35 m of gravel, followed by a nonwoven geotextile layer. The pig target was positioned at a depth of 0.50 m, with the dimensions specified in Table 1. A mixture comprising 30% clay and 70% sand was employed to bury the target and complete the grave filling [Castro, 2021].

Experimental Grave 04 (SEP04) measured 2.00 m in length, 0.80 m in width, and 0.87 m depth. The filling process (Figure 3d) proceeded as follows, from bottom to top: a layer of 0.37 m of gravel, followed by a nonwoven geotextile layer. The pig target was positioned at a depth of 0.50 m, with the dimensions specified in Table 1. A mixture comprising 70% clay and 30% sand was used to bury the target and complete the grave filling [Castro, 2021].

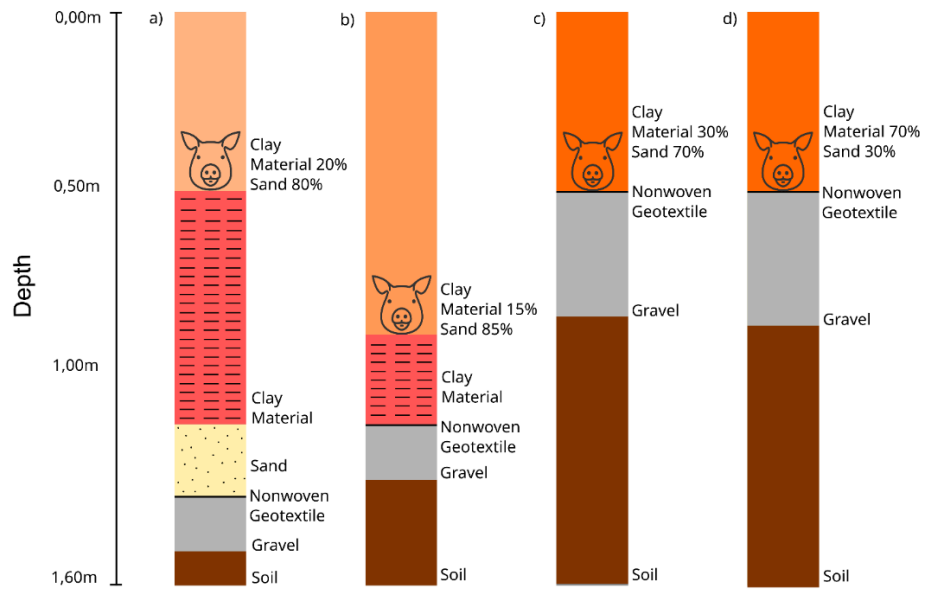


Figure 3 - Illustration depicting the sequence of filling for the experimental graves: (a) SEP01 filled with gravel, nonwoven geotextile, sand, clay material, and sand-clay proportion. (b) SEP02 filled with gravel, nonwoven geotextile, clay material, and sand-clay proportion. (c) SEP03 filled with gravel, nonwoven geotextile, and sand-clay proportion. (d) SEP04 filled with gravel, nonwoven geotextile, and sand-clay proportion.

2.3 Data Acquisition

Ground-penetrating radar (GPR) is a geophysical method for mapping subsurface structures using electromagnetic energy. Various deployment methods exist, but all approaches involve a transmitter generating radiofrequency signals, typically in the 1–5,000 MHz frequency range, and a receiver detecting similar signals. The objective is to measure the impulse response, or the transfer function of the surrounding medium, to reconstruct the material's property structure. In its simplest form, a GPR system with a transmitter and receiver is moved over the ground surface and reflections returning from subsurface objects are detected, recorded, and displayed for the user [Annan, 2004].

As the GPR system is moved over the ground, a shallow image of the subsurface is obtained along the survey line. These images, called radargrams (Figure 5), are two-dimensional graphical representations (XZ) of the detected reflections. The X-axis represents the antenna displacement along the survey line, while the Z-axis represents the two-way travel time of the emitted pulse (in nanoseconds). If the time it takes the electromagnetic pulse to travel from the transmission antenna to the reflector in the soil and back to the receiving antenna is measured, then the velocity of this pulse in the subsurface medium is known and the reflector's position can be determined [Solla et al., 2012].

Data acquisition was conducted using Geophysical Survey System Inc. (GSSI) GPR SIR3000 equipment, equipped with both 400 MHz and 900 MHz antennas. The data collection process took place on 3rd August 2021 (Figure 4), with the 400 MHz antenna and on 18th August 2021,

with the 900 MHz antenna. During the field operation, a total of 385 radargrams were acquired across the controlled site.



Figure 4 - Photograph of the GPR data acquisition in the controlled site area with the 400 MHz antenna.

To ensure precise profile orientation, two tape measures were employed and a rope was stretched between them to demarcate the start and end points of the surveyed lines. The spacing between these data collection lines was set at 0.05 m and the radargrams were acquired in a northeast to southwest direction. In addition, a steel cable was employed to facilitate the 3D processing of GPR data methods [Castro et al., 2024].

2.4 Processing

For the processing of the radargrams, Reflex-Win 7.5.2 software was employed [Sandmeier, 2014]. The processing sequence used for the data was:

- Static correction - the determination of the initial arrival point of electromagnetic energy directly propagated by the acquisition surface [Olhoeft, 2000].
- Energy decay function - enhances reflectors through an iterative process that can be applied linearly and exponentially at a specified depth.
- Bandpass frequency - filters out undesired frequencies and reduces noise from various sources, permitting frequencies to pass within the specified band [Gomes et al., 2011].
- Background removal - eliminates any background noise.
- FK filter - a two-dimensional filter defined in the frequency and wave number domain ($F - K$), which enables the suppression of electromagnetic signal noise [Cavalcanti, 2017].

- Migration (Kirchhoff) - migration relocates reflections to their accurate positions in the subsurface and collapses diffractions, thereby improving spatial resolution [Yilmaz, 2001]. With the known depth (h) of the buried targets and the double transit time values of the electromagnetic wave (t) over each hyperbolic event assigned to the buried targets, the average propagation velocities of the electromagnetic waves (v) were determined. The average electromagnetic wave propagation velocities used for migration were calculated using Equation 1. The velocities (V) ranged from 0.07 to 0.10 m/ns.

$$V = \frac{2h}{t} \text{ (Equation 1)}$$

3 Results

3.1 Area Background

The processing procedure for the radargrams depicted in Figures 5a-b adhered to the same methodology outlined in the preceding section. Figure 5a illustrates the radargram acquired with the 400 MHz antenna outside SEP01 and SEP02, for background validation. The geophysical response received elucidates the characteristics of the homogeneous latosol, exhibiting disordered hyperbolas that may correspond to probable tree roots or animal burrows. A persistent hyperbola is evident at the 3.2 m position, corresponding to the steel cable introduced prior to the GPR survey. Figure 5b displays the radargram obtained with the 900 MHz antenna outside SEP01 and SEP02, for background validation. The received response delineates the behavior of the homogeneous oxisols, revealing certain reflectors undergoing attenuation with increasing depth. Additionally, a hyperbola is discernible around the 3.4 m position, associated with the steel cable introduced during the GPR survey.

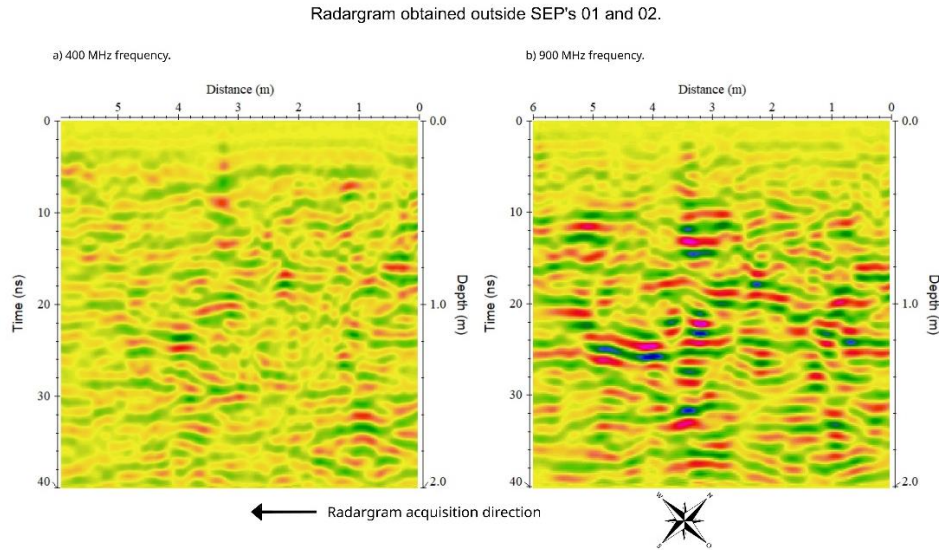


Figure 5 - GPR profile acquired outside SEP's 01 and 02 to verify the background. a) profile obtained with the 400MHz antenna. b) profile obtained with the 900MHz antenna.

3.2 2D Parallel Profiles

The selected 2D parallel radargrams chosen for interpreting the data of the targets below were acquired over the abdominal region of the pig carcass due to its wider dimensions.

Figures 6a-c depict radargrams obtained over SEP01 and SEP02 at a 400 MHz frequency. In Figure 6a, the radargram spans the grave but not the target, showing disordered reflectors primarily attributed to the clay material layer, when compared with the burial scenario (Figure 6c). Figure 6b reveals hyperbolas at depths corresponding to well-defined targets, with SEP01 exhibiting pronounced reflections from the underlying clay material, followed by the sand layer, while SEP02 shows the top of the target followed by the clay material layer.

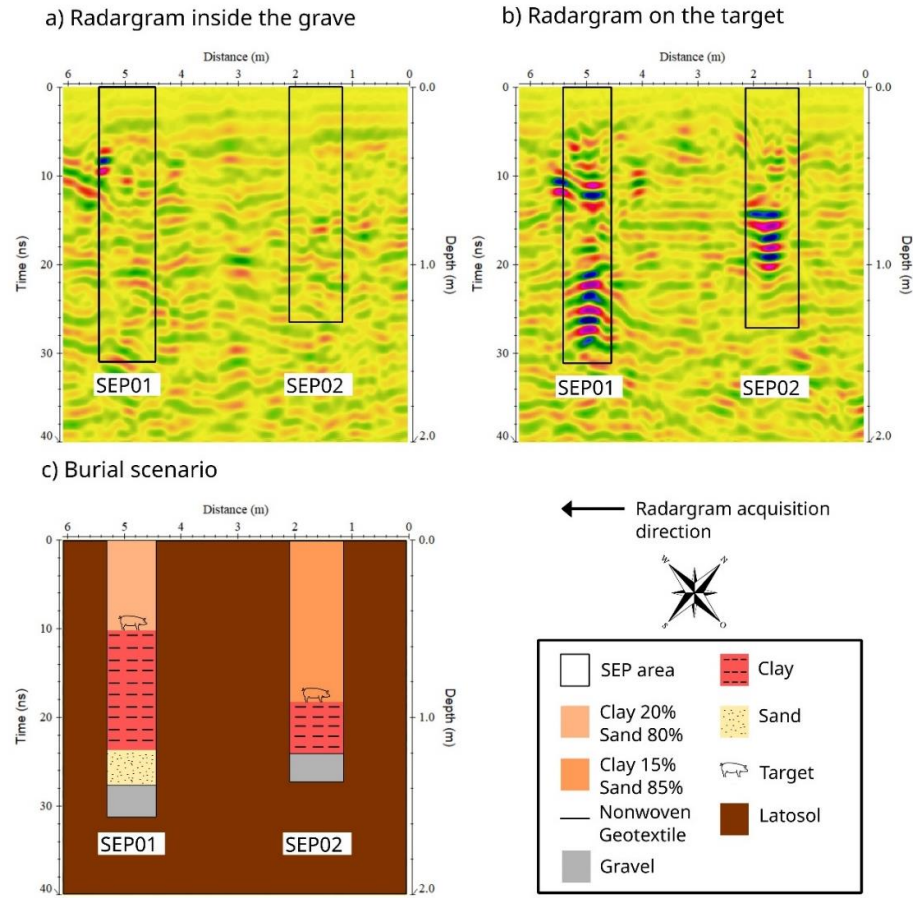


Figure 6 - Radargrams obtained over the experimental graves 01 and 02. Data acquired a) inside the grave. b) over the target with the 400MHz antenna during dry season. c) illustrative model of the buried target burial scenario.

The radargrams acquired over SEP03 at a 400 MHz frequency are presented in Figures 7a-c. Figure 7a shows a radargram traversing the grave without covering the target, with a notable reflector (medium amplitude) at 10 ns, corresponding to the interface between the sand-clay layer and the gravel layer. Figures 7b and 7c display the radargram obtained over the buried target and a model of the burial scenario, respectively, with a conspicuous hyperbola (high amplitude) signifying the target in Figure 7b and a reflection below the target representing the gravel base, along with a hyperbola (medium amplitude) attributed to a tree root in Figure 7c.

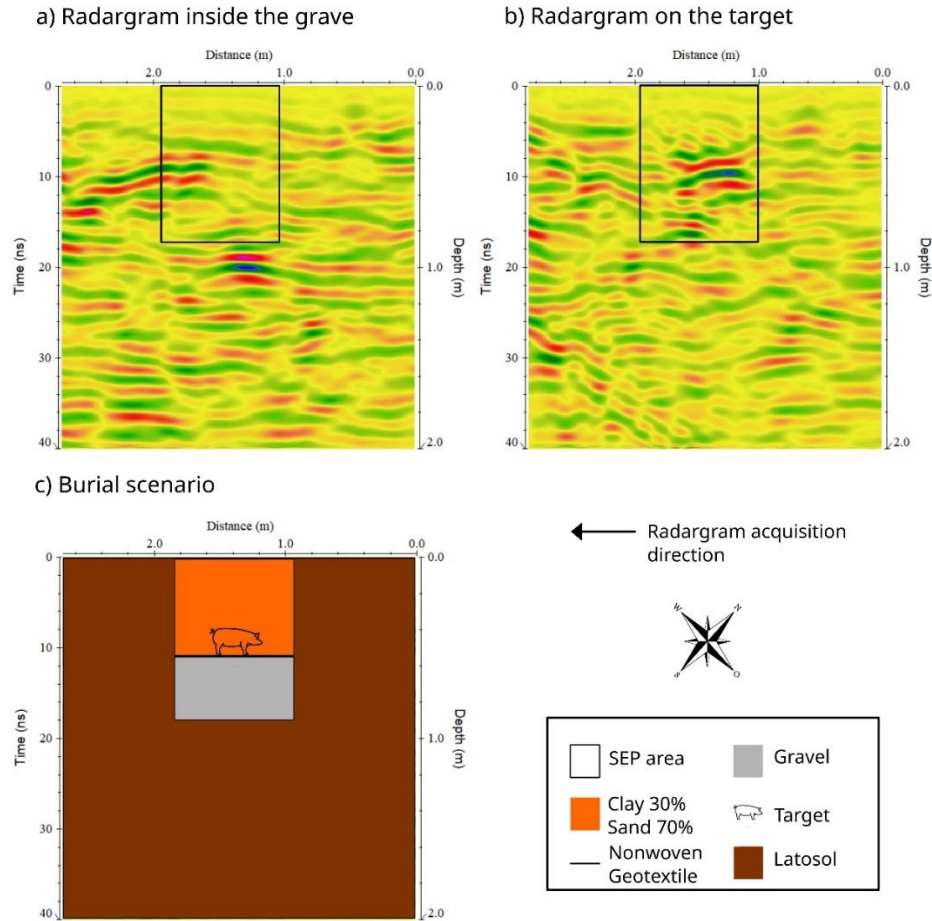


Figure 7 - Radargrams obtained over SEP03. Data acquired a) inside the grave. b) over the target with the 400MHz antenna during dry season. c) illustrative model of the buried target burial scenario.

Radargrams obtained over SEP04 at a 400 MHz frequency are depicted in Figures 8a-c. Figure 8a depicts a radargram traversing the grave without covering the target and with no notable anomalies, due to its composition resembling the surrounding ground. In Figure 8b, the radargram over the buried target reveals a hyperbola (high amplitude) at 6 ns and 0.3 m depth signifying the target, while Figure 8c depicts a model of the burial scenario.

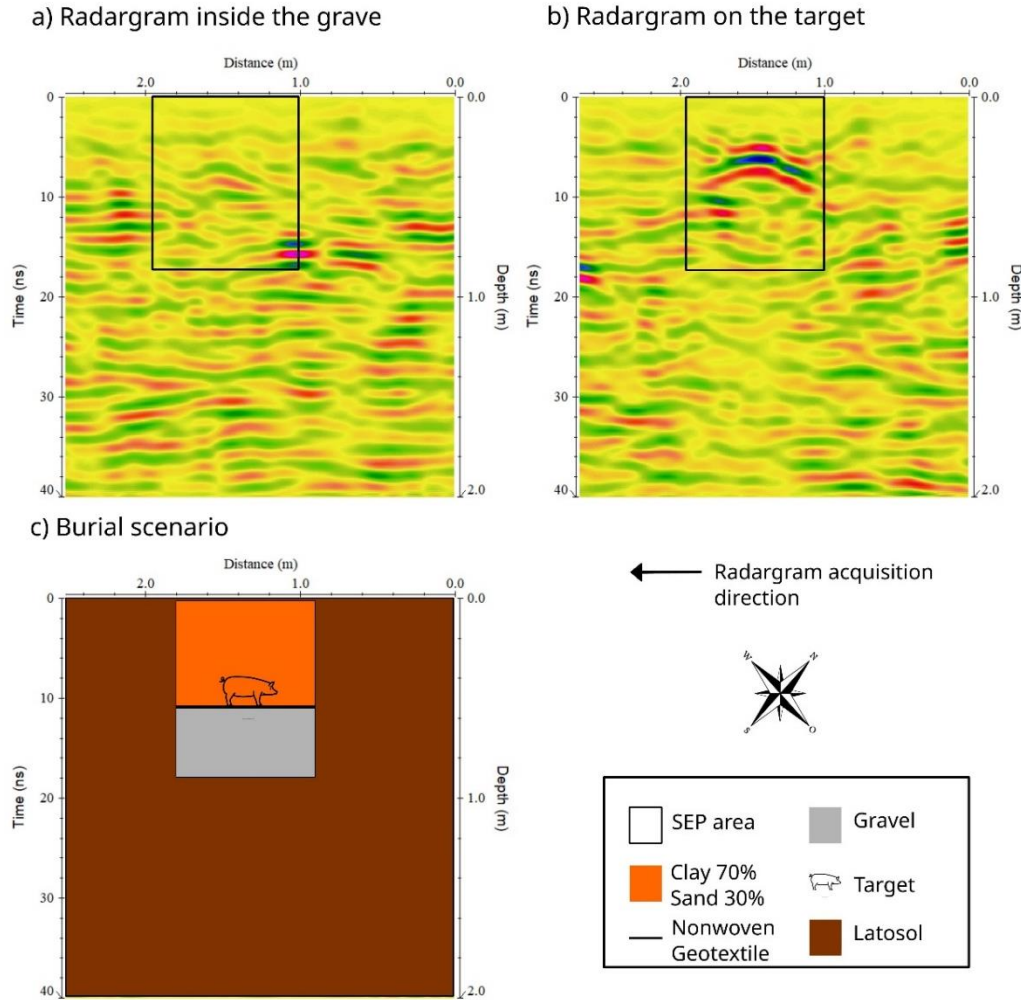


Figure 8 - Radargrams obtained over SEP04. Data acquired a) inside the grave. b) over the target with the 400MHz antenna during dry season. c) illustrative model of the buried target burial scenario.

Figures 9a-c showcase radargrams acquired over SEP01 and SEP02 at a 900 MHz frequency. Figure 9a shows reflections from all layers depicted in the burial scenario (Figure 9c) within SEP01, while the signal in SEP02 appears to be slightly attenuated. Figure 9b presents the radargram over the buried target, with SEP01 displaying a hyperbola (medium amplitude) at 10 ns and 0.5 m depth, relative to the target, and SEP02 revealing a well-defined hyperbola (low amplitude) at 18 ns and 0.9 m depth, near the target.

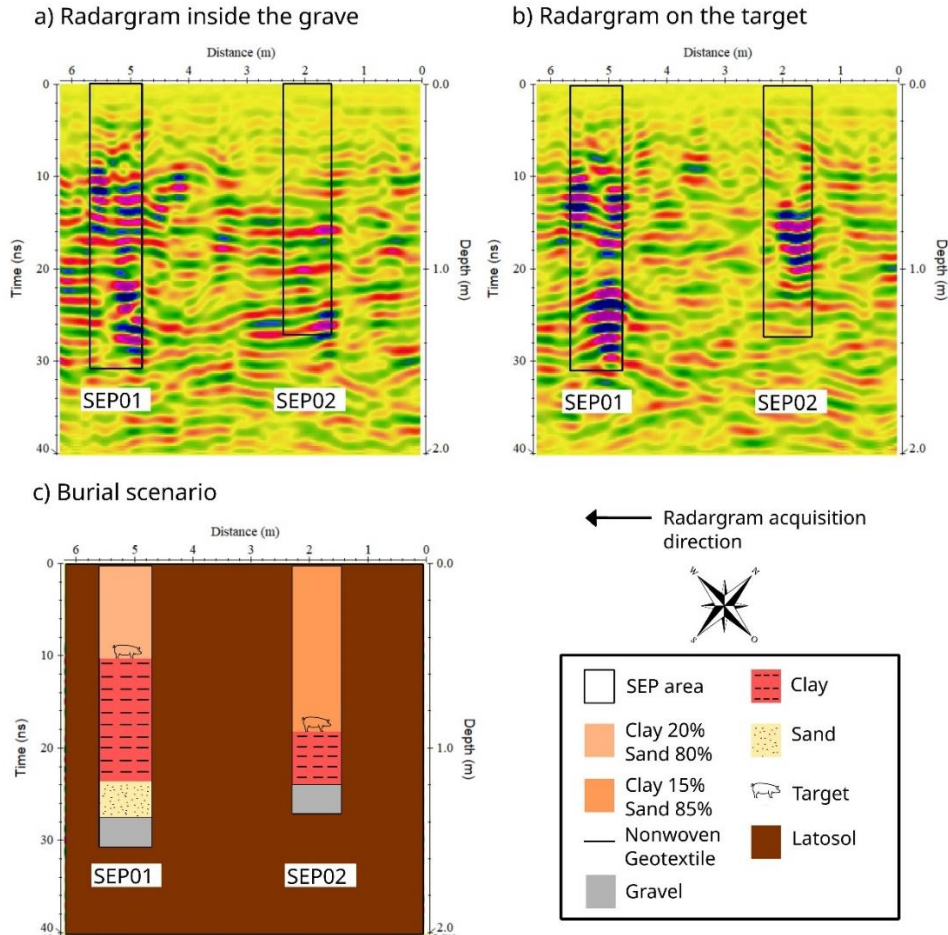


Figure 9 - Radargrams obtained over SEPs 01 and 02. Data acquired a) inside the grave. b) over the target with the 900MHz antenna during dry season. c) illustrative model of the buried target burial scenario.

Radargrams obtained over SEP03 at a 900 MHz frequency are illustrated in Figures 10a-c, showing a reflection at 2.0 m depth, corresponding to a PVC tube intended for future studies on decomposition gases in Figure 10a, a reflection at 10 ns indicative of the target's location in Figure 10b, and linear reflectors associated with the onset of the gravel layer in Figure 10c.

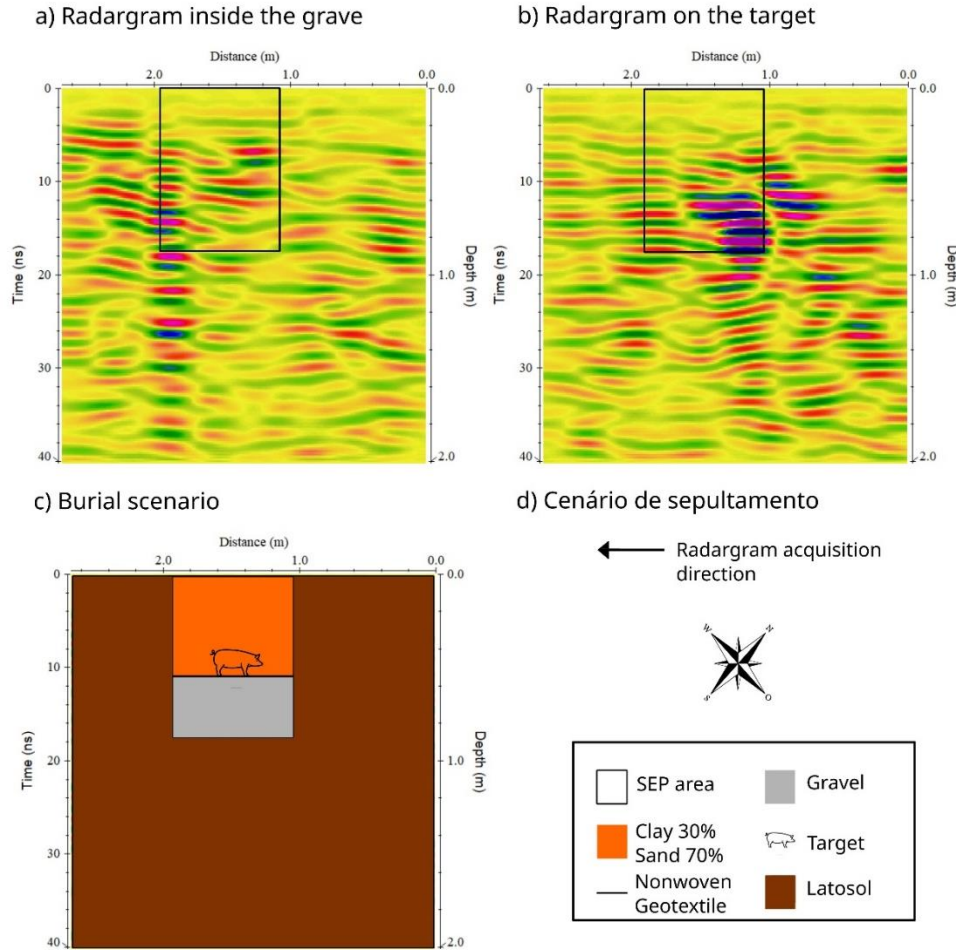


Figure 10 - Radargrams obtained over the experimental grave 03. Data acquired a) inside the grave. b) over the target with the 900MHz antenna during dry season. c) illustrative model of the buried target burial scenario.

Figures 11a-c depict radargrams acquired over SEP04 at a 900 MHz frequency, with reflections of higher amplitudes at the base corresponding to the gravel layer in Figure 11a. A reflection with a high amplitude from the top to the middle of the gravel can also be seen, along with a likely tree root reflection a nearby tree on the left side, ending at 20 ns in Figure 10b.

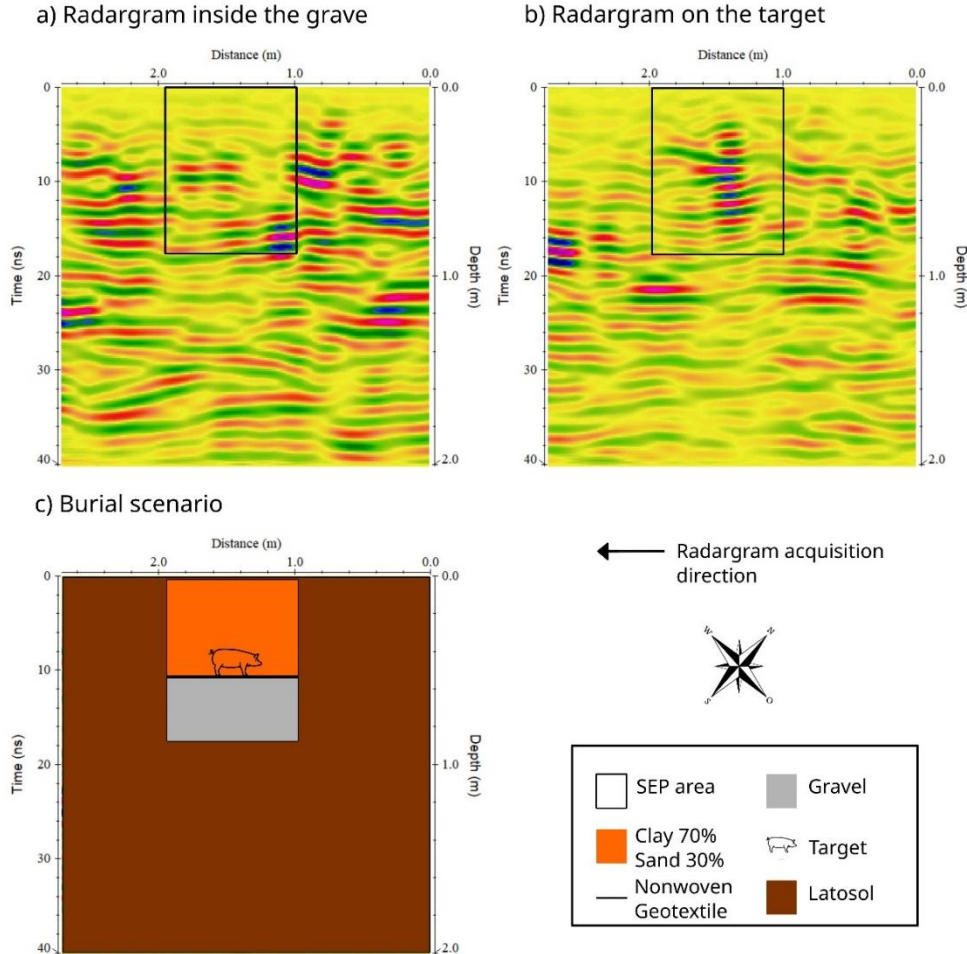


Figure 11 - Radargrams obtained over the experimental grave 04. Data acquired a) inside the grave. b) over the target with the 900MHz antenna during dry season. c) illustrative model of the buried target burial scenario.

3.3 2D Transversal Profiles

The radargrams acquired across SEPs 01 to 04 are depicted in Figures 12a-f, alongside their corresponding burial scenario models, utilizing a 400 MHz frequency. In Figure 12a, a GPR profile over SEP01 reveals various reflections within the grave, exhibiting heterogeneity, disorder, or diffraction, and suggesting ground disturbance. A faint hyperbola at a distance of 2.0 m and a depth of 0.5 m is discernible, indicating the target, compared to the burial scene in Figure 12b. Additionally, reflections corresponding to the clay, sand, and gravel layers are observed along the right-side boundary within the grave.

Figure 12c presents the radargram of a GPR profile over SEP02. A distinct noteworthy reflection commences at approximately 0.7 m depth, between 2.0-3.0 m. Comparison with the burial scenario in Figure 12d indicates its association with the target. Anomalous reflections along the grave boundary on the right-hand side, correspond to the interfaces of the clay, sand,

and gravel layers, indicating excavation at the site. There is a noticeable difference in reflection patterns between the interior and exterior of the grave, suggesting site disturbance.

The radargrams of GPR profiles over SEP03 and SEP04 are depicted in Figure 12e. Each grave exhibits a distinctive reflection. In SEP03, the reflection initiates at a depth corresponding to the top of the target, which is evident when compared with the burial scenario in Figure 12f. In SEP04, the highlighted reflection corresponds to the marker, as depicted in the burial scenario in Figure 12f. Attention is drawn to the signal attenuation beneath SEP04.

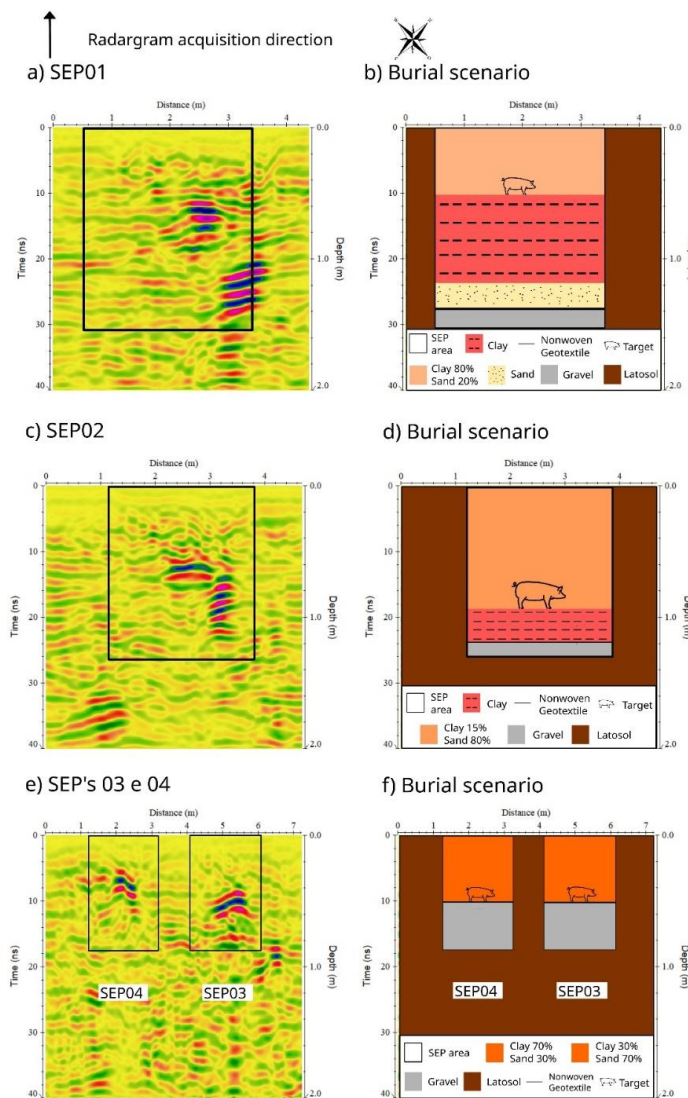


Figure 12 - Radargrams obtained transversely over the SEPs, and their respective models illustrate the buried targets' burial scenario. Data were acquired with the 400MHz antenna during dry season.

Figures 13a-f showcase the radargrams of GPR profiles over SEPs 01 to 04, alongside their corresponding burial scenario models, utilizing a 900 MHz frequency. Figure 13a displays a

GPR profile transversal to SEP01, where several reflections are identified. However, the absence of a signal at the beginning of the grave suggests interference, likely caused by an obstacle such as a root. Reflectors corresponding to all layers of the burial scene are observed in Figure 13b.

Figure 13c illustrates a radargram of a GPR profile over SEP02. A distinct reflection, occurring at 15 ns and a depth of 0.8 m, corresponds to the target closest to the pig's head, compared with the burial scenario in Figure 13d. Inside the grave, another prominent reflection above 1.0 m depth is associated with the clay layer up to the gravel layer.

Figure 13e displays a radargram of a GPR profile over SEP03 and SEP04. In SEP03, reflections commencing at 10 ns and a depth of 0.5 m correspond to the top of the gravel layer, as depicted in the burial scenario in Figure 13f. A high-amplitude reflection above this indicates the target. In SEP04, anomalous hyperbolas in the target region are observable.

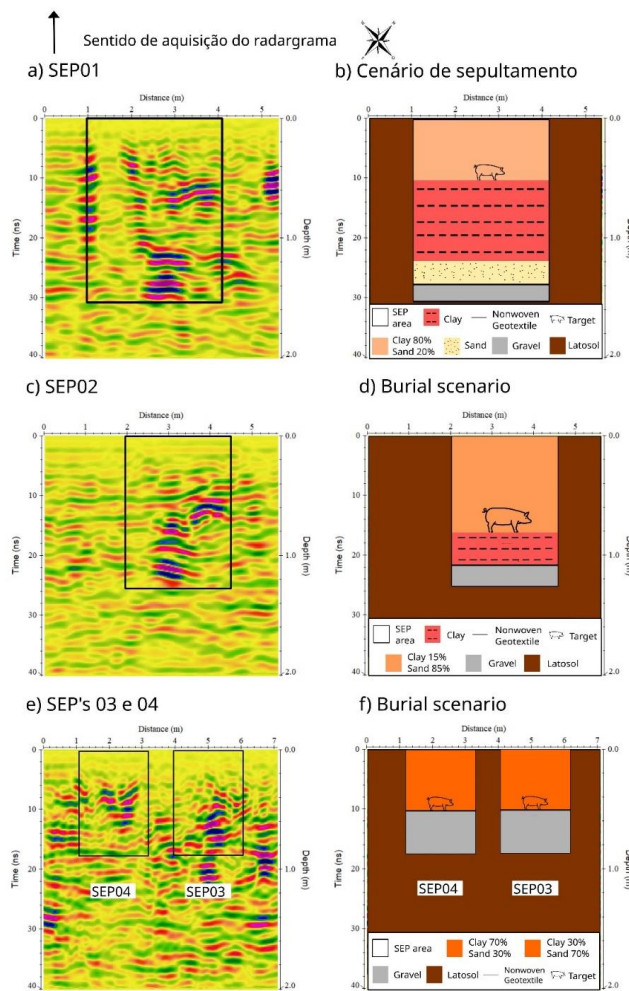


Figure 13 - Radargrams obtained transversely over the SEPs, and their respective models illustrate the buried targets' burial scenario. Data were acquired with the 900MHz antenna during dry season.

3.4 Block Diagram - Pseudo-3D Acquisition

GPR cubes are presented in Figures 14a-c, each compiled from radargrams acquired during GPR profiling over SEP's 01 to 04. Using a 400 MHz frequency in the depth cut mode, Figure 14a showcases the burial sites of SEP01 and SEP02, displaying depth slices at 0.5 m and delineating intervals at 0.9 m in SEP02. Meanwhile, Figure 14b displays the burial site of SEP03, with a depth slice at 0.5 m. Similarly, Figure 14c exhibits the burial site of SEP04, presenting buried targets with medium to high amplitude reflections.

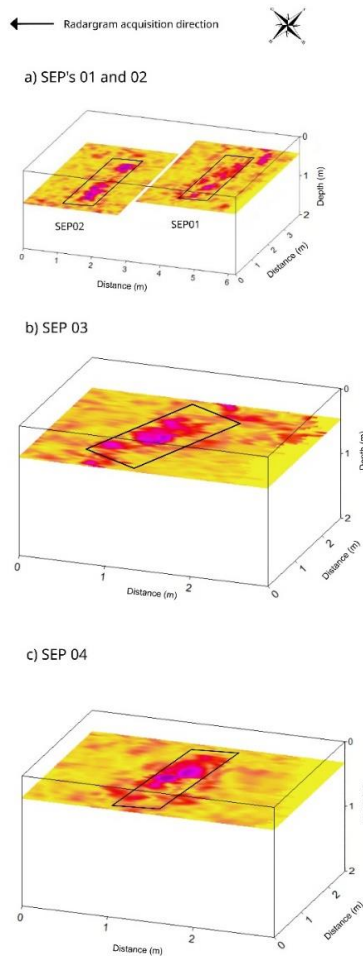


Figure 14 - a) Block diagram formed with the radargrams obtained over SEP01 and SEP02 in the depth slicing mode during dry season. Data were acquired with 400MHz. b) Block diagram formed with the radargrams obtained over SEP03 in the depth slicing mode during dry season. Data were acquired with 400MHz. c) Block diagram formed with the radargrams obtained over the SEP04 in the depth slicing mode during dry season. Data were acquired with 400MHz.

In Figures 15a-c, the GPR cubes depict radargrams obtained during GPR profiling over SEP's 01 to 04, employing a 900 MHz frequency in the depth cut mode. In Figure 15a, the burial sites of SEP01 and SEP02 are displayed, featuring a depth slice at 0.5 m for SEP01 and delineated intervals at 0.9 m in SEP02. Additionally, a medium amplitude reflection is observed at the 3.0 m position, corresponding to the steel cable added during the survey. Meanwhile, Figures 15b and 15c showcase the burial sites of SEP03 and SEP04, respectively, with depth slices at 0.5 m, illustrating buried targets with medium to high amplitude reflections.

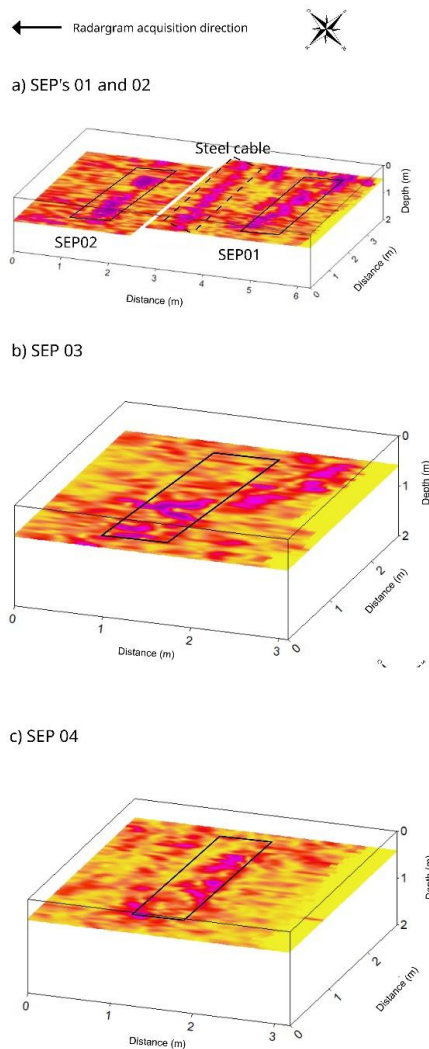


Figure 15 - a) Block diagram formed with the radargrams obtained over SEP01 and SEP02 in the depth slicing mode during dry season. Data were acquired with 900MHz. b) Block diagram formed with the radargrams obtained over SEP03 in the depth slicing mode during dry season. Data were acquired with 900MHz. c) Block diagram formed with the radargrams obtained over the SEP04 in the depth slicing mode during dry season. Data were acquired with 900MHz.

4 Discussion

With additional information on the actual positions of the buried targets, it is possible to assign their location in the interpretation of the obtained radargrams. This means that the optimal frequency and grave composition can be evaluated with precision, to accurately identify buried forensic targets.

In Figures 6b (SEP02), 8b, 9b (SEP02), 11b, 12c-e (SEP04), and 13c-e (SEP04), a discernible attenuation of the GPR post-target reflection signal is evident, exhibiting variability, which is contingent upon target size and grave filling composition. Notably, SEP02 and SEP04 indicate larger dimensions for their respective targets. In particular, in SEP04, characterized by a higher concentration of clay material compared to the others, the GPR signal experiences heightened attenuation, as exemplified by the notable visual decrease from 25 ns in Figure 9b (SEP02) and 15 ns in Figure 12e (SEP04).

By juxtaposing the GPR profiles conducted outside the grave with those on the targets, evidence of overturned soil in SEP areas is apparent. The 400 MHz frequency exhibits superior discernment of overturned soil, as exemplified in Figure 12c (within a span of 1.2-3.8 m) and Figure 7b (from 1.0-2.0 m). The most pronounced reflection outcomes from the parallel 2D GPR profiles performed on the targets are observed in SEP04, and are attributed to its larger target size, yielding a superior signal reflection across the 400 MHz and 900 MHz frequencies.

Considering the sand-clay ratio within the graves and the parallel 2D GPR profiles on targets, SEP04 presents the second-best outcomes across both frequencies studied. Despite exhibiting suboptimal target visualization, the primary contributing factor is the target's significant dimensions, rather than the sand (30%) and clay material (70%) composition, underscoring that clay material abundance in the soil does not impede forensic target detection.

Conversely, SEP03 demonstrates the most limited reflection outcomes due to target dimensions and grave fill composition, resulting in imprecise pig identification at both frequencies, via parallel 2D radargrams, even failing to yield a clear reflection from the gravel layer. Superior reflection outcomes, from transverse 2D GPR profiles over the targets, are observed in SEP01 and SEP02 and characterized by lower clay material concentrations, resulting in diminished GPR signal attenuation and heightened subsurface detailing, facilitating target identification across both 400 MHz and 900 MHz frequencies.

In relation to the grave filling material composition and transverse 2D GPR profiles, SEP03 displays the second-best detailed outcomes across both frequencies, enabling identification of the target and its layered characteristics. Lastly, SEP04's detection of the pig at both frequencies is marred by GPR signal attenuation, precluding finer layer identification, particularly the gravel layer.

5 Conclusions

As previously mentioned, the main objective of this work was to evaluate the influence of clay soil content and GPR frequency on the recognition of forensic targets in a controlled environment that simulates human burial evidence. The objective was achieved, as can be seen

in the results and discussion described above, allowing visualization of the geophysical response of the GPR method over graves with different sand-clay ratios and varied target sizes in the period with low soil moisture.

The investigation successfully elucidated the impact of clay soil content and GPR frequency on the detection of forensic targets in a controlled environment mimicking burial scenarios. Through meticulous analysis, it was evident that variations in sand-clay ratios and target sizes significantly influenced the geophysical response of the GPR method.

The utilization of a controlled site emerged as an invaluable asset for conducting geophysical studies. By meticulously controlling geometric configurations, target characteristics, and soil composition, the study facilitated a more precise examination of GPR results, thereby minimizing potential errors in radargram analysis.

Comparative analysis of different antenna frequencies revealed distinct performance characteristics. While the 400 MHz antenna yielded satisfactory results, providing detailed insights into grave structures and target localization, the 900 MHz frequency exhibited inferior performance, particularly in delineating SEP horizons.

The study underscored the significance of clay material proportion in graves, with optimal results observed in SEPs characterized by a lower clay content (85% sand and 15% clay material). Conversely, SEPs with higher clay content (30% sand and 70% clay material), such as SEP03, exhibited less accurate outcomes, attributed to the smaller target size and increased clay presence.

To mitigate ambiguities in data interpretation, the integration of GPR with complementary geophysical methods, such as magnetic susceptibility and electrical geophysics, is recommended. This approach enables more comprehensive data analysis, particularly in scenarios involving metal objects or expedited data processing requirements.

The study advocates the acquisition of multiple cross-sectional 2D radargrams to facilitate comparative analysis between areas inside and outside graves, enhancing the accuracy of target identification. Additionally, optimizing the positioning of reference markers, such as steel cables, is crucial for ensuring data integrity during 3D data acquisition.

In summary, this study provides valuable insights into optimizing GPR-based forensic investigations, highlighting the importance of meticulous data analysis, controlled experimental settings, and strategic methodological enhancements for enhanced target detection and interpretation accuracy.

6 Acknowledgments

The authors thank all the employees of Fazenda Água Limpa (FAL)/UnB for the project. The authors thank the Geosciences Institute/UnB for their support. The authors thank Hartos Agropecuária Cenci for donating the pig carcasses.

7 References

- Abate, D., Colls, S.C., Moyssi, N., Karsili, D., Faka, M., Anilir, A., Manolis, S. (2019). Optimizing search strategies in mass grave location through the combination of digital technologies. *Forensic Science International* 1: 95–107. DOI: 10.1016/j.fsisyn.2019.05.002

- ABNT (1989). Brazilian association of norms techniques. Peneiras para ensaio com telas de tecido metálico. NBR 5734.
- Annan, A.P. (2004) Ground penetrating radar: principles, procedures and applications, Sensors & Software Inc. Technical paper
- Aziz, A.S., Stewart, R., Green, S., Flores, J. (2016). Locating and characterizing burials using 3D ground-penetrating radar (GPR) and terrestrial laser scanning (TLS) at the historic Mueschke Cemetery, Houston, Texas. *Journal of Archaeological Science: Reports* 8: 392–405. DOI: 10.1016/j.jasrep.2016.06.035
- Barone, P.M., Di Maggio, R.M. (2019). Forensic geophysics: ground penetrating radar (GPR) techniques and missing persons investigations. *Forensic Sciences Research* 4: 337–340. DOI: 10.1080/20961790.2019.1675353
- Castro, K.C.P.L., Cunha, L.S., Sousa, A.C.A., Nogueira, P.V., Borges, W.R. (2024) Influence of the sand-clay ratio of the burial material of forensic targets on ground-penetrating radar (GPR) responses—comparison of dry and rainy season data. *Front. Earth Sci.* 12:1305496. doi: 10.3389/feart.2024.1305496
- Castro, K.C.P.L., Cunha, L.S. (2021). Forensic Investigations with the Identification of Human Remains with Ground Penetrating Radar (GPR): A Review. *Estudos Geológicos* 31(2): 64–86. DOI: 10.18190/estudosgeologicos.v31n2p64-86
- Castro, K.C.P.L. (2021). Ground Penetrating Radar (GPR) for the Identification of Forensic Evidence in the Controlled Site Fazenda Água Limpa/University of Brasília - DF. 100pp. Trabalho de Conclusão de Curso (Bacharelado em Geofísica) – University of Brasília – UnB. Brasília, Brazil.
- Cavalcanti, M.M Rocha, M.P., Blum M.L.B., Borges W.R. (2018). The forensic geophysical controlled research site of the University of Brasilia, Brazil: Results from methods GPR and electrical resistivity tomography. *Forensic Science International* 293: e1–101.e21. DOI: 10.1016/j.forsciint.2018.09.033
- Cavalcanti, M.M. (2017). Estudo da Resposta Geofísica em Diferentes Cenários de Sepultamento. 197 pp. Ph. D. Thesis. University of Brasilia - IG. Brasília, Brazil.
- Dick, H.C., Pringle, J.K. (2018). Inorganic elemental analysis of decomposition fluids of an in situ animal burial. *Forensic Science International* 289: 130–139. DOI: 10.1016/j.forsciint.2018.05.034
- Gomes, M.P., Vital, H., Macedo, J.W.P. (2011). Fluxo de Processamento Aplicado a Dados de Sísmica de Alta Resolução em Ambiente de Plataforma Continental. Exemplo: Macau-RN. *Revista Brasileira de Geofísica* 29(1): 173-186.
- Hansen, J.D., Pringle, J.K. (2013). Comparison of magnetic, electrical and ground penetrating radar surveys to detect buried forensic objects in semi-urban and domestic patio environments. *Geological Society, London, Special Publications* 384: 229–251. DOI: 10.1144/sp384.13
- Lester, J., Bernold, L.E. (2006). Innovative process to characterize buried utilities using Ground Penetrating Radar. *Automation in Construction* 16: 546–555.
- Molina, C.M., Pringle, J.K., Saumett, M., and Evans, G.T. (2016). Geophysical and botanical monitoring of simulated graves in a tropical rainforest, Colombia, South America. *Journal of Applied Geophysics* 135: 232–242. DOI: 10.1016/j.jappgeo.2016.10.002

- Molina, C.M., Pringle, J.K., Saumett, M., and Hernández, O. (2015). Preliminary results of sequential monitoring of simulated clandestine graves in Colombia, South America, using ground penetrating radar and botany. *Forensic Science International* 248: 61–70. DOI: 10.1016/j.forsciint.2014.12.011
- Olhoeft, G.R. (2000). Maximizing the information return from ground penetrating radar. *Journal of Applied Geophysics* 43: 175–187. DOI: 10.1016/S0926-9851(99)00057-9
- Parker, R., Ruffell, A., Hughes, D., and Pringle, J.K. (2010). Geophysics and the search of freshwater bodies: A review. *Science & Justice* 50: 141–149. DOI: 10.1016/j.scijus.2009.09.001
- Pringle, J.K., Stimpson, I.G., Wisniewski, K.C., Heaton, V., Davenward, B., Mirosch, N., Spencer, F., and Jervis, J.R. (2020). Geophysical monitoring of simulated homicide burials for forensic investigations. *Scientific Reports* 10. DOI: 10.1038/s41598-020-64262-3
- Pringle, J.K., Jervis, J.R., Roberts, D., Dick, H.C., Wisniewski, K.C., Cassidy, N.J., and Cassella, J.P. (2016). Long-term Geophysical Monitoring of Simulated Clandestine Graves using Electrical and Ground Penetrating Radar Methods: 4–6 Years After Burial. *Journal of Forensic Sciences* 61: 309–321. DOI: 10.1111/1556-4029.13009
- Rubio-Melendi, D., González-Quirós, A., Roberts, D., García, M.C.G., Domínguez, A.C., Pringle, J.K., and Fernández-Álvarez, J.P. (2018). GPR and ERT detection and characterization of a mass burial, Spanish Civil War, Northern Spain. *Forensic Science International* 287: e1–e9. DOI: 10.1016/j.forsciint.2018.03.034
- Ruffell, A., Pringle, J.K., Cassella, J.P., Morgan, R.M., Ferguson, M., Heaton, V., Hope, C., and McKinley, J.M. (2017). The use of geoscience methods for aquatic forensic searches. *Earth-Science 660 Reviews* 171:323–337. DOI: 10.1016/j.earscirev.2017.04.012
- Sandmeier, K.J. (2014). REFLEXW Version 7.5, Windows 9x/2000/NT. Program for the processing of seismic, acoustic or electromagnetic reflection, refraction and transmission data. Manual of Software, Karlsruhe, Germany.
- Schoor, M., Nienaber, W.C., and Marais-Werner, A. (2017). A controlled monitoring study of simulated clandestine graves using 3D ground penetrating radar. *Near Surface Geophysics* 15: 274–284. DOI: 10.3997/1873-0604.2017007
- Schultz, J.J., Walter, B.S., and Healy, C. (2016). Long-term sequential monitoring of controlled graves representing common burial scenarios with ground penetrating radar: Years 2 and 3. *Journal of Applied Geophysics* 132: 60–74. DOI: 10.1016/j.jappgeo.2016.06.015
- Schultz, J.J., Healy, C., Parker, K., and Lowers, B. (2013). Detecting submerged objects: The application of side scan sonar to forensic contexts. *Forensic Science International* 231: 306–316. DOI: 10.1016/j.forsciint.2013.05.032
- Schultz, J.J. (2008). Sequential Monitoring of Burials Containing Small Pig Cadavers Using Ground Penetrating Radar. *Journal of Forensic Sciences* 53: 279–287. DOI: 10.1111/j.1556-4029.2008.00665.x
- Schultz, J.J., Collins, M.E., and Falsetti, A.B. (2006). Sequential Monitoring of Burials Containing Large Pig Cadavers Using Ground-Penetrating Radar. *Journal of Forensic Sciences* 51: 607–616. DOI: 10.1111/j.1556-4029.2006.00129.x

Schultz, J.J., Falsetti, A.B., Collins, M., Koppenjan, S., and Warren, M.W. (2002). Detection of forensic burials in Florida using GPR. Ninth International Conference on Ground Penetrating Radar 4758. DOI: 10.1117/12.462239

Solla, M., Riveiro, B., Álvarez, M.X., and Arias, P. (2012). Experimental forensic scenes for the characterization of ground-penetrating radar wave response. Forensic Science International 220: 50–58. DOI: 10.1016/j.forsciint.2012.01.025

Yilmaz, O. (2001). Seismic Data Analysis, Society of Exploration Geophysicists, Tulsa, 2065pp. The following formatting styles are meant as a guide, as long as the full citation is complete and clear, Frontiers referencing style will be applied during typesetting.

Table 1 - Identification of the experimental burial sites, the composition of the cover textures, and the dimensions of the buried targets.

Experimental Graves	Target Dimension			Cover Texture Composition
	Weight (kg)	Length (m)	Width (m)	
SEP01	15.00	0.58	0.11	Clay 20% - Sand 80%
SEP02	55.60	1.26	0.33	Clay 15% - Sand 85%
SEP03	16.80	0.74	0.21	Clay 30% - Sand 70%
SEP04	84.20	1.40	0.43	Clay 70% - Sand 30%

Table 2 - Granulometric analysis results for the sand and clay materials used as cover for the targets.

Grain Size	SEP01	SEP02	SEP03	SEP04
	%	%	%	%
Gravel + Coarse Sand + Middle - Fine Sand	80.88	85.02	69.37	30.05
Silt + Clay	19.12	14.98	30.63	69.95
Total	100.00	100.00	100.00	100.00



OPEN ACCESS

EDITED BY

Marcelo Cohen,
 Federal University of Pará, Brazil

REVIEWED BY

Pier Matteo Barone,
 American University of Rome, Italy
 Elena Marrocchino,
 University of Ferrara, Italy

*CORRESPONDENCE

Kimberly Coutinho Paes Leme de Castro,
 kimberlycplcastro@yahoo.com

RECEIVED 01 October 2023

ACCEPTED 28 February 2024

PUBLISHED 20 March 2024

CITATION

Castro KCPL, Cunha LS, Sousa ACA, Nogueira PV and Borges WR (2024). Influence of the sand-clay ratio of the burial material of forensic targets on ground-penetrating radar (GPR) responses—comparison of dry and rainy season data.

Front. Earth Sci. 12:1305496.

doi: 10.3389/feart.2024.1305496

COPYRIGHT

© 2024 Castro, Cunha, Sousa, Nogueira and Borges. This is an open-access article distributed under the terms of the [Creative Commons Attribution License \(CC BY\)](#). The use, distribution or reproduction in other forums is permitted, provided the original author(s) and the copyright owner(s) are credited and that the original publication in this journal is cited, in accordance with accepted academic practice. No use, distribution or reproduction is permitted which does not comply with these terms.

Influence of the sand-clay ratio of the burial material of forensic targets on ground-penetrating radar (GPR) responses—comparison of dry and rainy season data

Kimberly Coutinho Paes Leme de Castro*,
 Luciano Soares da Cunha, Ana Clara de Araujo Sousa,
 Pedro Vencovský Nogueira and Weliton Rodrigues Borges

University of Brasília, Institute of Geosciences, Graduate Program in Applied Geosciences and Geodynamics, Brasília, Brazil

This study aims to assess the impact of the sand-clay ratio on the detection of simulated forensic targets resembling human burial evidence using ground-penetrating radar (GPR). To achieve this goal, we established a controlled site consisting of four experimental graves (SEPs), with each SEP representing a distinct burial scenario. The project's objectives encompass evaluating how varying the clay soil content influences the detection of swine targets using 2D, quasi-3D, and 4D GPR imaging techniques. We observed signal attenuation in the GPR data during the rainy season and after reflection from larger targets, primarily due to the conductive behavior of the soft tissues within the targets. We achieved more precise results in an SEP that was 85% sand and 15% clay material, regardless of seasonality. We obtained better results in the dry season due to the greater penetrability of electromagnetic waves and more explicit reflections. In comparison, we achieved more precise results for SEP03, which was 70% sand and 30% clay material. In conclusion, controlled sites are invaluable tools for geophysical investigations, as they provide a controlled environment where we can meticulously adjust various parameters, leading to a more precise and insightful analysis of the results. By systematically manipulating factors such as the soil composition, target depth, and environmental conditions, researchers can effectively calibrate their instruments and methodologies, enhancing the accuracy and reliability of their findings. Therefore, controlled sites not only facilitate comprehensive data collection but also serve as essential platforms for refining and validating geophysical techniques, ultimately advancing the field of geophysical forensics.

KEYWORDS

clandestine grave, controlled research site, forensic science, burials, GPR, ground penetrating radar

1 Introduction

Forensic geophysics research employing ground-penetrating radar (GPR) exhibits substantial potential for the non-destructive detection of concealed or interred objects. The forensic application of GPR has demonstrated notable progress across diverse scientific domains. It has been incorporated into various lines of investigation, encompassing the decomposition of organic matter (Schultz et al., 2016; Ruffell et al., 2017; Schoor et al., 2017; Dick and Pringle, 2018; Pringle et al., 2020), the examination of submerged environments (Parker et al., 2010; Schultz et al., 2013), controlled sites (Barone et al., 2022; Pringle et al., 2020; Cavalcanti et al., 2018; Schoor et al., 2017; Booth and Pringle, 2016; Molina et al., 2016a; b; Pringle et al., 2016; Schultz et al., 2016; Almeida et al., 2015; Molina et al., 2015; Almeida et al., 2014; Lowe et al., 2013; González-Jorge et al., 2012; Pringle et al., 2020; Schultz and Martin, 2012; Solla et al., 2012; Schultz and Martin, 2011; Parker et al., 2010; Schultz, 2008; Schultz et al., 2006; Powell, 2004; Schultz et al., 2002), and its synergistic utilization in conjunction with complementary methodologies (Hansen and Pringle, 2013; Molina et al., 2016a; Aziz et al., 2016; Cavalcanti et al., 2018; Rubio-Melendi et al., 2018; Abate et al., 2019; Pringle et al., 2020).

GPR is overwhelmingly the most commonly used geophysical technique for the detection of subsurface human remains, but resistivity, electromagnetic induction, magnetics, acoustic techniques, and gravity data are also applied depending on the particular burial circumstances (Berezowski et al., 2021). Nevertheless, applying the GPR technique for this purpose presents inherent limitations contingent upon site-specific characteristics, the soil composition, and the extent of decomposition exhibited by the target materials (Lester and Bernold, 2006; Barone and Di Maggio, 2019).

The principal advancements identified were in research conducted within controlled sites, which were systematically examined and cultivated under tightly monitored conditions. These conditions encompassed a comprehensive set of parameters, including the depth, dimensions, target type, soil characteristics, frequency, and the integration of supplementary methodologies, which were all meticulously controlled. Some objectives were facilitating comparisons across various antenna frequencies, establishing foundational principles for forensic research, and delineating optimal practices and methodologies for detecting inhumations. This research direction, recognized as promising in a systematic literature review (SLR) (Castro and Cunha, 2021), is the central objective of this work.

The primary goal of this study is to assess how the clay soil content, GPR frequency, and data collected under both dry and rainy conditions influence the recognition of forensic targets within a controlled environment designed to simulate human burial evidence. We monitored the spatial-temporal variations in the moisture content with depth and made measurements by employing electrical tomography and the spontaneous potential within this controlled site.

2 Materials and methods

2.1 Study area

The controlled site for the conducted experiments was established within an approximate area of 100 m² situated within the Experimental Farm (FAL) of the Federal University of Brasília (UnB). The vegetation at the site had already undergone partial suppression, with shrubs, medium-sized trees, and grasses remaining. Figure 1 provides a visual representation of the specific location of the controlled site (Castro, 2021).

Our area of the controlled site is within the FAL in a region characterized by the presence of oxisols. The climate in the Federal District region, according to Koppen's classification, falls within the spectrum of a tropical savanna and rainy temperate climate, with a distinct dry winter season. This climate exhibits a clear seasonal division: a rainy and hot period occurs from October to April, and it is followed by a cold and dry phase from May to September. The temperature fluctuations are notable, with the coldest months registering temperatures as low as 12°C, while the hottest months can see temperatures exceeding 28.5°C (Cavalcanti, 2017). The average annual precipitation in this region is 1,600 mm (available at <https://tempo.inmet.gov.br/Graficos/A001>, accessed on 01 November 2021).

2.2 Implementation of the controlled site

In July 2021, the controlled site was established; it comprised four experimental inhumations involving the burial of target specimens (pigs) at depths of either 0.50 m or 0.90 m with different cover texture compositions (Figure 2). Detailed specifications regarding the targets' dimensions and the composition of the cover textures can be found in Table 1 (Castro, 2021).

The oxisols, sourced from the excavation of the graves, were employed as the clay material constituting the cover for the targets. We conducted a laboratory analysis to assess the granulometry of the clay and sand materials, and we present the results in Table 2. The technique used to analyze the fine particles in the granulometry analysis was the sedimentology test, while for the larger particles (>0.075 mm), the sieving test was used (NBR 5734/ABNT, 1989).

Experimental Sepulture 01 (SEP01) is 3.00 m in length, 0.80 m in width, and 1.50 m in depth. We filled it according to the following sequence (Figure 3A): first, for the base, there is a layer of 0.15 m of gravel, followed by a nonwoven geotextile layer. Then, there is 0.20 m of sand and 0.65 m of clay material. Finally, we placed the pig target at a depth of 0.50 m, with its specific dimensions outlined in Table 1. A mixture of 20% clay material and 80% sand was employed to bury the target and complete the grave filling (Castro, 2021).

Experimental Grave 02 (SEP02) is 2.50 m in length, 0.80 m in width, and 1.30 m in depth. The filling process (Figure 3B) proceeded as follows, from bottom to top: there is a layer of 0.15 m of gravel, followed by a nonwoven geotextile layer. Then, there is 0.25 m of clay material. We positioned the pig target at a depth

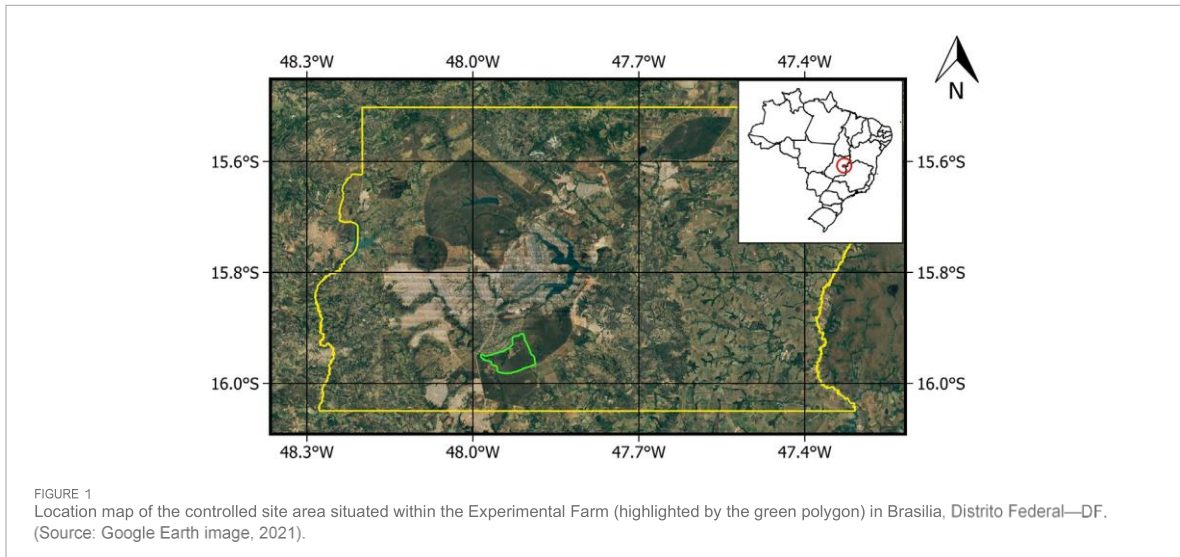


FIGURE 1
Location map of the controlled site area situated within the Experimental Farm (highlighted by the green polygon) in Brasilia, Distrito Federal—DF.
(Source: Google Earth image, 2021).

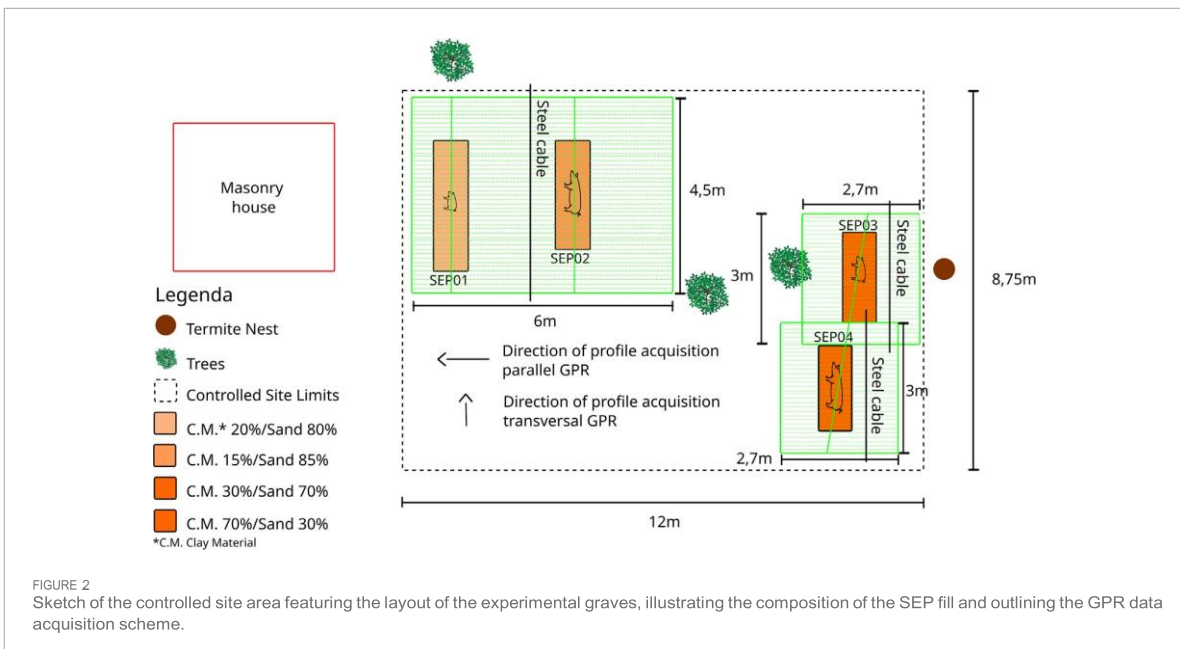


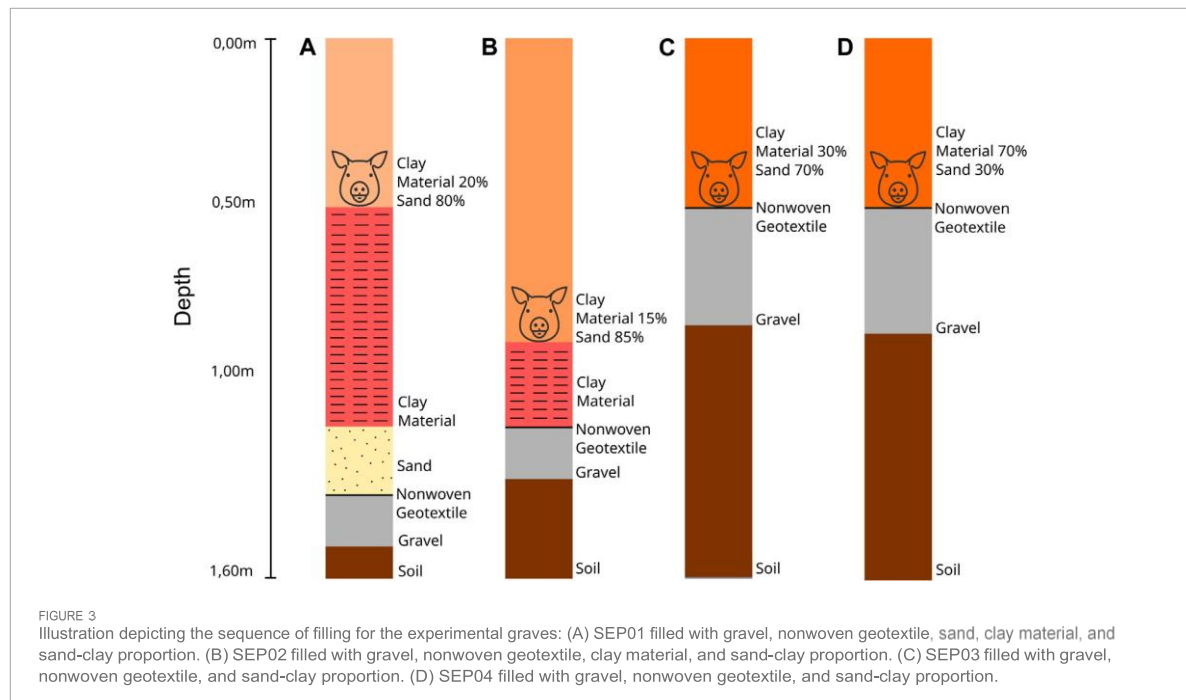
FIGURE 2
Sketch of the controlled site area featuring the layout of the experimental graves, illustrating the composition of the SEP fill and outlining the GPR data acquisition scheme.

TABLE 1 Identification of the experimental burial sites, the composition of the cover textures, and the dimensions of the buried targets.

Experimental graves	Target dimension			Cover texture composition (%)
	Weight (kg)	Length (m)	Width (m)	
SEP01	15.00	0.58	0.11	Clay: 20%, Sand: 80
SEP02	55.60	1.26	0.33	Clay: 15%, Sand: 85
SEP03	16.80	0.74	0.21	Clay: 30%, Sand: 70
SEP04	84.20	1.40	0.43	Clay: 70%, Sand: 30

TABLE 2 Granulometric analysis results for the sand and clay materials used as cover for the targets.

Grain size	SEP01	SEP02	SEP03	SEP04
	%	%	%	%
Gravel + Coarse Sand + Middle - Fine Sand	80.88	85.02	69.37	30.05
Silt + Clay	19.12	14.98	30.63	69.95
Total	100.00	100.00	100.00	100.00



of 0.90 m, with the dimensions specified in Table 1. We utilized a mixture comprising 15% clay and 85% sand to bury the target and complete the grave filling (Castro, 2021).

Experimental Grave 03 (SEP03) is 2.10 m in length, 0.80 m in width, and 0.85 m in depth. The filling process (Figure 3C) proceeded as follows, from bottom to top: there is a layer of 0.35 m of gravel, followed by a nonwoven geotextile layer. We positioned the pig target at a depth of 0.50 m, with the dimensions specified in Table 1. A mixture comprising 30% clay and 70% sand was employed to bury the target and complete the grave filling (Castro, 2021).

Experimental Grave 04 (SEP04) is 2.00 m in length, 0.80 m in width, and 0.87 m in depth. The filling process (Figure 3D) proceeded as follows, from bottom to top: there is a layer of 0.37 m of gravel, followed by a nonwoven geotextile layer. We positioned the pig target at a depth of 0.50 m, with the dimensions specified in Table 1. A mixture comprising 70% clay and 30% sand was employed to bury the target and complete the grave filling (Castro, 2021).

2.3 Data acquisition

The GPR is a geophysical method for mapping subsurface structures using electromagnetic energy. Various deployment methods exist, but all approaches involve a transmitter generating radiofrequency signals, which are typically in the 1–5,000 MHz frequency range, and a receiver detecting similar signals. The objective is to measure the impulse response or the transfer function of the surrounding medium to reconstruct the material's property structure. In its simplest form, a GPR system with a transmitter and receiver is moved over the ground surface, and reflections returning from subsurface objects are detected, recorded, and displayed for the user (Annan, 2004).

As the GPR system is moved over the ground, a shallow image of the subsurface is obtained along the survey line. These images, called radargrams (Figure 5), are two-dimensional graphical representations (XZ) of the detected reflections. The X-axis represents the antenna displacement along the survey line, while the Z-axis represents the two-way travel time of the emitted



FIGURE 4
Photograph of the GPR data acquisition in the controlled site area with the 400 MHz antenna.

pulse (in nanoseconds). Suppose that the time taken for the electromagnetic pulse to travel from the transmission antenna to the reflector in the soil and back to the receiving antenna is measured. In that case, the velocity of this pulse in the subsurface medium is known, and the reflector's position can be determined (Solla et al., 2012).

We acquired data using the Geophysical Survey System Inc. (GSSI) GPR SIR3000 equipment with 400 MHz and 900 MHz antennas. The dry data collection process occurred on 03 August 2021 (Figure 4) and on 18 August 2021. The rainy data collection process occurred on 23 February 2023. During the dry field operation, we acquired 385 radargrams across the controlled site area, and 377 radargrams were acquired during the rainy field operation.

We employed two tape measures to ensure precise profile orientation, and a rope was stretched between them to demarcate the starting and ending points of the surveyed lines. We acquired data with the spacing between these lines set to 0.05 m, moving from northeast to southwest. A steel cable was also employed to facilitate the 3D processing of GPR data.

2.4 Processing

For the processing of the radargrams, the Reflex-Win 7.5.2 software was employed (Sandmeier, 2014). Below is the processing sequence utilized for dry season data.

- Static correction—the determination of the initial arrival point of electromagnetic energy directly propagated by the acquisition surface (Olhoeft, 2000).
- Energy decay function—enhances reflectors through an iterative process that can be applied linearly and exponentially at a specified depth.
- Bandpass frequency—filters out undesired frequencies and reduces noise from various sources, permitting frequencies within the specified band to pass (Gomes et al., 2011).

- Background removal—eliminates any background noise.
- FK filter—a two-dimensional filter defined in the frequency and wave number domain (F-K) that enables the suppression of electromagnetic signal noise (Cavalcanti, 2017).
- Migration (Kirchhoff)—relocates reflections to their accurate positions in the subsurface and collapses diffractions, thereby improving the spatial resolution (Yilmaz 2001). We determined the velocities of the electromagnetic waves based on the known depth (h) of the buried targets and the double transit time values of the electromagnetic wave (t) over each hyperbolic event assigned to the buried targets. We calculated the average electromagnetic wave propagation velocities used for migration using Eq. 1. The velocities (V) ranged from 0.07 to 0.1 m/ns in the dry season and from 0.1 to 0.12 m/ns in the rainy season:

$$V = \frac{2h}{t} \quad (1)$$

We applied the same processing steps for the rainy season data, except for the bandpass frequency filter, which could have yielded more satisfactory results in assessing the clay and sand content and the moisture content.

3 Results

3.1 Area background

The radargram processing routine for Figures 5A–D followed the same procedures outlined in the previous section. Figure 5A displays the radargram obtained using the 400 MHz antenna outside SEP01 and SEP02 during the dry season to assess the background. The geophysical response highlights the behavior of the homogeneous latosol, where disordered hyperbolas are observed, likely representing tree roots or animal burrows. Shortly after the 3.0 m position, a hyperbola corresponding to the steel cable added during the GPR survey is visible. Figure 5B shows the radargram obtained using the 900 MHz antenna outside SEP01 and SEP02 during the dry season for background verification. The response emphasizes the behavior of the homogeneous latosol, revealing some reflectors that attenuate as depth increases. Additionally, at approximately 3.4 m, there is a hyperbola that corresponds to the steel cable added during the GPR survey. Figure 5C presents the radargram acquired using the 400 MHz antenna outside SEP01 and SEP02 during the rainy season for background verification. The geophysical response illustrates the behavior of the homogeneous latosol, displaying less prominent, disordered hyperbolas that likely represent tree roots or animal burrows. Around the 3.0 m position, a hyperbola corresponding to the steel cable added during the GPR survey is visible. Lastly, Figure 5D exhibits the radargram obtained using the 900 MHz antenna outside SEP01 and SEP02 during the rainy season for background verification. The response underscores the behavior of the homogeneous latosol, revealing some reflectors that attenuate as the depth increases; they are particularly noticeable after 30 ns.

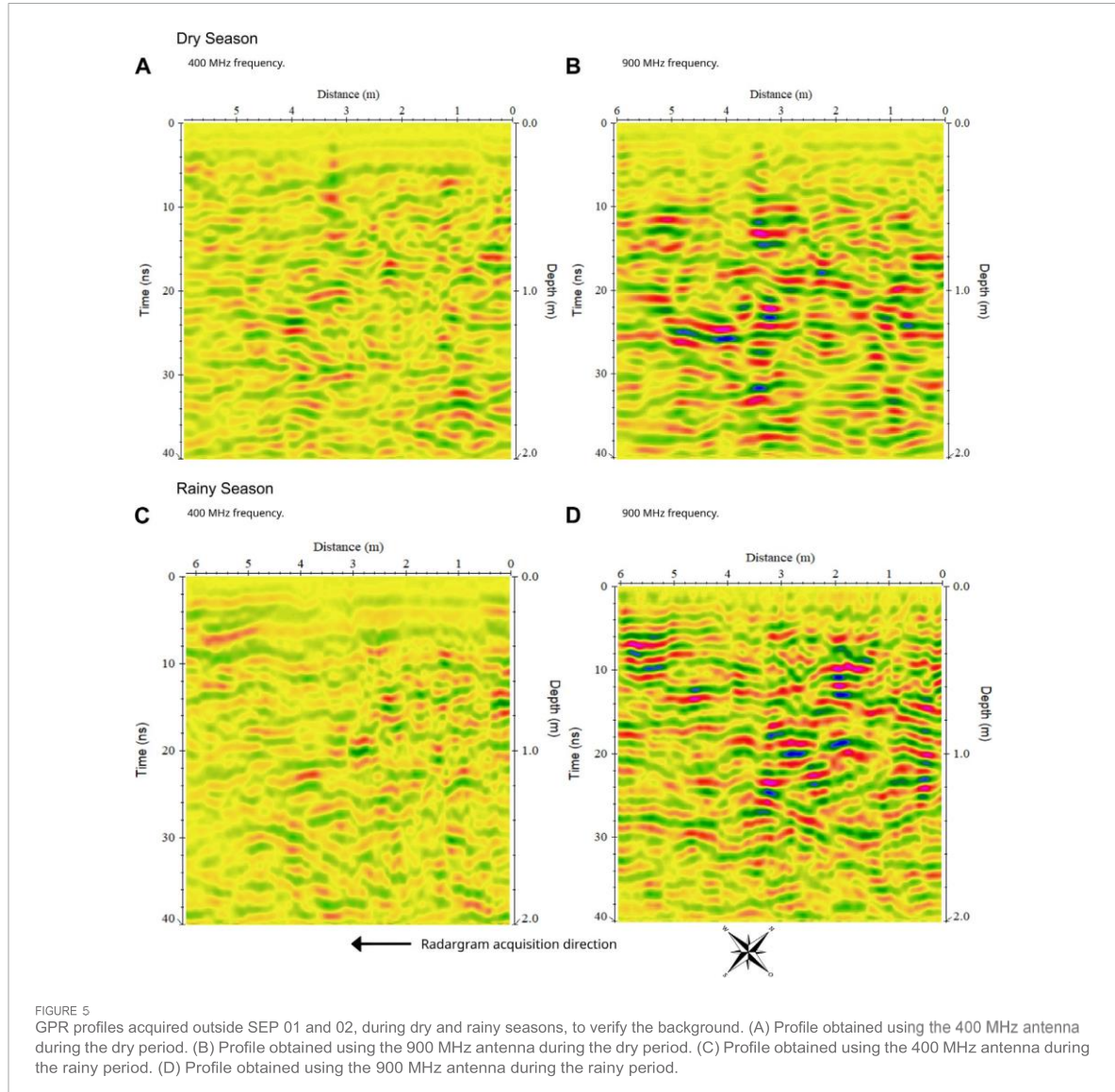


FIGURE 5
GPR profiles acquired outside SEP 01 and 02, during dry and rainy seasons, to verify the background. (A) Profile obtained using the 400 MHz antenna during the dry period. (B) Profile obtained using the 900 MHz antenna during the dry period. (C) Profile obtained using the 400 MHz antenna during the rainy period. (D) Profile obtained using the 900 MHz antenna during the rainy period.

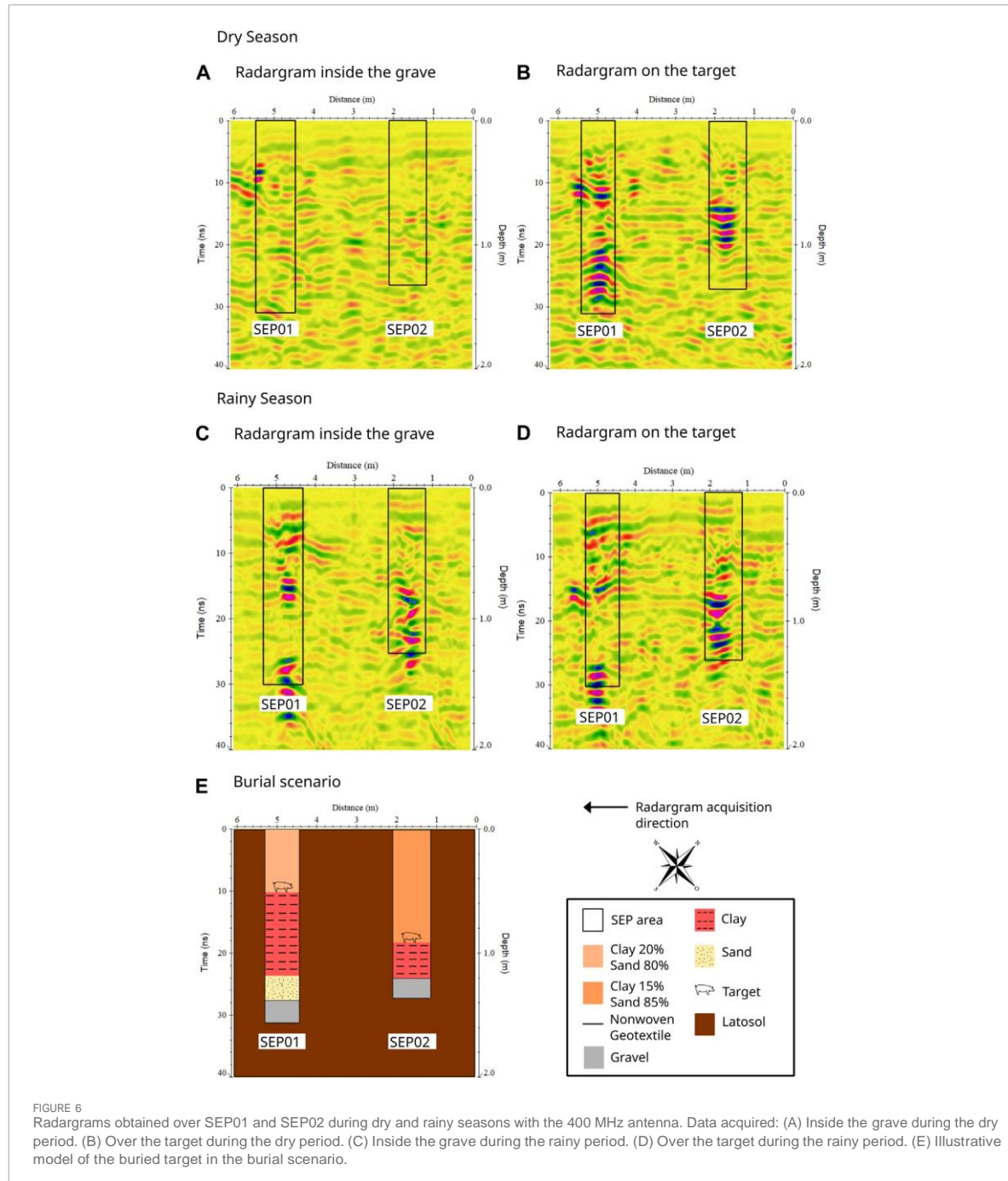
3.2 2D parallel profiles

In this method, the radargrams are acquired parallel to the axis of the buried target. This means that the electromagnetic waves travel along the length of the target. This approach is useful for mapping the layers of the soil in depth and assessing the composition and distribution of the soil along the profile. Parallel radargrams offer a vertical view of the target, which can aid in assessing its depth and internal structure. We chose to use 2D parallel radargrams to interpret the targets' data below and over the pig carcass's abdominal region due to its wider dimension.

Figures 6A–D depict radargrams obtained over SEP01 and SEP02, captured with a 400 MHz frequency during both the dry and rainy periods. Figure 6A shows the radargram obtained

inside the grave during the dry season, excluding the buried pig's location. In SEP01, disordered reflectors were observed, primarily corresponding to the layer of clayey material, as evidenced by a comparison with the burial scenario (Figure 6E). In Figure 6B, which was obtained during the dry season, well-defined hyperbolas indicate the targets' depths, particularly in SEP01, where the clayey material is visible below the target, followed by a layer of sand. SEP02 also exhibits distinct layers, with the top of the target and the layer of clayey material being evident.

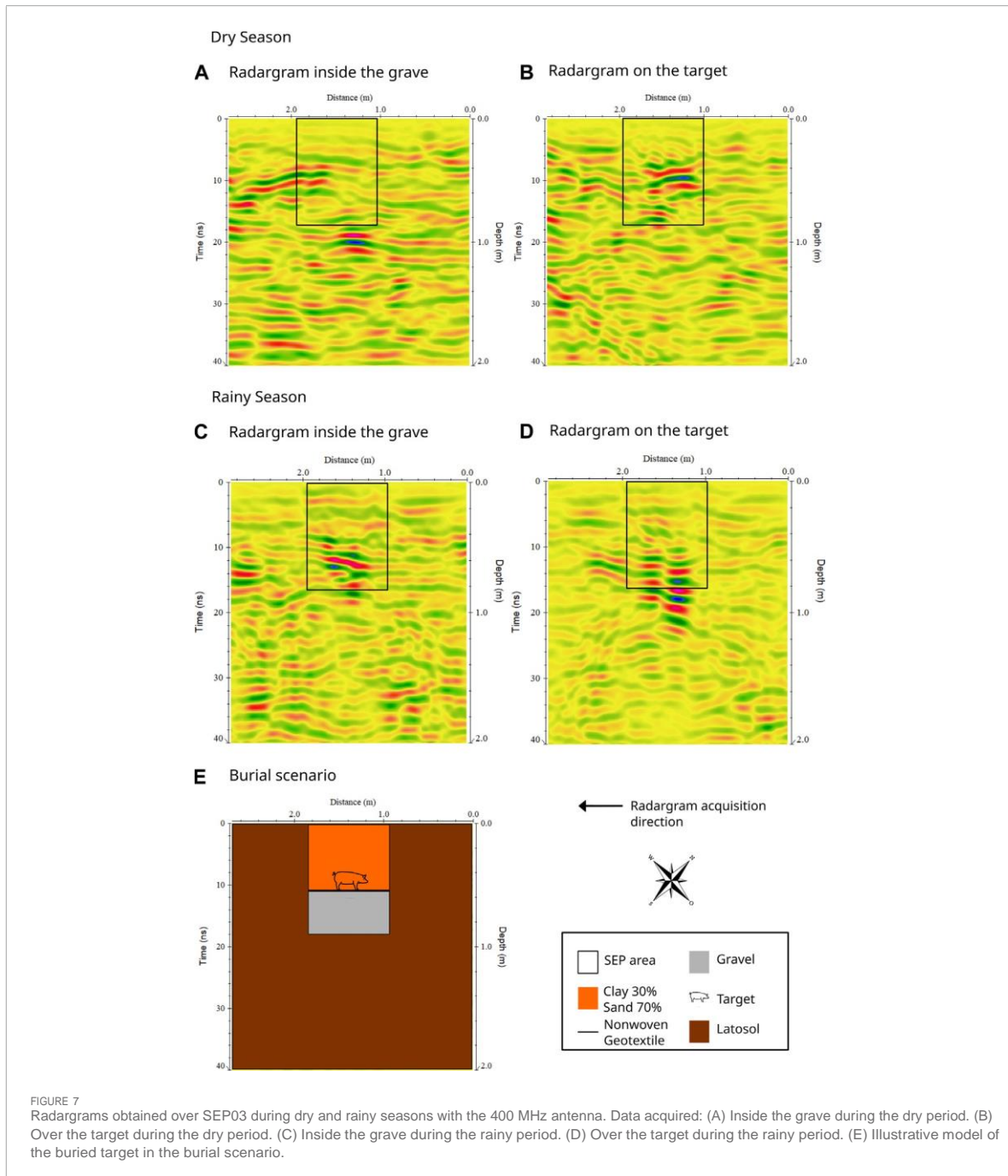
Figure 6C presents the radargram inside the grave during the rainy season, again without the buried pig; it shows disordered hyperbolas, especially in SEP02, indicating the end of the sand-clay mixture layer and the presence of the clayey



layer. Figure 6D displays the radargram over the buried targets during the rainy season, revealing moderate-to high-amplitude hyperbolas, which are particularly clear at the depths corresponding to SEP02.

Figures 7A–D depict radargrams captured over SEP03 with a 400 MHz frequency during the dry and rainy periods. Figure 7A

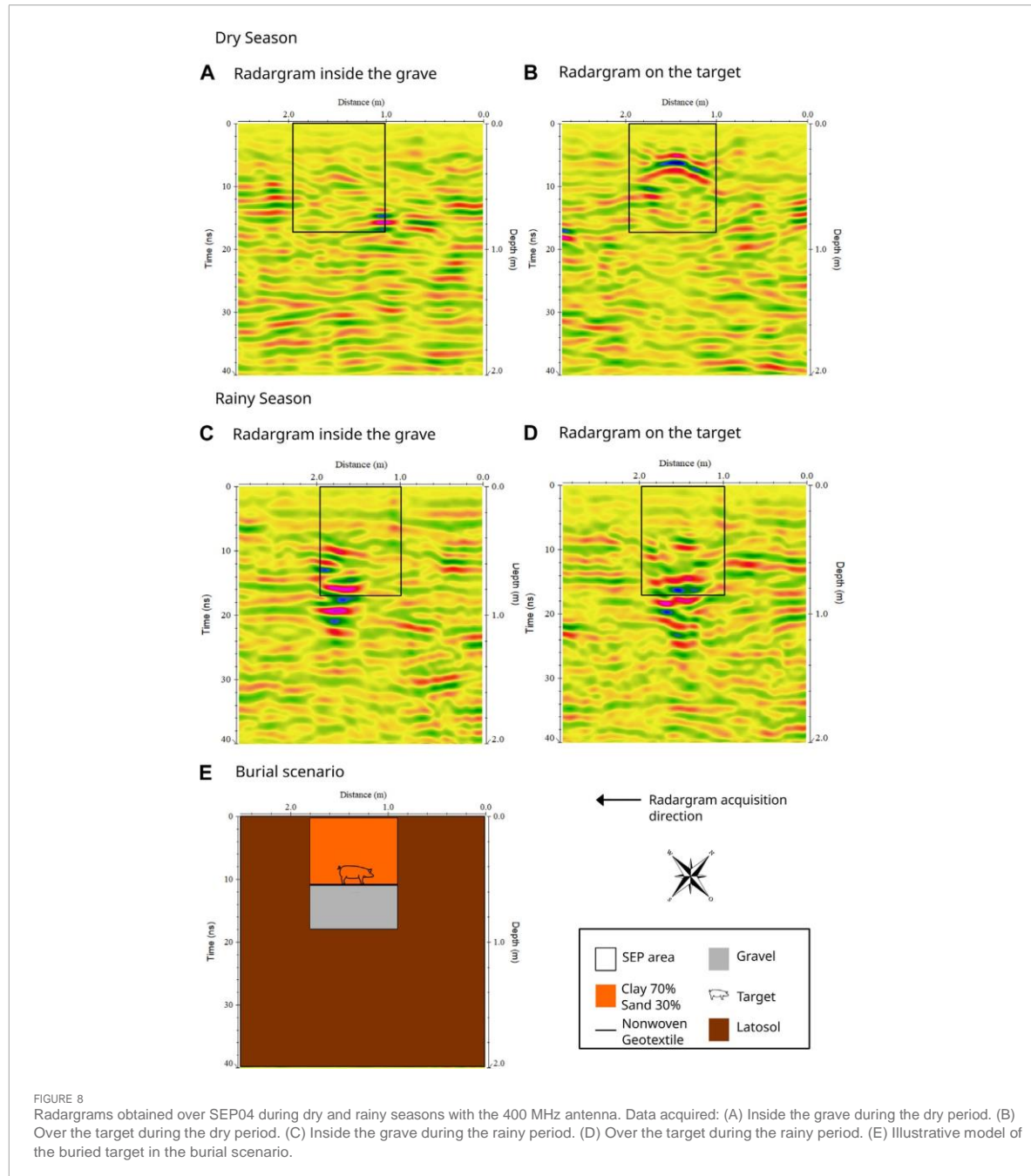
displays the radargram inside the grave during the dry season, again excluding the buried pig's location, revealing reflectors corresponding to the sand-clay mixture and gravel layers. In Figure 7B, which displays the radargram over the buried target during the dry season, a clear hyperbola indicates the target's depth. Figure 7C shows the radargram inside the grave during the rainy



season, indicating signal attenuation and reflectors corresponding to the sand-clay mixture layer. In Figure 7D, which shows the radargram over the buried target during the rainy season, a single anomalous hyperbola corresponds to the sand-clay mixture layer.

Figures 8A–D exhibit radargrams over SEP04 captured with a 400 MHz frequency during the dry and rainy periods. Figure 8A displays the radargram inside the grave during the dry season, where

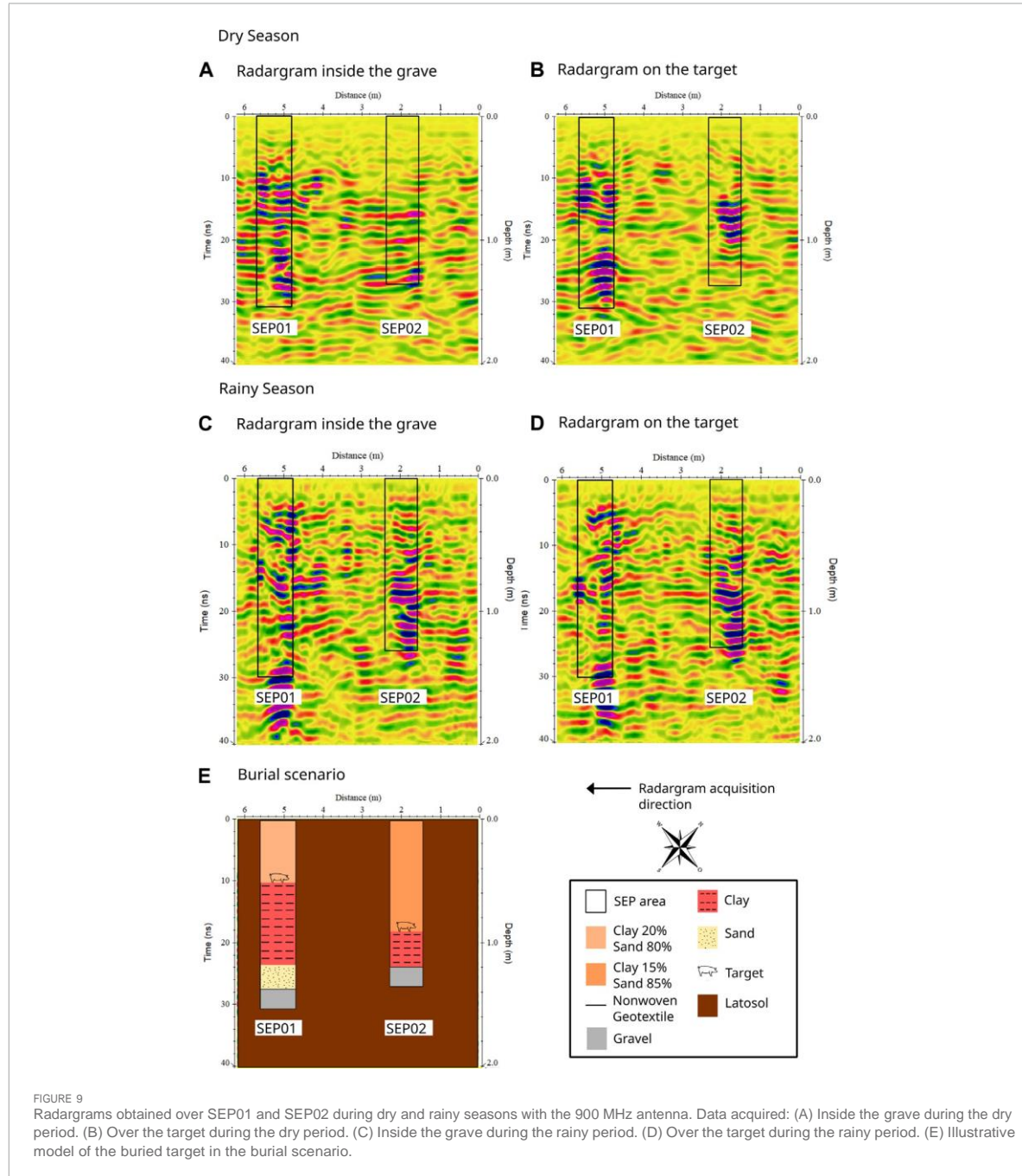
no notable anomalies are observed. Figure 8B shows the radargram over the buried target during the dry season, revealing the target's hyperbola. In Figure 8C, inside the grave during the rainy season, a medium-to high-amplitude hyperbola corresponds to the sand-clay mixture and gravel layers. Figure 8D displays the radargram over the buried target during the rainy season, indicating signal attenuation and hyperbolas corresponding to the target's position.



Figures 9A–D present radargrams over SEP01 and SEP02 captured with a 900 MHz frequency during dry and rainy periods. Figure 9A shows the radargram inside the grave during the dry season, revealing reflections from all the layers observed in the burial scenario. Figure 9B displays the radargram over the buried targets during the dry season, indicating hyperbolas corresponding to the targets. Figures 9C, D show radargrams during the rainy

season; they exhibit reflections from all layers observed in the burial scenario, with Figure 8D indicating hyperbolas corresponding to the targets.

Figures 10A–D present radargrams over SEP03 using a 900 MHz frequency during the dry and rainy periods, with Figure 10A showing the radargram inside the grave during the dry season, indicating a reflection corresponding to the PVC pipe.



Figures 10B,D display radargrams over the buried target during both dry and rainy seasons; they indicate hyperbolas corresponding to the targets.

Figures 11A–D show radargrams over SEP04 using a 900 MHz frequency during the dry and rainy periods, with **Figure 11A** revealing a reflection corresponding to the gravel layer during the dry season. **Figures 11B,D** display radargrams over the buried target during both the dry and

rainy seasons; they indicate hyperbolas corresponding to the targets.

3.3 2D transversal profiles

In this method, the radargrams are acquired perpendicular to the axis of the buried target. This means that the electromagnetic

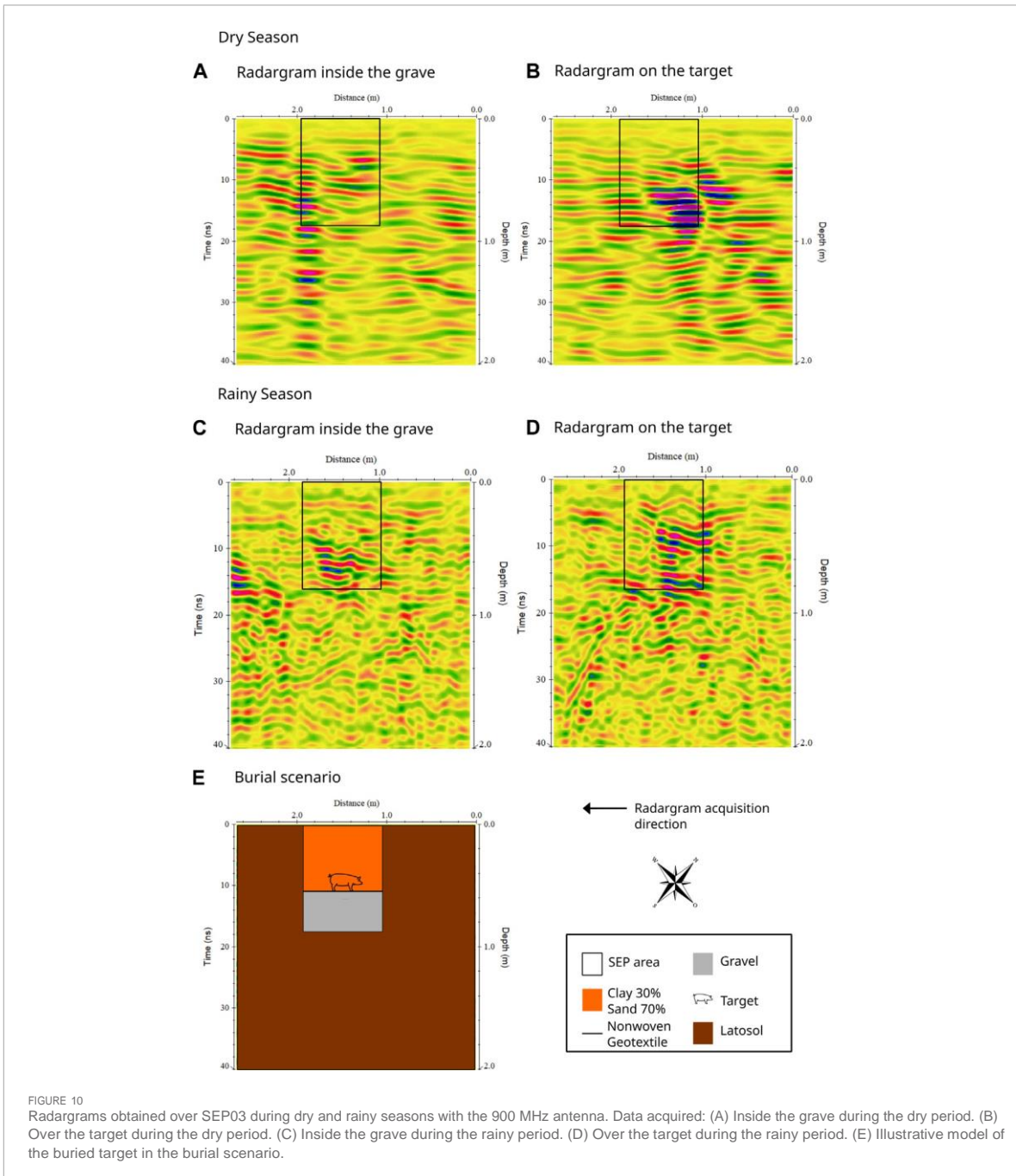


FIGURE 10
Radargrams obtained over SEP03 during dry and rainy seasons with the 900 MHz antenna. Data acquired: (A) Inside the grave during the dry period. (B) Over the target during the dry period. (C) Inside the grave during the rainy period. (D) Over the target during the rainy period. (E) Illustrative model of the buried target in the burial scenario.

waves travel from one side of the target to the other. This type of acquisition is useful for detecting abrupt changes in subsurface properties, such as interfaces between different layers or the presence of buried objects, such as a tomb or a buried box. Transverse radargrams offer a lateral view of the target, which can aid in assessing its shape and lateral extent.

In Figures 12A–I, radargrams transversely obtained over SEP01 to SEP04 and their respective burial scenario models are presented; they were acquired by utilizing a 400 MHz frequency during both the dry and rainy periods.

Figure 12A depicts a GPR profile over SEP01 during the dry season, revealing heterogeneous reflectors within the grave and a less prominent hyperbola representing the target. Figure 12B

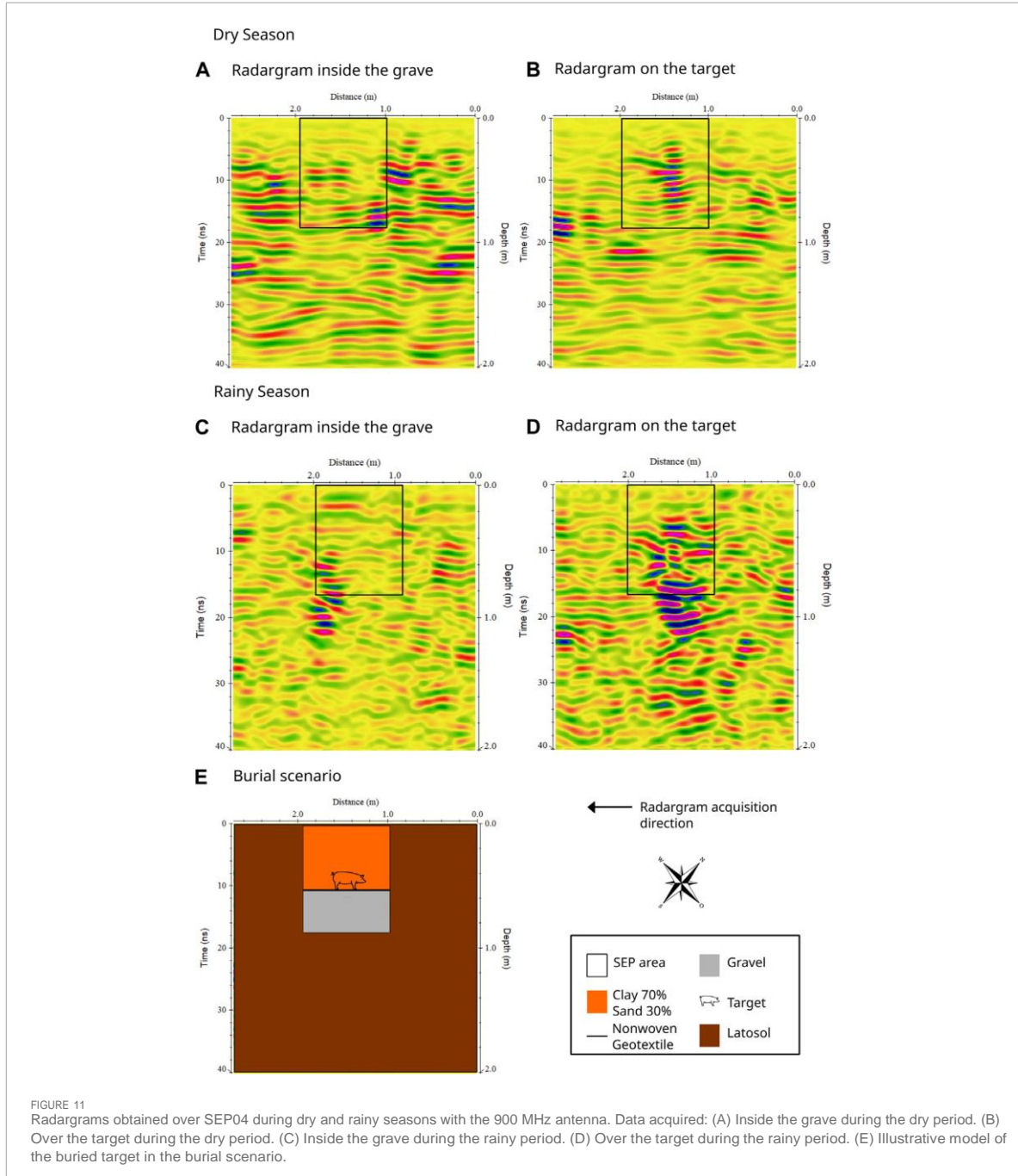


FIGURE 11

Radargrams obtained over SEP04 during dry and rainy seasons with the 900 MHz antenna. Data acquired: (A) Inside the grave during the dry period. (B) Over the target during the dry period. (C) Inside the grave during the rainy period. (D) Over the target during the rainy period. (E) Illustrative model of the buried target in the burial scenario.

shows a GPR profile over SEP01 during the rainy season, with distinct hyperbolas indicating soil layers and the target's position. Figure 12D presents a GPR profile taken transversely over SEP02 during the dry season, showing reflections suggesting the target's presence and layer interfaces. In contrast, Figure 12E displays a GPR profile over SEP02 during the rainy season, highlighting hyperbolas corresponding to different soil layers and the target's position.

In Figures 12G, H, GPR profiles taken transversely over SEP03 and SEP04 during both the dry and rainy seasons are depicted. Reflectors corresponding to gravel layers and targets are visible, with notable differences in the signal strength and attenuation between seasons.

In Figures 13A–I, GPR profiles conducted transversely over SEP01 to SEP04 and their respective burial scenario models are

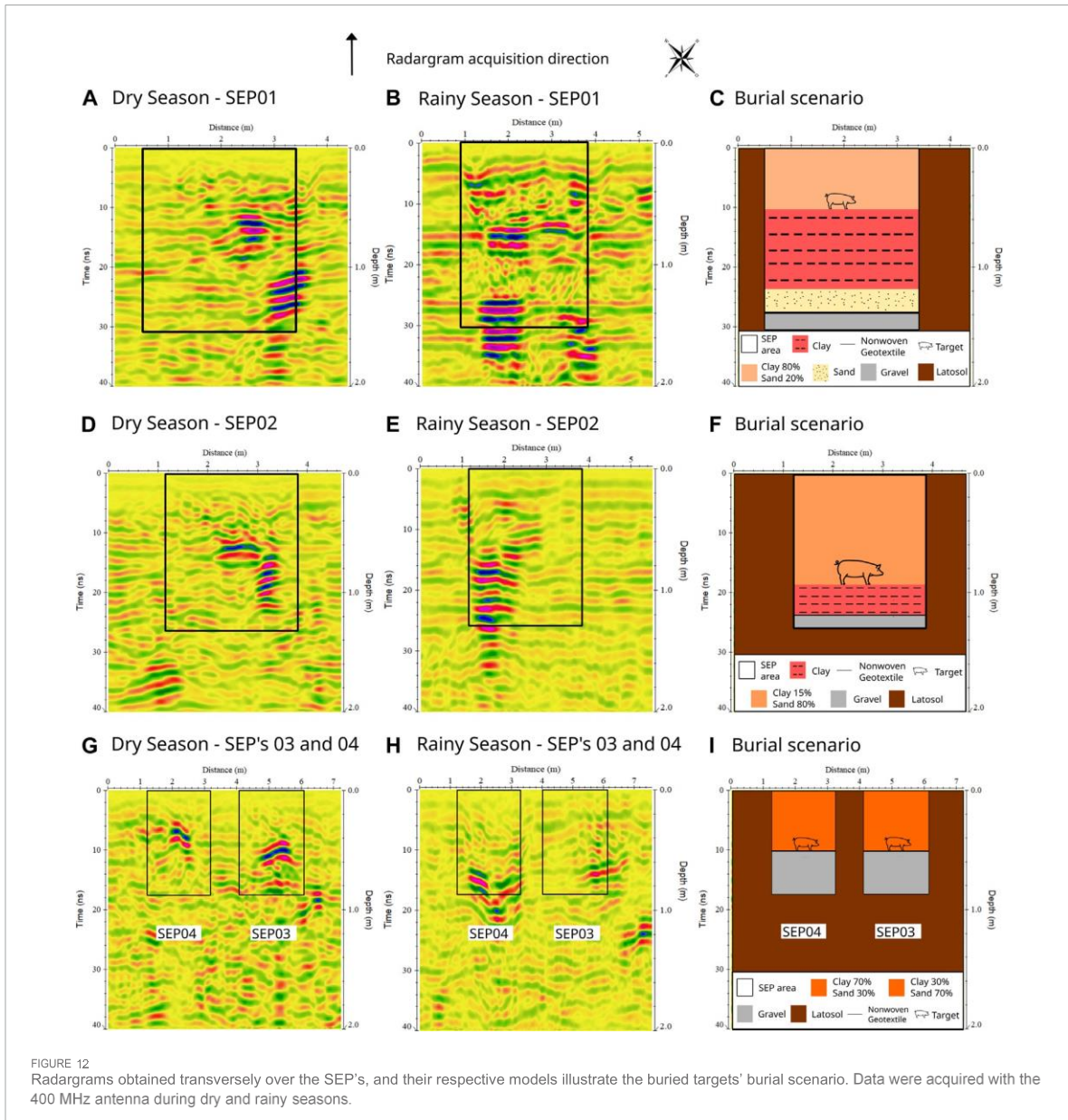


FIGURE 12
Radargrams obtained transversely over the SEP's, and their respective models illustrate the buried targets' burial scenario. Data were acquired with the 400 MHz antenna during dry and rainy seasons.

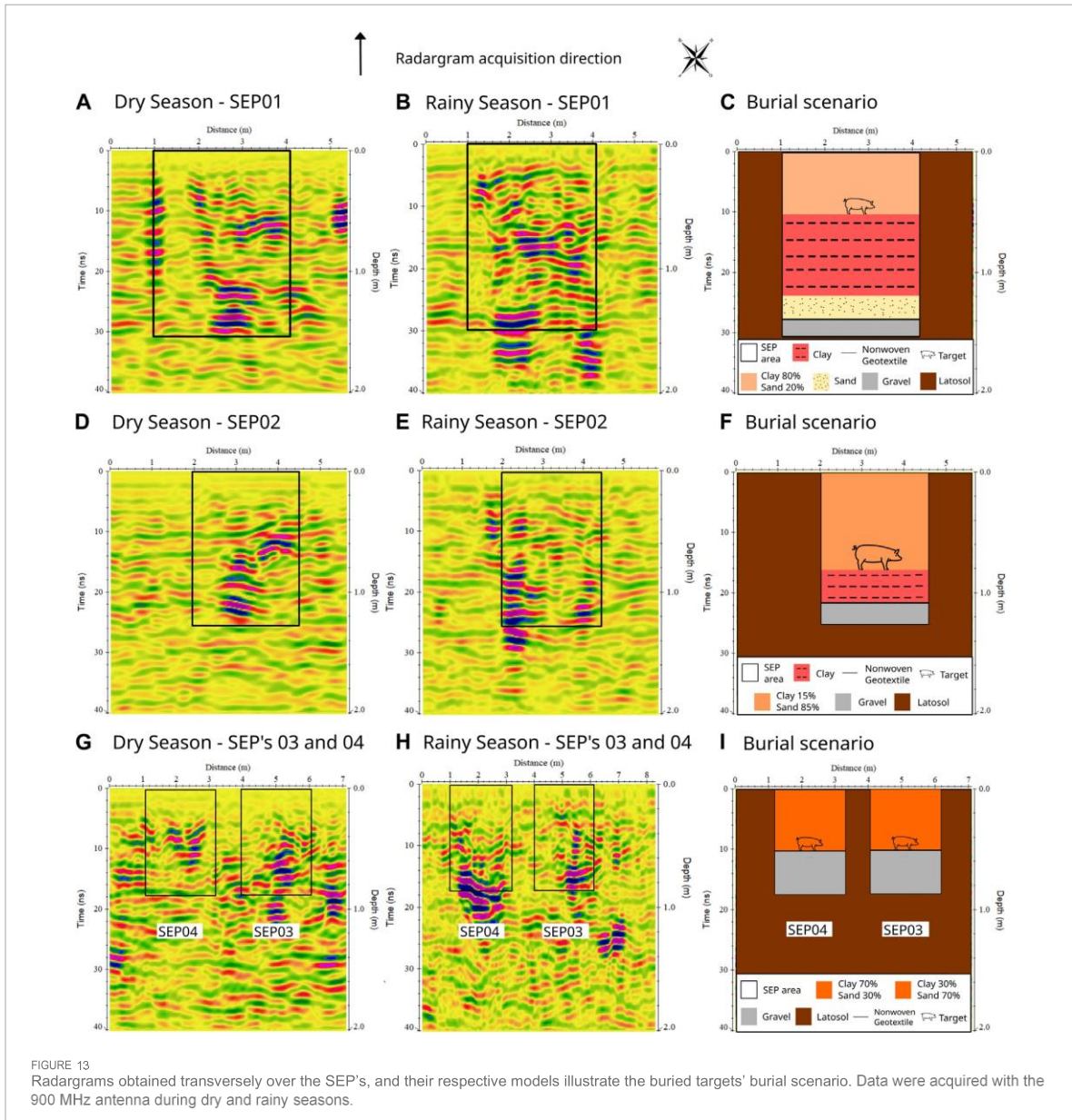
presented; they were acquired by utilizing a 900 MHz frequency during both the dry and rainy periods.

Figure 13A displays a GPR profile over SEP01 during the dry season; it shows various reflections and the absence of a signal at the grave's beginning. Figure 13B shows a GPR profile over SEP01 during the rainy season; it indicates signal attenuation near the target's position. Figure 13D presents a GPR profile taken transversely over SEP02 during the dry season, highlighting reflections indicating the target's position and soil layer interfaces. In contrast, Figure 13E displays a GPR profile over SEP02 during the rainy season; it shows hyperbolas corresponding to different soil

layers and the target's position. In Figures 13G, H, transverse GPR profiles over SEP03 and SEP04 during both the dry and rainy seasons are depicted; they show reflectors corresponding to gravel layers and targets, with variations in the signal strength and attenuation between seasons.

3.4 Block Diagram—Pseudo-3D acquisition

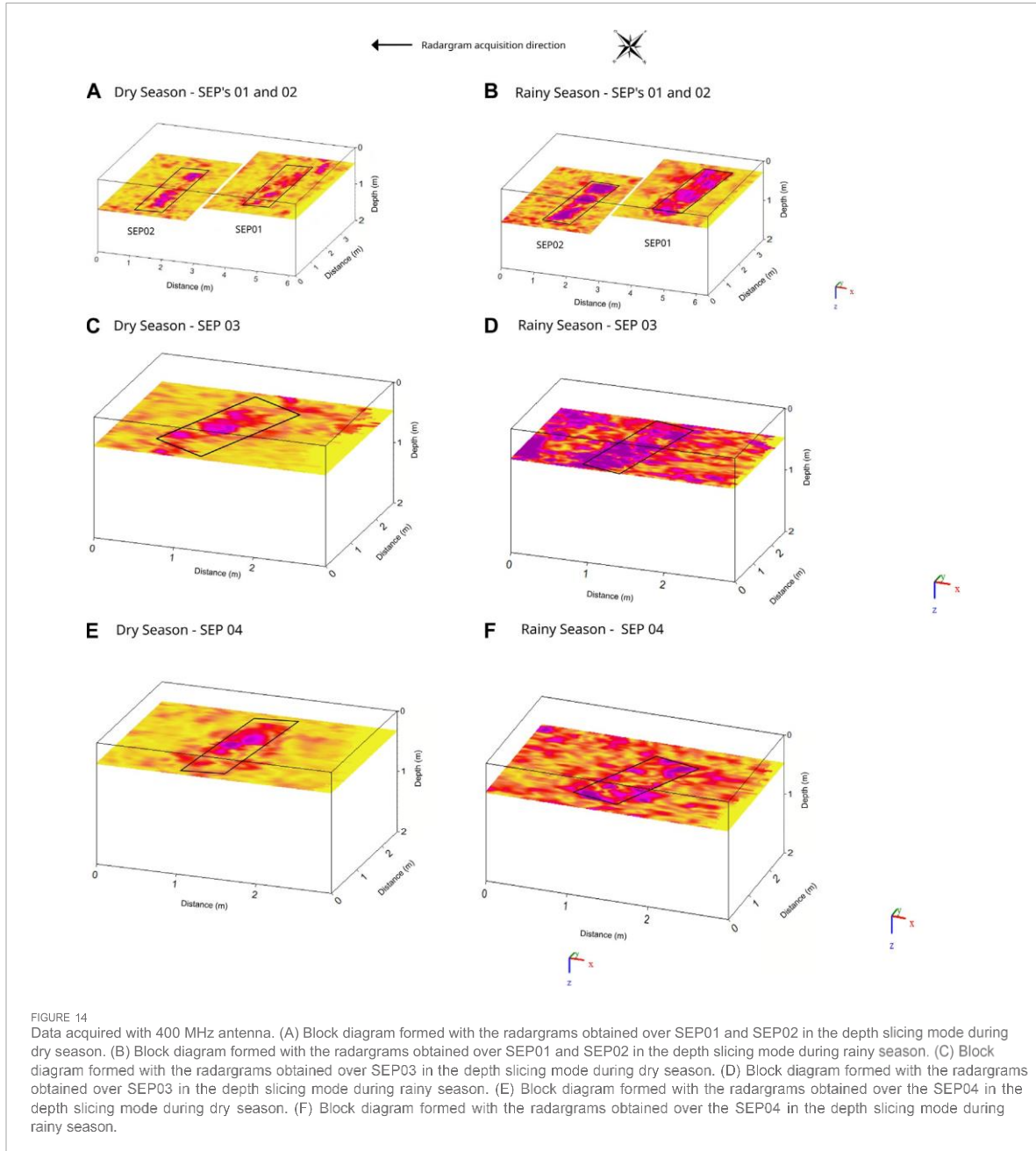
In Figures 14A-F, the depth-sliced diagram blocks from the GPR profile radargrams conducted on SEPs with a 400 MHz



frequency are presented for the dry and rainy periods, respectively; Figures 15A–F present the same data but with a 900 MHz frequency. The depth slicing for SEP01 (Figures 14A,B; Figures 15A,B) was performed at 0.5 m, while for SEP02, it was performed at 0.9 m. Black rectangles outline the burials, and the targets exhibit medium to high amplitudes. The depth slicing for SEP03 was at a depth of 0.5 m, and the black rectangle outlines the interment (Figures 14C, D; Figures 15C, D). The buried target exhibits medium to high amplitudes, with a notable shift in fluid migration observed in the depth slices. The depth slicing for SEP04 was at a depth of 0.5 m, with the buried target exhibiting medium to high amplitudes (Figures 14C, D; Figures 15C, D). A distinct

downward displacement due to fluid migration is observed in these depth slices.

We observed a remarkable migration of fluids in the direction of the gravitational force, leading to a consequential alteration in the position of the anomaly relative to the target. We observed this phenomenon better in in-depth slices, where a downward displacement of a few centimeters occurred. The displacement is more distinctly observable in the depth slices acquired with the 400 MHz antenna. In the depth slices observed in Figures 14C, D, this displacement occurred at depths of 0.47–0.50 m, while in Figures 14E, F, we observed this displacement in the depth range of 0.32–0.46 m.

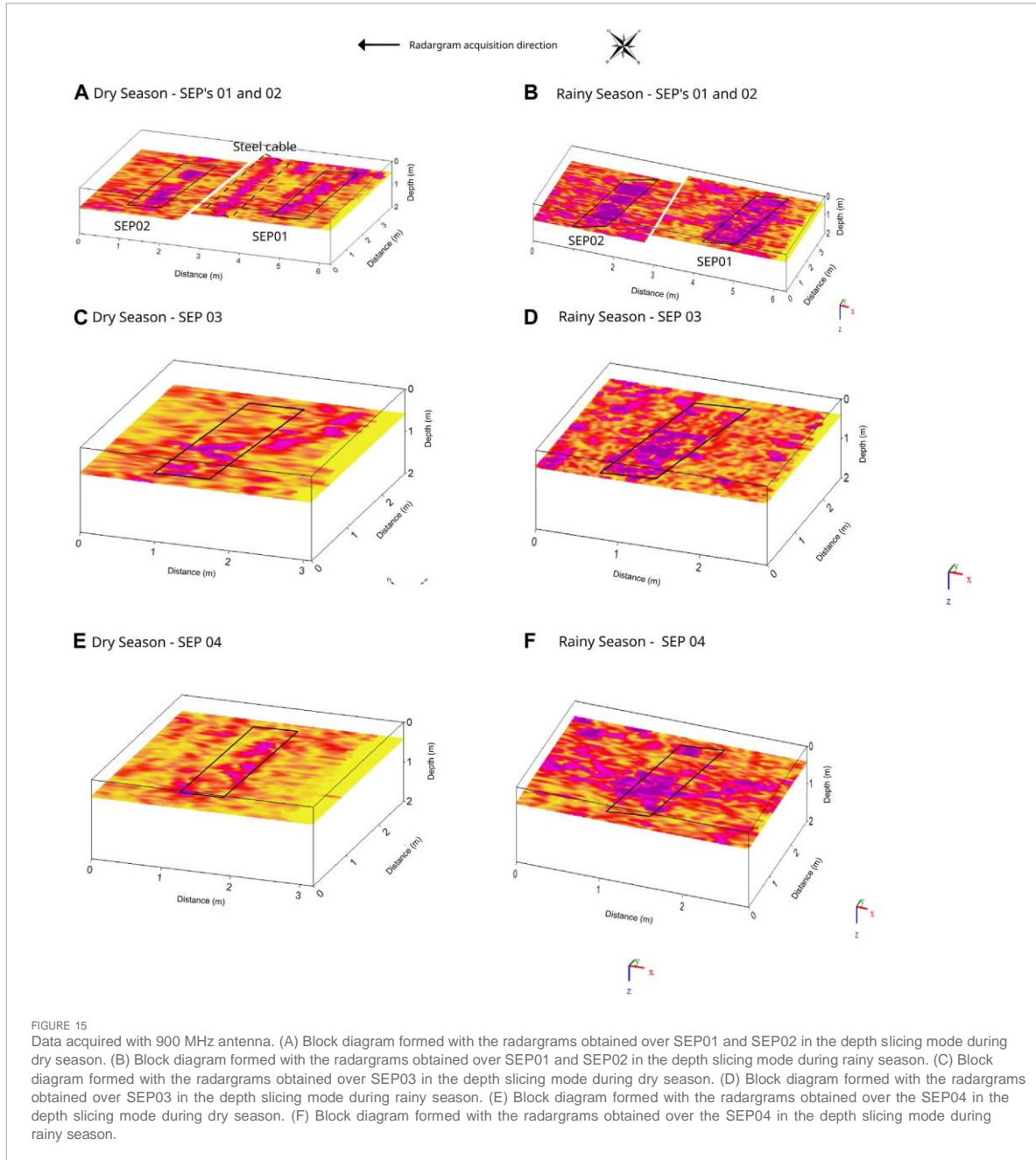


4 Discussion

With information about the actual positions of buried targets, it is possible to determine their locations when interpreting the radargrams obtained. Furthermore, it is possible to accurately assess the ideal frequency, grave composition, and season (dry or rainy) for identifying buried forensic targets with more precision.

4.1 Dry season

In Figure 6B (SEP02), 8b, 9b (SEP02), 11b, 12d–g (SEP04), and 13d–g (SEP04), we observed the attenuation of the GPR signal after the target reflection, varying according to the size of the targets and the filling mixture of the graves, as shown in Table 1. In SEP02 and SEP04, these targets have larger dimensions. In SEP04, the



concentration of clayey material is higher than in the other SEPs, causing a more significant attenuation of the GPR signal, which is visible, for example, starting at 25 ns in [Figure 9B](#) (SEP02) and 15 ns in [Figure 12G](#) (SEP04).

We observed indicators of the presence of disturbed soil in areas corresponding to the grave by comparing the radargrams of GPR profiles executed outside the grave and over the targets. As seen in the radargrams presented in the results, the 400 MHz frequency provides a better identification of the disturbed soil, which is visible,

for example, in [Figure 12D](#) from 1.2 m to 3.8 m and [Figure 6B](#) from 1.0 m to 2.0 m.

The best reflection results obtained with the 2D GPR profile radargrams conducted parallel to the targeted areas were observed in SEP01 and SEP02. These sites, characterized by a lower proportion of clayey material, exhibit minimal attenuation of the GPR signal, resulting in optimal detection outcomes. Remarkably, these outcomes were consistently achieved across both the 400 MHz and 900 MHz frequencies.

Regarding the sand-clay composition within the burial sites and the parallel 2D GPR profile radargrams, the second-best outcomes were observed in SEP04 at both frequency ranges. Despite presenting the second-highest efficacy in target visualization, credit is attributed to the balanced sand (30%) and clay (70%) mixture rather than the target size. This underscores that the presence of clayey material in the soil does not hinder the detection process, especially for larger forensic targets.

Lastly, considering the influence of the sand-clay proportion in detecting the buried target, SEP03, due to the target's dimensions and the texture composition of the grave fill material (Table 1), resulted in an imprecise identification of the pig at both studied frequencies with parallel 2D radargrams. Even the layer of crushed stone did not show a clear reflection.

The best reflection results obtained with the 2D GPR profile radargrams executed transversely over the sought-after targets were observed in SEP01 and SEP02, which exhibit a lower attenuation of the GPR signal due to their composition, which has a lower concentration of clayey material. Consequently, the radargrams provide more detailed subsurface information and indicate the sought-after targets at both the 400 MHz and 900 MHz frequencies.

SEP03 showed the second-best result in terms of the level of detail at both studied frequencies, making it possible to identify the sought-after target and obtain information about the sand and clay proportions in the graves.

Lastly, considering the influence of the texture composition of the grave fill material (Table 1) in detecting the buried target, SEP04 allowed the identification of the pig at both studied frequencies. Nevertheless, the attenuation of the GPR signal hindered the attainment of finer details, thereby impeding the identification of the gravel layer.

4.2 Rainy season

In Figures 6C, D (SEP01), with a frequency of 400 MHz, the attenuation of the electromagnetic wave signal transmitted by the GPR is observed in the layer of clayey material. Conversely, with the 900 MHz antenna, as seen in Figures 9C, D, there is a wealth of details in the graves (SEPs), albeit with diffuse reflections. In SEP02 (Figure 9D), the electromagnetic signal attenuates after the grave ends, unlike in SEP01, where the signal propagates with high-amplitude hyperbolas.

In Figure 8D (SEP03), with the 400 MHz antenna, there are no indications of the presence of a target, which we expected. This response occurs because, as stated in Table 1, the target has small dimensions, and data acquisition during the rainy season was conducted more than 6 months after the pig's burial. Additionally, the signal is heavily attenuated throughout the SEP, displaying low-to medium-amplitude hyperbolas only in the area corresponding to the gravel layer. Figure 11D (SEP03), with the 900 MHz antenna, exhibits diffuse reflections and hyperbolas in the region of the buried target, but they are inconclusive regarding the presence of a buried object.

Signal attenuation in the region corresponding to the target and some reflections appeared in the region corresponding to the gravel layer in SEP04, with the 400 MHz antenna (Figure 8D).

Strong signal attenuation with the 900 MHz antenna was recorded in the grave without the target until the gravel layer was reached (Figure 11C), while reflections appear very diffusely (Figure 11D).

The radargrams obtained transversely over the graves at a frequency of 400 MHz did not highlight the target location in any of the graves (Figures 12B–H), because SEP01 displays highly diffuse reflections (Figure 12B) and SEP02 shows high signal attenuation. The left side of the grave shows hyperbolas with higher amplitude, none of which correspond to the pig's location (Figures 12E). In SEP03 and SEP04, the signal exhibits high attenuation, and clear hyperbolas are only visible in the region corresponding to the gravel layer.

Figures 13B,E, H showcase radargrams captured transversely over the graves using a 900 MHz antenna. In SEP01 (Figure 13B), despite diffuse reflections, detailed layers of the grave are discernible. Conversely, in SEP02 (Figure 13E), significant signal attenuation is evident, with hyperbolas exhibiting lower attenuation visible only along the grave's periphery. Similarly, in SEP03 and SEP04, pronounced signal attenuation is observed around the target's area, accompanied by hyperbolas displaying higher amplitudes within the gravel layer.

The best reflection was obtained with the 2D GPR profiles (400 MHz and 900 MHz frequencies) executed parallel to the sought-after targets in SEP01 and SEP02 due to their composition; they had a lower concentration of clayey material that exhibited less attenuation of the GPR signal. This is in contrast with the 2D GPR profile radargrams executed transversely over the targets at the 400 MHz and 900 MHz frequencies, which provided imprecise results in almost all graves due to the high signal attenuation.

4.3 Dry and rainy seasons

Moist and clay-rich soils generally cause high signal attenuation in GPR (Doolittle and Collins, 1995; Annan, 2004; Linford and Linford, 2004; Schulze, 2005). However, some authors have indicated that the penetration depth is directly related to the clay mineralogy. For instance, Conyers and Connell (2007) demonstrate that kaolinite clay allows electromagnetic energy transmission. In contrast, McDonald et al. (2005) show that montmorillonite clay significantly diminishes most of the radar signal in the subsurface (Barone et al., 2013).

As expected, electromagnetic waves exhibited reduced penetrability during the rainy season due to water absorbing and dispersing a significant amount of energy, as shown in Figures 6, 7. Given that the buried targets were at shallow depths, this characteristic of electromagnetic waves in moist soils was not a hindrance. We also noted that the signal attenuation increased with a higher clay content in the layer mixture.

The 2D GPR profiles conducted parallel to the targets in SEP01 and SEP02 during the rainy period revealed hyperbolas with higher amplitudes and occasionally even greater layer detail at both frequencies. However, the dry season offered more clarity for target visualization in the region where the pig was buried. More imprecision in identifying the position's target occurred in SEP03 during the dry and rainy periods (Figures 7, 10).

We attributed this imprecision to the small dimensions of the target ([Table 1](#)). During the rainy season, SEP03 displayed more detailed layers, although the influence of the PVC pipe observed in the dry season was absent. In SEP04 ([Figures 8, 11](#)), the target was distinctly visible during the dry season, whereas we observed that the signal significantly attenuated in the rainy season. Hyperbolas referring to the target were observable only with the 900 MHz antenna.

In the 2D GPR profiles conducted transversely to the targets during the rainy season at both frequencies ([Figures 12, 13](#)), there was substantial signal attenuation, diffuse reflections due to water molecule absorption and dispersion, reduced clarity in the disturbed soil compared to dry season data, and limited target visibility. In the pseudo-3D block diagrams, it was evident that the burials displayed higher amplitudes during the rainy periods due to the higher dielectric constant of moist soil.

The migration process of decomposition fluids is prominently emphasized in the pseudo-3D acquisition depth slices ([Figures 14C–F](#)). This is relevant for understanding geophysical phenomena associated with clandestinely buried targets. Factors such as the composition of the SEPs or climatic conditions influence the percolation of fluids resulting from decomposition. Additional experiments are required to determine the most influential factors affecting the outcomes of this experiment. It is noteworthy that in SEP04 ([Figures 14E, F](#)), fluid percolation was high compared to SEP03 ([Figures 14C, D](#)); this is potentially explained by the larger dimensions of the buried target ([Table 1](#)).

Upon comparing the dry and rainy seasons, we can conclude that the best results with 2D GPR profiles executed parallel and transversely to the sought targets were achieved during the dry season. During this period, GPR waves produced more evident reflections, facilitating target detection, and there was less absorption or dispersion of energy due to the reduced water content. Unlike the dry season, larger targets did not exhibit better reflections during the rainy season. In the rainy season, the most influential parameter was the proportions of sand and clay material, which had a lesser impact during the dry season.

In summary, transverse radargrams are more suitable for identifying the presence and shape of buried objects, while parallel radargrams are more suitable for mapping subsurface characteristics in depth and assessing the composition of the subsurface along the profile. Both methods can be complementary and used together for a comprehensive assessment of a forensic site of interest.

5 Conclusion

As mentioned, this study aimed to evaluate how the clayey soil content, GPR frequency, and data collected under dry and rainy conditions influence the recognition of forensic targets in a controlled environment designed to simulate human burial evidence. We achieved the objective, as evidenced in the above results and discussions, allowing the visualization of the geophysical response of the GPR method on graves with different sand-clay proportions and varying target dimensions in periods of low and high soil moisture.

After analyzing the obtained results, it is noteworthy that soils with higher moisture and clay content typically lead to significant GPR signal attenuation, as indicated by various studies. However, some research suggests that the penetration depth is directly linked to the clay mineralogy. For instance, while kaolinite allows the transmission of electromagnetic energy, montmorillonite can significantly diminish radar signals in the subsurface.

During the rainy season, we observed a reduction in the penetrability of electromagnetic waves due to water absorption and dispersion, as evidenced in our results. However, since our targets were at shallow depths, this characteristic of electromagnetic waves in moist soils did not pose a significant obstacle. Additionally, we observed that signal attenuation increased with a higher clay content in the soil mixture.

The 2D GPR profiles conducted parallel to the targets in SEP01 and SEP02 during the rainy season revealed hyperbolas with higher amplitudes and occasionally greater layer detail at both frequencies. However, the dry season provided more clarity for target visualization in the region where the pig was buried. In SEP03, during both the dry and rainy seasons, we observed more imprecision in identifying the target's position, attributed to its smaller dimensions.

In the 2D GPR profiles conducted transversely to the targets during the rainy season at both frequencies, there was significant signal attenuation, diffuse reflections due to the absorption and dispersion of water molecules, reduced clarity in the disturbed soil compared to dry season data, and limited target visibility.

The pseudo-3D diagrams highlighted the migration process of decomposition fluids, a crucial aspect for understanding geophysical phenomena associated with clandestinely buried targets. The composition of burial sites and climatic conditions influence the percolation of fluids resulting from decomposition. Further experiments are necessary to determine the most influential factors in the outcomes of this experiment.

Comparing the dry and rainy seasons, we conclude that the best results with 2D GPR profiles executed parallel and transversely to the targets were achieved during the dry season. During this period, GPR waves produced more evident reflections, facilitating target detection, and there was less absorption or dispersion of energy due to the reduced water content. Unlike the dry season, larger targets did not exhibit better reflections during the rainy season. In this season, the most influential parameter was the proportions of sand and clay material, which had less impact during the dry season.

Combining GPR with another geophysical method is recommended to resolve any ambiguities in data interpretation. Other research has already been done with this procedure using electrical tomography and spontaneous potential measurements due to their excellent detection rates, even in clayey soils, and more straightforward data processing compared to GPR.

Data availability statement

The raw data supporting the conclusion of this article will be made available by the authors, without undue reservation.

Ethics statement

The animal study was approved by the Comitê de ética da Universidade de Brasília, Brasil. The study was conducted in accordance with the local legislation and institutional requirements.

Author contributions

KP Castro: Conceptualization, Formal Analysis, Investigation, Methodology, Project administration, Supervision, Validation, Visualization, Writing-original draft. LS: Conceptualization, Investigation, Methodology, Project administration, Supervision, Validation, Visualization, Writing-review and editing. AS: Investigation, Writing-review and editing. PN: Formal Analysis, Investigation, Writing-review and editing. WB: Investigation, Project administration, Supervision, Writing-review and editing.

Funding

The author(s) declare financial support was received for the research, authorship, and/or publication of this article. The authors declare that financial support was received of the CAPES PROAP program, totaling R\$7350.

References

- Abate, D., Colls, S. C., Moyssi, N., Karsili, D., Faka, M., Anilir, A., et al. (2019). Optimizing search strategies in mass grave location through the combination of digital technologies. *Forensic Sci. Int.*, 1, 95–107. doi:10.1016/j.fsisyn.2019.05.002
- ABNT (1989). *Brazilian association of norms techniques. Peneiras para ensaio com telas de tecido metálico. NBR 5734*.
- Almeida, E. R., Porsani, J. L., Catapano, I., Gennarelli, G., and Soldovieri, F. (2014). GPR data analysis enhanced by microwave tomography for forensic archaeology. *Proc. 15th Int. Conf. Ground Penetrating Radar*, 474–478. doi:10.1109/ICGPR.2014.6970470
- Almeida, E. R., Porsani, J. L., Catapano, I., Gennarelli, G., and Soldovieri, F. (2015). Microwave tomography-enhanced GPR in forensic surveys: the case study of a tropical environment. *IEEE J. Sel. Top. Appl. Earth Observations Remote Sens.* 9, 115–124. doi:10.1109/jstars.2015.2466556
- Annan, A. P. (2004). Ground penetrating radar: principles, procedures and applications. *Sensors Softw. Inc.* Technical paper.
- Aziz, A. S., Stewart, R., Green, S., and Flores, J. (2016). Locating and characterizing burials using 3D ground-penetrating radar (GPR) and terrestrial laser scanning (TLS) at the historic Mueschke Cemetery, Houston, Texas. *J. Archaeol. Sci. Rep.* 8, 392–405. doi:10.1016/j.jasrep.2016.06.035
- Barone, P. M., and Di Maggio, R. M. (2019). Forensic geophysics: ground penetrating radar (GPR) techniques and missing persons investigations. *Forensic Sci. Res.* 4, 337–340. doi:10.1080/20961790.2019.1675353
- Barone, P. M., Matsentidi, D., Mollard, A., Kulengowska, N., and Mistry, M. (2022). Mapping decomposition: a preliminary study of non-destructive detection of simulated body fluids in the shallow subsurface. *Forensic Sci.* 2, 620–634. doi:10.3390/forensicsci2040046
- Barone, P. M., Mattei, E., and Pettinelli, E. (2013). Non-invasive archaeological exploration in stratigraphically complex rural settings: an example from Ferento (Viterbo, Italy). *Archaeol. Anthropol. Sci.* 5, 267–273. doi:10.1007/s12520-013-0138-3
- Berezowski, V., Mallett, X., Ellis, J., and Moffat, I. (2021). Using ground penetrating radar and resistivity methods to locate unmarked graves: a review. *Remote Sens.* 13, 2880. doi:10.3390/rs13152880
- Booth, A. D., and Pringle, J. K. (2016). Semblance analysis to assess GPR data from a five-year forensic study of simulated clandestine graves. *J. Appl. Geophys.* 125, 37–44. doi:10.1016/j.jappgeo.2015.11.016
- Castro, K. C. P. L. (2021). *Aplicação de Ground Penetrating Radar (GPR) para Identificação de Evidências Forenses no Sítio Controlado Fazenda Água Limpa/Universidade de Brasília - DF. 100pp. Trabalho de Conclusão de Curso (Bacharelado em Geofísica) – Universidade de Brasília - UnB*. Brasil: Brasília.
- Castro, K. C. P. L., and Cunha, L. S. (2021). Forensic investigations with the identification of human remains with ground penetrating radar (GPR): a review. *Estud. Geol.* 31 (2), 64–86. doi:10.51359/1980-8208/estudosgeologicos.v31n2p64-86
- Caivalcanti, M. M. (2017). *Estudo da Resposta Geofísica em Diferentes Cenários de Sepultamento*. Brazil: Ph. D. Thesis. University of Brasília - IG. Brasília, 197.
- Caivalcanti, M. M., Rocha, M. P., Blum, M. L. B., and Borges, W. R. (2018). The forensic geophysical controlled research site of the University of Brasília, Brazil: results from methods GPR and electrical resistivity tomography. *Forensic Sci. Int.* 293, 101.e1–101.e21. doi:10.1016/j.forsciint.2018.09.033
- Conyers, L. B., and Connell, S. (2007). “An analysis of ground-penetrating radar’s ability to discover and map buried archaeological sites in Hawaii,” in *Hawaiian archaeology*. Editors M. Desilets, and M. T. Carson 11th edn. (Honolulu, ISSN: Society for Hawaiian Archaeology).
- Dick, H. C., and Pringle, J. K. (2018). Inorganic elemental analysis of decomposing fluids of an *in situ* animal burial. *Forensic Sci. Int.* 289, 130–139. doi:10.1016/j.forsciint.2018.05.034
- Doolittle, J. A., and Collins, M. E. (1995). Use of soil information to determine application of ground penetrating radar. *J. Appl. Geophys.* 33, 101–108. doi:10.1016/0926-9851(94)00031-i
- Gomes, M. P., Vital, H., and Macedo, J. W. P. (2011). Fluxo de Processamento aplicado a dados de Sísmica de Alta resolução em ambiente de Plataforma continental. Exemplo: Macau-m. *Rev. Bras. Geofísica* 29 (1), 173–186. doi:10.1590/s0102-261x2011000100012
- González-Jorge, H., Solla, M., Martínez-Sánchez, J., and Arias, P. (2012). Comparison between laser scanning, single-image rectification and ground-penetrating radar technologies in forensic science. *Measurement* 45, 836–843. doi:10.1016/j.measurement.2012.02.013
- Hansen, J. D., and Pringle, J. K. (2013). Comparison of magnetic, electrical and ground penetrating radar surveys to detect buried forensic objects in semi-urban and domestic patio environments. *Geol. Soc. Lond. Spec. Publ.* 384, 229–251. doi:10.1144/sp384.13
- Lester, J., and Bernold, L. E. (2006). Innovative process to characterize buried utilities using Ground Penetrating Radar. *Automation Constr.* 16, 546–555. doi:10.1016/j.autcon.2006.09.004

Acknowledgments

The authors thank all the employees of Fazenda Água Limpa (FAL)/UnB for their work on this project. The authors thank the Geosciences Institute/UnB for their support. The authors thank Hartos Agropecuária Cenci for donating the pig carcasses.

Conflict of interest

The authors declare that the research was conducted in the absence of any commercial or financial relationships that could be construed as a potential conflict of interest.

Publisher's note

All claims expressed in this article are solely those of the authors and do not necessarily represent those of their affiliated organizations, or those of the publisher, the editors and the reviewers. Any product that may be evaluated in this article, or claim that may be made by its manufacturer, is not guaranteed or endorsed by the publisher.

- Linford, N., and Linford, P. (2004). Ground penetrating radar survey over a roman building at groundwell ridge, blunsdon st andrew, swindon, UK. *Archaeol. Prospect* 11, 49–55. doi:10.1002/arp.220
- Lowe, A., Beresford, D., Carter, D., Gaspari, F., O'brien, R., and Forbes, S. (2013). Ground penetrating radar use in three contrasting soil textures in southern Ontario. *Geol. Soc. Lond. Spec. Publ.* 384, 221–228. doi:10.1144/sp384.12
- McDonald, L. M., Evangelou, V. P., and Chappel, M. A. (2005). “Cation exchange,” in *Encyclopedia of soils in the environment*. Editor H. Daniel (Amsterdam: Elsevier Academic Press), Vol. 1, 180–188.
- Molina, C. M., Pringle, J. K., Saumett, M., and Evans, G. T. (2016a). Geophysical and botanical monitoring of simulated graves in a tropical rainforest, Colombia, South America. *J. Appl. Geophys.* 135, 232–242. doi:10.1016/j.jappgeo.2016.10.002
- Molina, C. M., Pringle, J. K., Saumett, M., and Evans, G. T. (2016b). Geophysical monitoring of simulated graves with resistivity, magnetic susceptibility, conductivity and GPR in Colombia, South America. *Forensic Sci. Int.* 261, 106–115. doi:10.1016/j.forsciint.2016.02.009
- Molina, C. M., Pringle, J. K., Saumett, M., and Hernández, O. (2015). Preliminary results of sequential monitoring of simulated clandestine graves in Colombia, South America, using ground penetrating radar and botany. *Forensic Sci. Int.* 248, 61–70. doi:10.1016/j.forsciint.2014.12.011
- Olhoeft, G. R. (2000). Maximizing the information return from ground penetrating radar. *J. Appl. Geophys.* 43, 175–187. doi:10.1016/S0926-9851(99)00057-9
- Parker, R., Ruffell, A., Hughes, D., and Pringle, J. K. (2010). Geophysics and the search of freshwater bodies: a review. *Sci. Justice* 50, 141–149. doi:10.1016/j.scijus.2009.09.001
- Powell, K. (2004). Detecting buried human remains using near-surface geophysical instruments. *Explor. Geophys.* 35, 88–92. doi:10.1071/eg04088
- Pringle, J. K., Jervis, J. R., Roberts, D., Dick, H. C., Wisniewski, K. C., Cassidy, N. J., et al. (2016). Long-term geophysical monitoring of simulated clandestine graves using electrical and ground penetrating radar methods: 4–6 Years after burial. *J. Forensic Sci.* 61, 309–321. doi:10.1111/1556-4029.13009
- Pringle, J. K., Stimpson, I. G., Wisniewski, K. C., Heaton, V., Davenward, B., Mirosch, N., et al. (2020). Geophysical monitoring of simulated homicide burials for forensic investigations. *Sci. Rep.* 10, 7544. doi:10.1038/s41598-020-64262-3
- Rubio-Melendi, D., Gonzalez-Quirós, A., Roberts, D., García, M. C. G., Domínguez, A. C., Pringle, J. K., et al. (2018). GPR and ERT detection and characterization of a mass burial, Spanish Civil War, Northern Spain. *Forensic Sci. Int.* 287, e1–e9. doi:10.1016/j.forsciint.2018.03.034
- Ruffell, A., Pringle, J. K., Cassella, J. P., Morgan, R. M., Ferguson, M., Heaton, V., et al. (2017). The use of geoscience methods for aquatic forensic searches. *Earth-Science Rev.* 171, 323–337. doi:10.1016/j.earscirev.2017.04.012
- Sandmeier, K. J. (2014). *REFLEXW Version 7.5. Windows 9x/2000/NT. Program for the processing of seismic, acoustic or electromagnetic reflection, refraction and transmission data*. Karlsruhe, Germany: Manual of Software.
- Schoor, M., Nienaber, W. C., and Marais-Werner, A. (2017). A controlled monitoring study of simulated clandestine graves using 3D ground penetrating radar. *Near Surf. Geophys.* 15, 274–284. doi:10.3997/1873-0604.2017007
- Schultz, J. J. (2008). Sequential monitoring of burials containing small pig cadavers using ground penetrating radar. *J. Forensic Sci.* 53, 279–287. doi:10.1111/j.1556-4029.2008.00665.x
- Schultz, J. J., Collins, M. E., and Falsetti, A. B. (2006). Sequential monitoring of burials containing large pig cadavers using ground-penetrating radar. *J. Forensic Sci.* 51, 607–616. doi:10.1111/j.1556-4029.2006.00129.x
- Schultz, J. J., Falsetti, A. B., Collins, M., Koppenjan, S., and Warren, M. W. (2002). Detection of forensic burials in Florida using GPR. *Ninth Int. Conf. Ground Penetrating Radar* 4758. doi:10.1117/12.462239
- Schultz, J. J., Healy, C., Parker, K., and Lowers, B. (2013). Detecting submerged objects: the application of side scan sonar to forensic contexts. *Forensic Sci. Int.* 231, 306–316. doi:10.1016/j.forsciint.2013.05.032
- Schultz, J. J., and Martin, M. M. (2011). Controlled GPR grave research: comparison of reflection profiles between 500 and 250MHz antennae. *Forensic Sci. Int.* 209, 64–69. doi:10.1016/j.forsciint.2010.12.012
- Schultz, J. J., and Martin, M. M. (2012). Monitoring controlled graves representing common burial scenarios with ground penetrating radar. *J. Appl. Geophys.* 83, 74–89. doi:10.1016/j.jappgeo.2012.05.006
- Schultz, J. J., Walter, B. S., and Healy, C. (2016). Long-term sequential monitoring of controlled graves representing common burial scenarios with ground penetrating radar: years 2 and 3. *J. Appl. Geophys.* 132, 60–74. doi:10.1016/j.jappgeo.2016.06.015
- Schulze, D. G. (2005). “Clay minerals,” in *Encyclopedia of soils in the environment*. Editor H. Daniel (Amsterdam: Elsevier Academic Press), Vol. 1, 246–254.
- Solla, M., Riveiro, B., Álvarez, M. X., and Arias, P. (2012). Experimental forensic scenes for the characterization of ground-penetrating radar wave response. *Forensic Sci. Int.* 220, 50–58. doi:10.1016/j.forsciint.2012.01.025

CAPÍTULO 4 – CONCLUSÕES E CONSIDERAÇÕES FINAIS

Conforme mencionado anteriormente, esta dissertação teve como principal objetivo avaliar a influência do conteúdo de solo argiloso e do teor de umidade na detecção de alvos forenses em um ambiente controlado que simula evidências de sepultamento humano utilizando o GPR. O objetivo foi alcançado através de uma abordagem meticulosa que incluiu a análise dos resultados e discussões nos dois artigos apresentados. Ao longo da investigação, foi possível não apenas atingir o objetivo principal, mas também obter clareza sobre a complexidade envolvida na detecção de sepulturas clandestinas e na interpretação dos dados geofísicos obtidos pelo GPR.

A detecção de sepulturas clandestinas é uma tarefa desafiadora que depende de diversos fatores, incluindo características do local, tipo de solo, estado de decomposição dos materiais sepultados e sazonalidade. Os métodos geofísicos desempenham um papel importante na detecção não destrutiva de alvos enterrados ou ocultos. A natureza não invasiva dos métodos geofísicos é de especial valor na geofísica forense e pode fornecer respostas rápidas em investigações criminais.

É importante notar que os solos com maior teor de umidade e argila geralmente levam a uma atenuação significativa do sinal de GPR, conforme indicado por vários estudos. No entanto, algumas pesquisas sugerem que a profundidade de penetração está diretamente ligada à mineralogia da argila. Por exemplo, enquanto a caulinita permite a transmissão de energia eletromagnética, a montmorilonita pode diminuir significativamente os sinais de radar na subsuperfície.

Durante a estação chuvosa, é observada uma redução na penetrabilidade das ondas eletromagnéticas devido à absorção e dispersão da água, conforme evidenciado nos resultados. No entanto, como os alvos estavam em profundidades rasas, essa característica das ondas eletromagnéticas em solos úmidos não representou um obstáculo significativo. Além disso, foi observado que a atenuação do sinal aumentou com um maior teor de argila na mistura do solo.

Os perfis de GPR 2D conduzidos paralelamente aos alvos nas SEP01 e SEP02 durante a estação chuvosa revelaram hipérboles com amplitudes mais altas e, ocasionalmente, maior detalhamento das camadas em ambas as frequências. No

entanto, a estação seca proporcionou mais clareza para a visualização do alvo na região onde houve o sepultamento. Na SEP03, tanto na estação seca quanto na chuvosa, foi observada maior imprecisão na identificação da posição do alvo, atribuída às suas dimensões menores.

Nos perfis GPR 2D conduzidos transversalmente sobre os alvos durante a estação chuvosa em ambas as frequências, houve atenuação significativa do sinal, reflexões difusas devido à absorção e dispersão das moléculas de água, clareza reduzida no solo perturbado em comparação com os dados da estação seca e visibilidade limitada do alvo.

Os diagramas pseudo-3D destacaram o processo de migração dos fluidos de decomposição, um aspecto fundamental para a compreensão dos fenômenos geofísicos associados a alvos sepultados clandestinamente. A composição dos locais de sepultamento e as condições climáticas influenciam a percolação dos fluidos resultantes da decomposição. São necessários mais experimentos para determinar os fatores mais influentes nos resultados desse experimento.

Comparando as estações seca e chuvosa, conclui-se que os melhores resultados com perfis GPR 2D executados paralela e transversalmente sobre alvos foram obtidos durante a estação seca. Durante esse período, as ondas de GPR produziram reflexões mais evidentes, facilitando a detecção do alvo, e houve uma menor absorção ou dispersão de energia devido a redução do teor de água. Ao contrário da estação seca, os alvos maiores não apresentaram melhores reflexões durante a estação chuvosa. Nessa estação, o parâmetro mais influente foi a proporção do teor de areia e argila, que teve menor impacto durante a estação seca.

A comparação entre diferentes frequências de antenas também revelou características de desempenho distintas. Embora a antena de 400 MHz tenha produzido resultados satisfatórios, fornecendo informações com bom detalhamento das sepulturas e localização de alvos, a antena de 900 MHz ofereceu resolução espacial mais alta sendo capaz de fornecer imagens mais detalhadas das sepulturas. Embora sua penetração seja menor em comparação com a antena de 400MHz, ela ainda pode ser eficaz para detectar alvos em profundidades mais rasas, comumente encontrados em cenas de crime.

Esta dissertação ressaltou a importância do efeito da proporção de material argiloso nas sepulturas, com resultados ótimos observados em SEPs caracterizadas por um menor teor de argila (85% de areia e 15% de material argiloso). Por outro lado, SEPs com maior teor de argila (30% de areia e 70% de material argiloso), como a SEP03, exibiram resultados menos precisos, atribuídos tanto ao tamanho menor do alvo quanto ao aumento da presença de argila.

O uso de todas as técnicas e dispositivos possíveis, embora abrangente, pode ser caro e demorado, uma boa abordagem é usar uma combinação de dois métodos que podem ser úteis em uma possível ambiguidade na interpretação dos dados. Pesquisas com a integração de GPR e suscetibilidade magnética são indicadas quando os alvos incluem pequenos objetos metálicos. A eletrorresistividade é outra técnica complementar com potencial, pois tem um tempo de coleta rápido, boas taxas de detecção e processamento de dados mais simples do que o GPR. Dessa forma recomenda-se a integração do GPR com métodos geofísicos complementares para mitigar ambiguidades na interpretação de dados. Essa abordagem permite uma análise de dados mais abrangente fornecendo informações complementares que ajudam a confirmar e enriquecer as descobertas obtidas com o GPR.

Para otimização de pesquisas futuras é recomendada a aquisição de múltiplos radargramas 2D transversais para facilitar a análise comparativa entre áreas dentro e fora da sepultura, melhorando a precisão da identificação do alvo. Além disso, otimizar o posicionamento de marcadores de referência, como cabos de aço, é fundamental para garantir a integridade dos dados durante a aquisição de dados *quasi-3D*.

Logo, esta dissertação contribui significativamente para o avanço das investigações forenses baseadas em GPR, destacando a importância da análise meticolosa de dados, configurações experimentais controladas e aprimoramentos metodológicos estratégicos para maior detecção de alvos e precisão de interpretação. Ao fornecer detalhamentos sobre os desafios e possibilidades associados à detecção de sepulturas clandestinas, este estudo abre caminho para futuras pesquisas e aplicações práticas no campo da geofísica forense.

CAPÍTULO 5 – REFERÊNCIAS BIBLIOGRÁFICAS

- ABATE, D. et al. 2019. Optimizing search strategies in mass grave location through the combination of digital technologies. *Forensic Science International* 1: 95–107.
- ANNAN, A.P. 2004 Ground penetrating radar: principles, procedures and applications, Sensors & Software Inc. Technical paper
- AZIZ, A.S. et al. 2016 Locating and characterizing burials using 3D ground-penetrating radar (GPR) and terrestrial laser scanning (TLS) at the historic Mueschke Cemetery, Houston, Texas. *Journal of Archaeological Science: Reports* 8: 392–405. DOI: 10.1016/j.jasrep.2016.06.035
- BILLINGER, M.S. 2009. Utilizing Ground Penetrating Radar for the Location of a Potential Human Burial under Concrete. *Canadian Society of Forensic Science Journal* 42: 200–209.
- BORGES, W.R. 2007. Caracterização Geofísica de Alvos Rasos com Aplicações no Planejamento Urbano e Meio Ambiente: Estudo sobre o Sítio Controlado do IAG / USP. Tese de doutorado. Instituto de Astronomia, Geofísica e Ciências Atmosféricas. 260p.
- BÜYÜKSARAÇ, A. et al. 2013. Geophysical investigations at Agadere Cemetery, Gallipoli Peninsular, NW Turkey. *Australian Journal of Forensic Sciences* 46: 111–123.
- CASTRO, K.C.P.L., CUNHA, L.S. 2021. Forensic Investigations with the Identification of Human Remains with Ground Penetrating Radar (GPR): A Review. *Estudos Geológicos* 31(2): 64–86. DOI 10.18190/estudosgeologicos.v31n2p64-86
- CASTRO, K.C.P.L., CUNHA, L.S., SOUSA, A.C.A., NOGUEIRA, P.V., BORGES, W.R. 2024 Influence of the sand-clay ratio of the burial material of forensic targets on ground-penetrating radar (GPR) responses—comparison of dry and rainy season data. *Front. Earth Sci.* 12:1305496. doi: 10.3389/feart.2024.1305496
- CAVALCANTI, M.M. 2017. Estudo da Resposta Geofísica em Diferentes Cenários de Sepultamento. Tese de doutorado. Instituto de Geociências. 197p.
- CAVALCANTI, M.M. et al. 2018. The forensic geophysical controlled research site of the University of Brasilia, Brazil: Results from methods GPR and electrical resistivity tomography. *Forensic Science International* 293: e1–101.e21.
- DANIELS, D.J. 1996. Surface Penetrating Radar. The Institution of Electrical Engineers, London, United Kingdom. 300p.
- DAVIS, J.L., ANNAN, A.P. 1989. Ground penetrating radar for high-resolution mapping of soil and rock stratigraphy. *Geophys. Prospect.* 37, 531–551p.

- DOOLITTLE, J.A., BELLANTONI NF. 2010. The search for graves with ground-penetrating radar in Connecticut. *Journal of Archaeological Science* 37: 941–949. DOI: 10.1016/j.jas.2009.11.027
- JOL, M.H. 2009. *Ground Penetrating Radar: Theory and Applications*. Elsevier Science, Oxford.
- MALA GEOSCIENCE. RAMAC/GPR. Versão 2.28. Software Manual, Agosto, 66p. 1997.
- MOLINA, C.M. et al. 2015. Preliminary results of sequential monitoring of simulated clandestine graves in Colombia, South America, using ground penetrating radar and botany. *Forensic Science International* 248: 61–70. DOI: 10.1016/j.forsciint.2014.12.011
- MOLINA, C.M. et al. 2016a. Geophysical and botanical monitoring of simulated graves in a tropical rainforest, Colombia, South America. *Journal of Applied Geophysics* 135: 232–242.
- MOLINA, C.M. et al. 2016b. Geophysical monitoring of simulated graves with resistivity, magnetic susceptibility, conductivity and GPR in Colombia, South America. *Forensic Science International* 261: 106–115.
- NOVO, A. et al. 2011. 3D GPR in forensics: Finding a clandestine grave in a mountainous environment. *Forensic Science International* 204: 134–138.
- PORSANI, J.L. 1999. *Ground Penetrating Radar (GPR): Proposta metodológica de emprego em estudos geológico-geotécnicos nas regiões de Rio Claro e Descalvado-SP*. Tese de Doutorado, Instituto de Geociências e Ciências Exatas, UNESP, Campus de Rio Claro-SP, 145p.
- POWERS, M.H. 1997. Modeling frequency-dependent GPR. *The Leading Edge* 16, 1657–1662.
- RUBIO-MELENDI, D. et al. 2018. GPR and ERT detection and characterization of a mass burial, Spanish Civil War, Northern Spain. *Forensic Science International* 287: e1–e9. DOI: 10.1016/j.forsciint.2018.03.034
- SANDMEIER, K.J. 2006. REFLEXW Version 7.4, Windows 9x/2000/NT. Program for the processing of seismic, acoustic or electromagnetic reflection, refraction and transmission data. Manual do Software, Karlsruhe, Germany, 209p.
- SCHOOR, M. et al. 2017. A controlled monitoring study of simulated clandestine graves using 3D ground penetrating radar. *Near Surface Geophysics* 15: 274–284.
- SCHULTZ, J.J., MARTIN, M.M. 2012. Monitoring controlled graves representing common burial scenarios with ground penetrating radar. *Journal of Applied Geophysics* 83: 74–89.

- SOLLA, M. et al. 2012. Experimental forensic scenes for the characterization of ground-penetrating radar wave response. *Forensic Science International* 220: 50–58.
- STRATTON, J.A. 1941. Electromagnetic Theory. McGraw-Hill Book Company, Inc., New York, 615p.
- WISNIEWSKI, K. et al. 2019. The Search for “Fred”: An Unusual Vertical Burial Case. *J Forensic Sci* 64: 1530–1539.
- YELF, R.J. 2004. Where is true time zero? *Proceedings of the Tenth International Conference on Grounds Penetrating Radar*. v. 1, 279–282.

ANEXOS

A – FUNDAMENTAÇÃO TEÓRICA

O Radar de Penetração no Solo (GPR) é um método não destrutivo de investigação geofísica que consiste na emissão de ondas de rádio em altas frequências (comumente entre 10MHz a 2500MHz), com o intuito de estudar estruturas e feições geológicas rasas, bem como a presença de materiais enterrados pelo homem (Porsani, 1999).

O GPR possui duas antenas, uma transmissora que emite ondas eletromagnéticas e uma antena receptora que capta o sinal refletido pelas diferentes estruturas do solo. As informações são transmitidas para o disco rígido e mostradas na tela de um *notebook* onde podem ser interpretadas.

Os sinais GPR são campos eletromagnéticos, que são definidos por meio de quatro expressões fundamentais conhecidas como Equações de Maxwell, que serão detalhadas mais à frente. Com o método GPR, a antena transmissora emite um pulso eletromagnético para o solo que é parcialmente refletido quando encontra o meio com diferentes propriedades dielétricas, e o resto do feixe é transmitido para camadas mais profundas. Então, o sinal refletido é gravado a partir da antena receptora (Solla et al., 2012) (Figura 1).

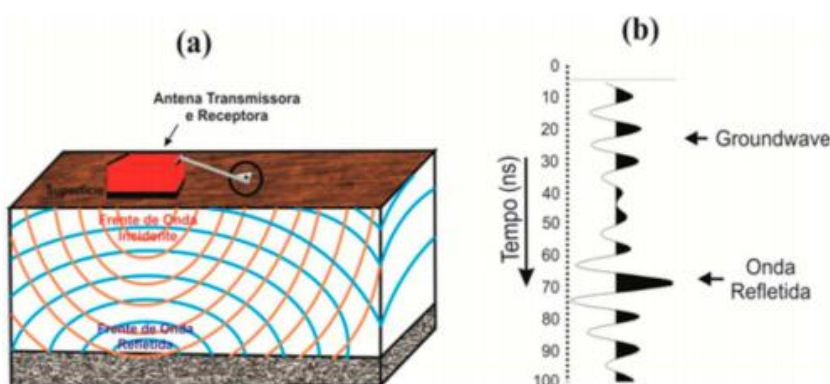


Figure 1 - (a) Diagrama de antenas GPR ilustrando o comportamento das frentes de onda. (b) Traço esquemático mostrando as chegadas das principais frentes de onda do GPR. (Cavalcanti, 2017)

Ao mover a antena sobre o solo, uma imagem rasa da subsuperfície é obtida sob a linha de deslocamento. Essas imagens, chamadas radargramas (Figura 2), são representações bidimensionais gráficas XZ das reflexões detectadas. O eixo X representa o deslocamento da antena ao longo da linha de levantamento e o eixo Z representa a viagem bidirecional do tempo do pulso emitido (em nanossegundos). Se o tempo necessário para o pulso eletromagnético ir da antena de transmissão para o refletor no solo e o retorno para a antena receptora é medido, então a velocidade deste pulso no meio subterrâneo é conhecida e a posição do refletor pode ser determinada. A frequência da antena transmissora determina a faixa de profundidade do GPR e deve ser cuidadosamente escolhida pois a energia da onda eletromagnética é atenuada durante a sua propagação. Um equilíbrio deve ser mantido entre uma baixa frequência, que fornece uma penetração de sinal mais profunda (Tabela 1), com resolução mais baixa e uma antena de maior frequência, que oferece melhor resolução (Tabela 2), mas penetração mais rasa (Solla et al., 2012).

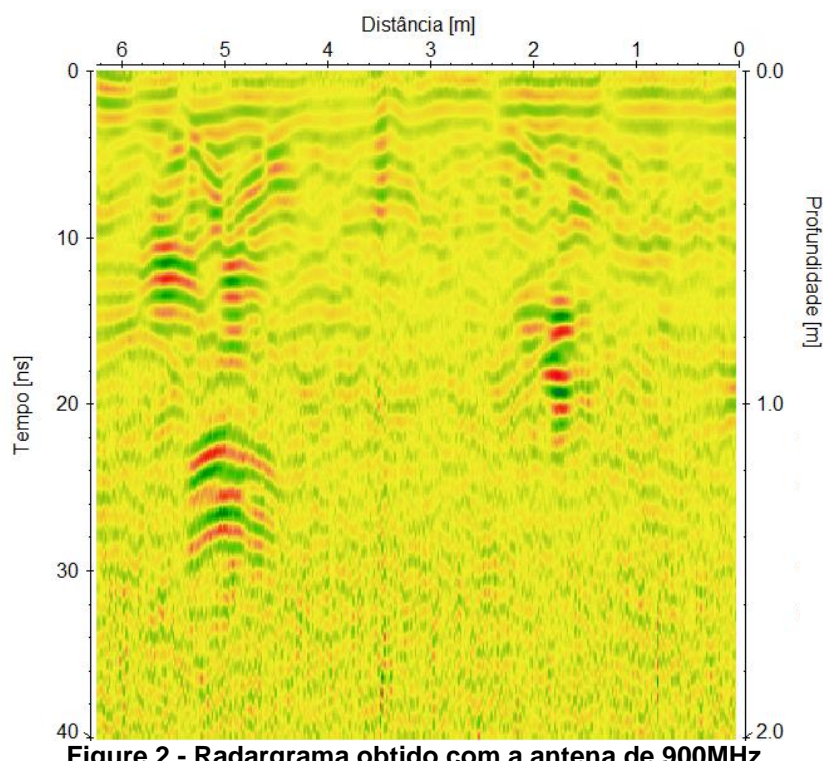


Figure 2 - Radargrama obtido com a antena de 900MHz.

Tabela 1 – Frequência versus profundidade de penetração do sinal (Mala, 1997 e Borges, 2007).

Frequência central (MHz)	10	25	50	100	200	400	500	1000
Profundidade de penetração (m)	50	40	30	25	3,4	1,6	1,5	0,8

A resolução vertical é a habilidade de distinguir as reflexões provenientes do topo e da base de camadas de pequena espessura (Davis & Annan, 1989)

Tabela 2 – Frequência central das antenas e sua resolução vertical (Annan, 2004).

Frequência central (MHz)	200	100	50	25
Resolução vertical (m)	0,25	0,50	1,00	2,00

A1 – PRINCÍPIOS MATEMÁTICOS

O método GPR é fundamentado nas relações entre campos elétricos e magnéticos que são expressas matematicamente por meio das equações de Maxwell:

$$\nabla \times E = -\frac{\partial B}{\partial t} \quad (\text{Equação 1})$$

$$\nabla \times H = J + \frac{\partial D}{\partial t} \quad (\text{Equação 2})$$

$$\nabla \cdot B = 0 \quad (\text{Equação 3})$$

$$\nabla \cdot D = \rho \quad (\text{Equação 4})$$

Onde: E é a intensidade do campo elétrico (Volts por metro - V/m);

H é o campo magnético (Ampère por metro - A/m);

J é o vetor densidade de fluxo de corrente (Ampère por metro quadrado – A/m²);

B é o vetor indução magnética (Weber por metro quadrado - Weber/m² ou Tesla)

D é a densidade do fluxo magnético (Coulomb por metro quadrado – C/m²)

ρ é a densidade de carga elétrica (Coulomb por metro cúbico – C/m³);

t é o tempo (segundos).

A equação 1 é a Lei de Faraday que relaciona o campo elétrico com o magnético. A equação 2 é a Lei de Ampère que mostra como o fluxo elétrico se modifica por meio do tempo. A equação 3 prova que por meio de qualquer superfície fechada o fluxo do vetor indução magnética é igual a 0, não existem polos magnéticos

isolados. A equação 4 é a Lei de Gauss que fornece o fluxo do campo elétrico em uma superfície fechada que é igual à carga líquida encerrada por ela (Stratton, 1941).

Tomando o gradiente nas equações 1 e 2, considerando E e H como funções contínuas, em uma região de estudo homogênea são obtidas as seguintes equações no domínio da frequência:

$$\mathbf{D} = \epsilon \cdot \mathbf{E} \text{ (Equação 5)}$$

$$\mathbf{B} = \mu \cdot \mathbf{H} \text{ (Equação 6)}$$

$$\mathbf{J} = \sigma \cdot \mathbf{E} \text{ (Equação 7)}$$

Onde: μ é a permeabilidade magnética (weber/Am);

ϵ é a permissividade dielétrica (C^2/Nm^2);

σ é a condutividade elétrica (Siemens/m).

A permeabilidade magnética (μ), permissividade dielétrica (ϵ) e a condutividade elétrica (σ) são as grandezas que controlam o comportamento da propagação do sinal eletromagnético no meio.

A permeabilidade magnética consiste na magnitude equivalente da permissividade dielétrica, ou seja, é a medida da energia do campo magnético armazenado e perdido através da magnetização induzida (Powers, 1997). A permissividade dielétrica expressa uma relação entre frequência e o campo elétrico induzido. Devido à presença de água em todos os materiais geológicos, à medida que a frequência da onda eletromagnética aumenta, a permissividade dielétrica da água também aumenta, chegando ao limite entre aproximadamente 10 GHz a 20 GHz, onde o efeito de relaxação é máximo, fazendo com que a molécula de água dissipe a energia acumulada na forma de calor (Powers, 1997). A condutividade elétrica expressa a facilidade de um corpo conduzir corrente elétrica, quanto maior a condutividade maior será a atenuação do sinal eletromagnético.

Para compreender melhor as relações destas grandezas a Tabela 3 mostra a variação na permissividade dielétrica (ϵ) e na condutividade elétrica (σ) para alguns materiais comumente estudados com o GPR.

Tabela 3 – Valores de permissividade dielétrica (ϵ) e condutividade elétrica (σ) determinados em materiais comuns para as frequências mais utilizadas no GPR (Adaptado Daniels, 1996).

Material	Permissividade dielétrica - ϵ	Condutividade elétrica - σ (mS/m)
Água fresca	81	0,5
Ar	1	0
Argila	5 – 40	2 – 1000
Concreto	4 – 10	1 – 0,1
Metal	300	10^{10}
PVC	3,3	0
Solo argiloso saturado	15	50
Solo argiloso seco	2,4	0,27

A2 – PROCESSAMENTO

Correção Estática (Static Correction)

É aplicada individualmente em cada traço, realizando uma correção temporal independente para cada um. Essa etapa é comumente utilizada para remover a onda aérea do sinal GPR. O primeiro pico positivo da onda eletromagnética refletida é considerado, pois representa o contato entre o ar e o solo nos radargramas (Yelf, 2004).

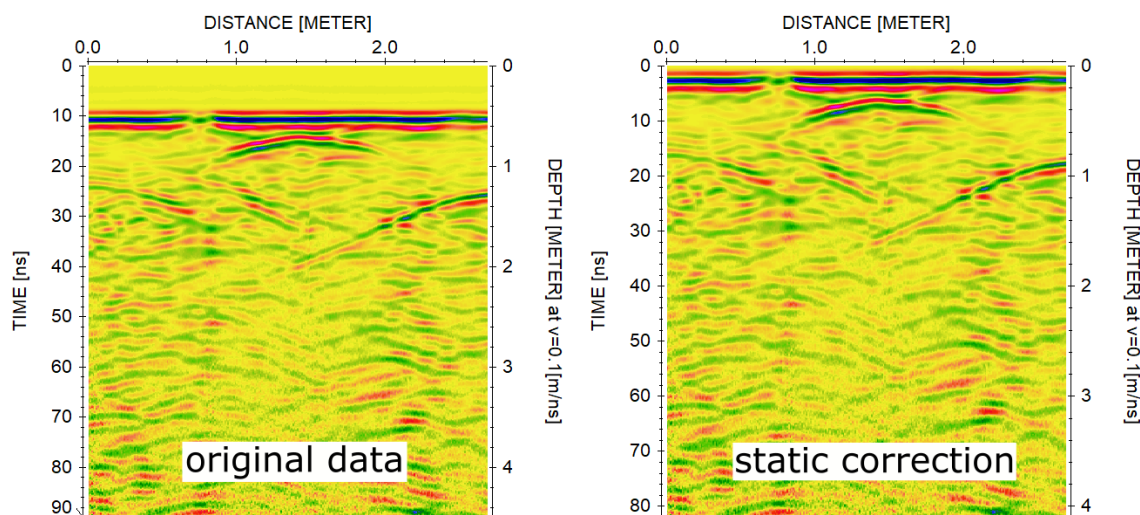


Figura 3 - Primeira etapa do fluxo de processamento usado em dados GPR onde a correção estática corrige o tempo zero.

Ganho – decaimento de energia (energy decay)

A atenuação das ondas eletromagnéticas aumenta conforme se propaga para o solo, resultando em sinais mais fracos em profundidades maiores. Para compensar essa perda de energia, utiliza-se a função de ganho com variação temporal. (Jol, 2009).

Para compensar a perda de energia devido ao decaimento, é aplicado um ganho temporal em cada traço. Esse ganho é baseado na curva de decaimento médio de amplitude. Primeiro, é determinada uma curva de decaimento médio a partir de todos os traços existentes no perfil. Em seguida, aplica-se um filtro de mediana nesta curva e cada amostra do traço é dividida pelo valor da curva de decaimento. Muitas vezes é necessário aplicar um fator de escala menor do que um, pois alguns valores de amplitude podem exceder a amplitude máxima do perfil original após a aplicação desse ganho (Sandmeier, 2006).

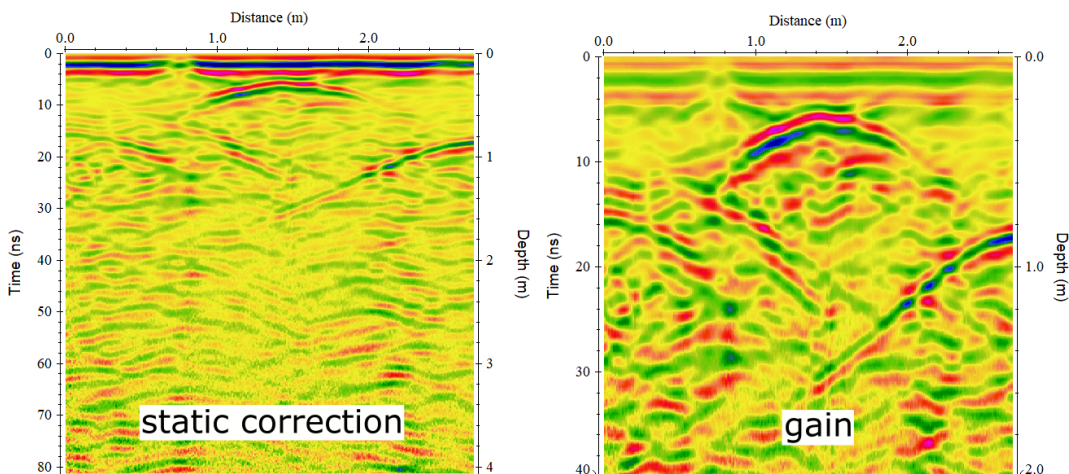


Figura 4 - Segunda etapa do fluxo de processamento usado em dados GPR onde o ganho melhorou a visualização de refletores fracos.

Remoção de fundo (background removal)

Técnica para eliminar sinais de baixa frequência do sinal de radar, destacando refletores pontuais e anomalias. Esse filtro é aplicado a um determinado número de traços, subtraindo um traçado médio (trace range) construído a partir do intervalo de tempo/distância escolhido no radargrama. Em outras palavras, é feita uma média da amplitude dos traços dentro de uma janela definida e essa média é subtraída dos traços originais (Sandmeier, 2006). A principal equação que obtém as remoções é mostrada abaixo:

$$A'n, a = An, a(t) - \left(\frac{1}{Na}\right) \sum_{a=1}^{Na} An, a(t) \quad (\text{Equação 8})$$

Onde: $n=1$ para N (números de amostras);
 $a=1$ para N_a (número de forma de onda A ou B-Scan);
 $A_n, a(t)=$ não processado;
 $A'_n, a(t)=$ processado.

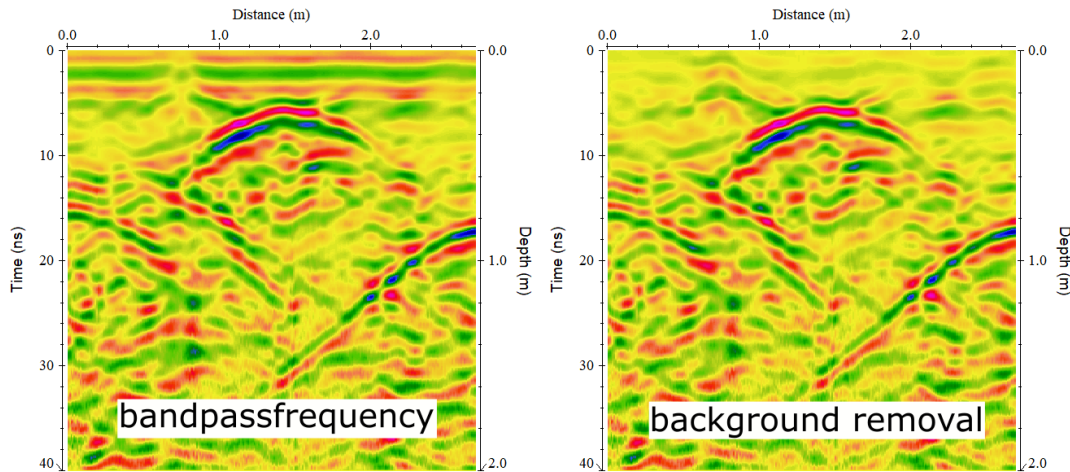


Figura 5 - Terceira etapa do fluxo de processamento usado em dados GPR onde a remoção de fundo promove a redução de eventuais ruídos de fundo.

Fk filter

O filtro Fk é uma técnica utilizada para remover distorções causadas por variações na velocidade de propagação da onda radar ao longo da profundidade em dados GPR.

Os dados GPR são geralmente registrados como secções de profundidade que mostram variações de impedância elétrica ao longo da profundidade. O filtro Fk é utilizado para remover distorções causadas por variações na velocidade de propagação da onda radar, como por exemplo, variações na densidade e na porosidade dos solos e rochas, ajudando a melhorar a qualidade da imagem.

A aplicação do filtro Fk aos dados GPR é realizada por meio da utilização da transformada de Fourier, que permite transformar os dados do domínio espacial para o domínio da frequência-número de onda (f - k), um espaço bidimensional onde a frequência é representada no eixo x e o número de onda é representado no eixo y. A representação f - k permite analisar como a frequência e o número de onda se relacionam entre si e como variam ao longo do tempo, permitindo identificar e remover distorções indesejadas do sinal.

Depois de transformar os dados para o domínio f - k , o filtro Fk utiliza técnicas de filtragem, como a aplicação de filtros de banda passante ou outras técnicas de filtragem, para remover ruído e outras distorções. Em seguida, a transformada inversa de Fourier é aplicada para trazer os dados de volta ao domínio espacial, resultando em dados limpos e processados.

Em resumo, o filtro Fk permite a aplicação de filtragem bidimensional no domínio da frequência e do número de onda, permitindo remover distorções causadas por variações na velocidade de propagação da onda eletromagnética, melhorando a qualidade dos dados e facilitando a identificação de estruturas subterrâneas.

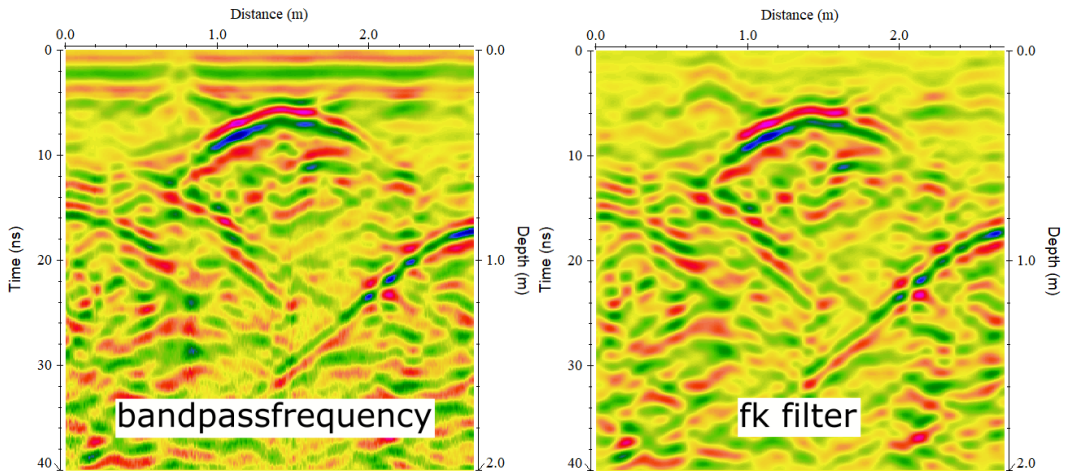


Figura 6 - Quarta etapa do fluxo de processamento usado em dados GPR onde o filtro fk realiza a supressão de ruídos no domínio fk do sinal eletromagnético.

Migração (Kirchhoff)

A migração tem como objetivo "colapsar" as difrações, ou seja, concentrar a energia da onda em seu ápice, para produzir uma imagem mais clara e precisa. Quando a onda sísmica ou radar atinge uma estrutura subterrânea, ela é refletida em vários ângulos, o que resulta em difrações ou "fantasmas" na imagem final. A migração busca corrigir essas difrações e concentrar a energia refletida em um único ponto, o que resulta em uma imagem mais clara e precisa.

A migração Kirchhoff é uma técnica utilizada para processar dados GPR para melhorar a qualidade da imagem e tornar mais fácil identificar estruturas subterrâneas. Ela é baseada na teoria da radiação Kirchhoff, que descreve como a radiação se propaga em um meio heterogêneo.

A migração Kirchhoff utiliza a teoria da radiação de Kirchhoff para calcular o caminho de reflexão de cada trajeto de onda, levando em conta as variações na velocidade de propagação da onda radar ao longo da profundidade. Isso permite remover distorções causadas por variações na velocidade de propagação e produzir uma imagem mais clara e precisa.

A teoria da radiação de Kirchhoff descreve como a radiação se propaga em um meio heterogêneo e é baseada na lei da conservação da energia, que afirma que a quantidade total de energia no sistema permanece constante.

De acordo com a teoria de Kirchhoff, a radiação incidente em uma interface entre dois meios é dividida em duas componentes: uma componente refletida e uma componente transmitida. A componente refletida é determinada pela relação entre as impedâncias acústicas dos meios e o ângulo de incidência da onda. Já a componente

transmitida é determinada pela relação entre a impedância do meio anterior e do meio posterior.

A teoria de Kirchhoff também descreve como a radiação se propaga em meios heterogêneos, como rochas e solos, e como a radiação é afetada por variações na velocidade de propagação e impedância. Isso é importante para aplicações como a identificação de estruturas subterrâneas.

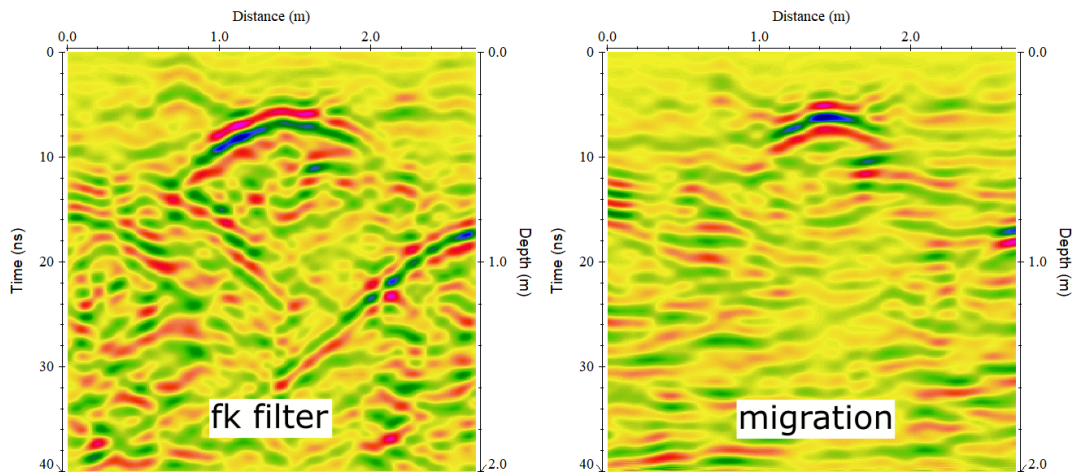


Figura 7 - Quinta etapa do fluxo de processamento usado em dados GPR onde por meio da migração as difrações são colapsadas tendendo a energia a se focar no seu ápice.

B – ARTIGO CIENTÍFICO – REVISÃO SISTEMÁTICA DA LITERATURA ([ACESSO AQUI](#))

**FORENSIC INVESTIGATIONS WITH THE IDENTIFICATION OF HUMAN REMAINS
WITH GROUND PENETRATING RADAR (GPR): A REVIEW**

**PESQUISAS FORENSES COM A IDENTIFICAÇÃO DE VESTÍGIOS HUMANOS COM
O RADAR DE PENETRAÇÃO DO SOLO (GPR): UMA REVISÃO**

Kimberly Coutinho Paes Leme de Castro
Luciano Soares da Cunha

10.18190/1980-8208/estudosgeologicos.v31n2p64-86

Instituto de Geociências da Universidade de Brasília - IG/UnB.

kimberlycplcastro@yahoo.com luciano.soares.unb@gmail.com

ABSTRACT

Forensic geophysics research using ground-penetrating radar (GPR) has the potential to non-destructively detect buried or hidden targets. A systematic literature review is a bibliographic technique that aims to answer a question objectively and impartially by evaluating a body of data from articles and other scientific documents. The question posed here was how GPR can assist in identifying bodies in different burial scenarios and where research on this topic is headed. The extracted articles were divided into two groups: controlled sites and uncontrolled sites. From the analysis of the results, it can be seen the most commonly used targets for research in controlled sites were pigs due to their anatomical similarity to humans. The articles reviewed involve the integration of more than one research method. As new scopes of investigations are a comparison of GPR image features for multiple burial scenarios, evaluation of the change in geophysical response of simulated mass graves over the years, and research about false-positive results which was discussed in only 2.1% of the reviewed articles.

Keywords: clandestine grave; uncontrolled and controlled research site; forensic Science; burials.

RESUMO

Pesquisas na área de geofísica forense com a utilização do radar de penetração no solo (GPR) têm o potencial de detectar de forma não destrutiva alvos enterrados ou ocultos. A revisão sistemática da literatura é uma técnica bibliográfica que se propõe a responder uma questão objetiva e imparcialmente avaliando um conjunto de dados oriundos de artigos e outros documentos científicos. A questão aqui posta foi saber como o GPR pode auxiliar na identificação de corpos em diferentes cenários de sepultamento e para onde pesquisas nesta temática estão se direcionando. Os artigos extraídos foram divididos em dois grupos: sítios controlados e sítios não controlados. Os alvos mais utilizados para pesquisas em sítios controlados são suínos devido à semelhança anatômica com os humanos. Como novos escopos de investigações estão a comparação de características de imagens de GPR para múltiplos cenários de sepultamento, avaliação da mudança na

FORENSIC INVESTIGATIONS WITH THE IDENTIFICATION OF HUMAN REMAINS...

resposta geofísica de sepulturas clandestinas simuladas ao longo dos anos e pesquisas acerca de resultados falsos positivos que foi discutida em apenas 2,1% dos artigos revisados.

Palavras-chave: sepultamentos clandestinos; sítios controlados e não controlados; ciências forenses; sepulturas simuladas.

INTRODUCTION

Forensic research by searching for human remains associated with the use of the geophysical method, Ground Penetrating Radar (GPR), is advancing in various areas of the sciences being incorporated in different lines of research such as decomposition of organic material (Pringle *et al.*, 2020; Dick & Pringle, 2018; Schoor *et al.*, 2017; Schultz, *et al.*, 2016), in submerged areas (Ruffell *et al.*, 2017; Schultz *et al.*, 2013; Parker *et al.*, 2010) controlled sites (Pringle *et al.*, 2020; Cavalcanti *et al.*, 2018; Schoor *et al.*, 2017; Schultz *et al.*, 2016; Molina *et al.*, 2016a; Pringle *et al.*, 2016; Molina *et al.*, 2016b; Booth & Pringle, 2016; Salsarola *et al.*, 2015; Almeida *et al.*, 2015; Molina *et al.*, 2015; Almeida *et al.*, 2014; Lowe *et al.*, 2013; Pringle *et al.*, 2012a; Solla *et al.*, 2012; Schultz & Martin, 2012; González-Jorge *et al.*, 2012; Schultz & Martin, 2011; Parker *et al.*, 2010; Schultz, 2008; Schultz *et al.*, 2006; Powell, 2004; Schultz *et al.*, 2002), use combined with other methods (Pringle *et al.*, 2020; Abate *et al.*, 2019; Rubio-Melendi *et al.*, 2018; Cavalcanti *et al.*, 2018; Molina *et al.*, 2016a; Aziz *et al.*, 2016; Hansen & Pringle, 2013).

These forensic researches aided by geophysical methods are relatively recent and coincident with greater and better development of geophysical equipment, mainly, in this specific case, as happened with GPR in the mid-1990s. The increasing scientific development on

the subject can be observed by the increase in the average publication of scientific articles that between 2000-2009 was 3.0 articles compared to the period 2010-2019 with an average of 6.9 according to data accessed on 03/15/2021 in the Web of Science.

In this context, the development of a Systematic Literature Review (SLR) is appropriate because it allows identifying both the evolution of scientific knowledge and evaluates it statistically. Thus, the present work had an as main objective: to analyze the advances obtained in forensic research of human remains identification with the help of the GPR geophysical method and, in a complementary way, to identify the common characteristics of the controlled sites, the limitations in the use of GPR and the real improvements in the use of complementary geophysical methods in this theme.

Systematic Review and Meta-Analysis

Systematic Literature Review (SLR) is a scientific research technique to gather, critically evaluate, and conducting a synthesis of the results of multiple primary studies (Benefield, 2003). It allows, within an area of knowledge, to identify, evaluate, and interpret the most relevant studies in a topic with the production of a critical synthesis of the main evidence, evolution, and highlights neglected themes that may indicate the proposition of future topics in the process for new research. SLR's concentrate on

the identification of previous research, evaluating the results in a systematic way and with statistical resources employing synthesis. Its main features are a predefined set of objectives and eligibility criteria.

It comprises three development stages (Planning, Execution, and Documentation). Planning begins with the definition of the protocol that specifies all the steps of the method that will be followed. The definition of the main question and other guiding parameters of the review ensures in advance that the methods employed will be standardized and the risk of bias reduced ("Systematic Reviews: CRD's guidance for undertaking reviews in health care", 2009). Execution objectively comprises the fulfillment of the protocol in its entirety, beginning with access to databases using keywords in advanced search processes utilizing strings. Documentation presents the product of the review that must have a minimum set of items (Checklist) comprising the final report document (Galvão *et al.*, 2015).

The steps involved are based on evidence-based searches and have as main steps (Porritt *et al.*, 2014): (i) Development of the review protocol that contains the formulation of the Main Question, Keywords, Inclusion/Exclusion Criteria and Selection of Databases; (ii) Search for the primary studies (articles) in the Databases; (iii) Selection of the primary studies (based on the inclusion/exclusion criteria); (iv) Data extraction using a summary sheet developed in parallel with the protocol; (v) Analysis and Synthesis of the extracted

data focused on formulating the answer to the Main Question; (vi) Thematic suggestion for further research.

MATERIALS AND METHODS

For this research, the StArt (State of the Art) software (http://lapes.dcc.ufscar.br/tools/start_tool), version 3.3 beta 03 (Lapes/UFSCar) was used. The steps performed in this research are: (i) defining the research protocol; (ii) importing the data from the articles obtained in the databases; (iii) selecting the articles; (iv) classifying the articles to be read; (v) summarizing using graphs with a statistical emphasis of the results. The searches were carried out in the Web of Science, Scopus, and Science Direct Databases considering the combination of keywords and the guiding delimiters (Table 1) that work as a first filtering process of the search.

As a result, a total of 890 articles were obtained: 651 in Science Direct, 201 in Scopus, and 38 in Web of Science. For each database, the searches containing the title, abstract, and keywords were exported in "bibtex" format and imported into StArt 3.0.3. After the selection 56 articles were accepted for the next step, 399 were rejected and 435 articles were duplicates. Initially, the stage of extraction of information from the articles occurs with the full-text search by accessing the Federated Academic Community (CAFe) (<http://periodicos.capes.gov.br/>). The summary table will not be displayed in this article due to the imposed page limit.

FORENSIC INVESTIGATIONS WITH
THE IDENTIFICATION OF HUMAN
REMAINS...

Table 1 - Protocol parameters defined for the research.

Parameters	Applied to the Systematic Review
Research Group Members	Reviewer A and Reviewer B.
Main Question	How can GPR assist in identifying bodies in different burial scenarios?
Keywords string structure	((("GPR" OR "ground penetrating radar") AND "forensic")) e (((("GPR" OR "ground penetrating radar") AND "forensic" AND ("burial" OR "burials" OR "buried")) AND ("graves" OR "grave"))).
Database	Web of Science/Scopus/Science Direct.
Delimiters	Year of publication: 2000 to 2020. Publication type: Only articles available online. Language: English. Area of research: unrestricted.
Inclusion (I)/Exclusion (E) Criteria	(I) Forensic research using GPR. (I) Studies published and fully available in the scientific databases searched. (E) Does not address GPR applied to forensics. (E) Not in the selected language. (E) Full text not found. (E) Records without abstract. (E) Full text not accessible by the Capes Portal and/or without return of the authors by the Research Gate.

RESULTS

The visualization of co-authorship is presented in Fig. 1 for the period 1990-2021 with authorships being the unit of analysis. This relationship reflects how the networks of researchers are structured when considering at least 2 documents per author and at least 1 citation of the publication. In this graphic form, the size of the symbol reflects the number of publications belonging to the researcher clusters. The intensity of the relationships is reflected in the thickness of the lines and the proximity between the centers of the clusters (circles). Six clusters are identified that have their common core in researcher Pringle, J.K (Table 2). Cluster 1 (in green) is composed of 4 researchers and coordinated by Pringle, J.K., the most cited researcher when the topic is forensic research in the identification of human remains with the aid of geophysical methods. Clusters 2 (in dark blue), 3 (in purple), and 4 (in red) represent clusters with repetitive contributions to each other and Cluster 1, and with their network being structured, but with very tenuous relationships. The distance of the Cluster 5 (in yellow) to the others reflects a co-authorship association that occurred in previous years and was not continued with an increase in new publications. Cluster 6 (in turquoise blue) reflects a more recent association among researcher clusters, but already with relationships with researchers from Clusters 1, 2, 3, and 4. The relations of association and intensity of coauthorship can be evaluated considering research institutes

as the unit of analysis, but the corresponding graph will not be presented here. The largest concentration is in institutions in the United Kingdom with a minority presence of institutions from Colombia (South America) and Spain (Europe).

For the same period, the cocitation map (Fig. 2) was prepared to identify the relevant authors and/or articles in the theme from the selected documents. The unit of analysis considered was cocitation when an article cites two articles in common. The parameters used were a minimum of 25 cocitations on the reference and the weight of the relations being calculated for the number of these cocitations. In order not to filter out articles that may be citation references, the period used did not compute the beginning year, only the end, 2020.

The authors with the highest reference of publications with at least 25 citations, according to the Web of Science, are respectively: France et al., 1992 (47), Nobes et al., 2001 (40), Schultz, 2007 (33), Schultz et al., 2006 (33), Schultz 2008 (29), Pringle et al., 2008 (28), Ruffell et al., 2005 (26), Owsley 1995 (26), Davenport, 2001 (26), Cheetham, 2005 (26), Pringle et al., 2012 (25), Novo et al., 2011 (25), and Bevan, 1991 (25). In addition to these 13 articles cited above another 43 articles that met the inclusion criteria outlined in the protocol were selected for full reading, extraction, and analysis. They were divided into 2 thematic groups, 48 articles, for a better presentation of the results: Controlled Sites (Table 3) and Non-Controlled Sites (Table 4).

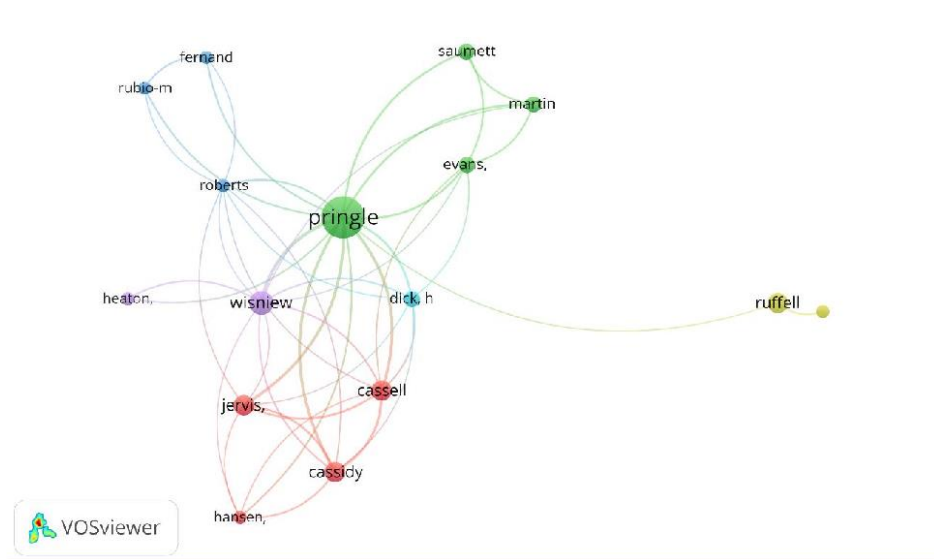


Figure 1 - Coauthorship network map between authors of the selected articles for the period 2000-2021 (Source: Web of Science). The most structured network is centered on the researcher with the most publications on the subject matter of this SLR. The thicker lines indicate direct citation and with greater intensity in the relationships of the researchers. The less thick lines indicate indirect citation and co-authorship.

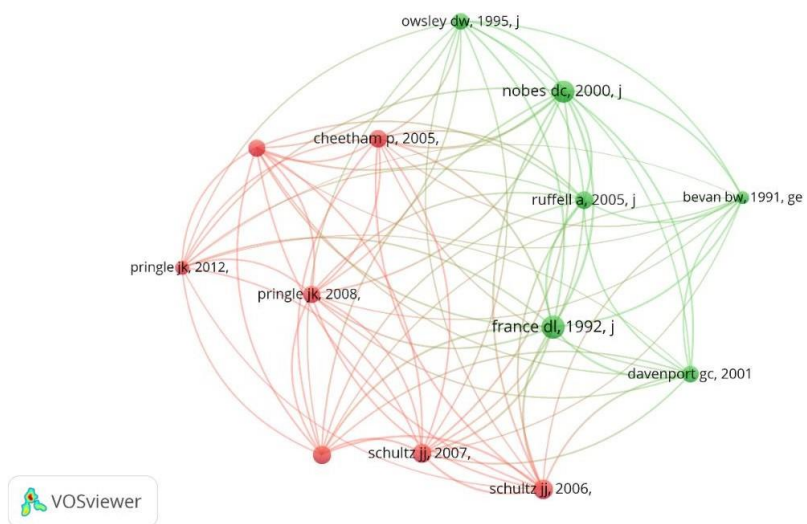


Figure 2 - The intensity of the cocitation network among the authors of the research on the topic in question (Source: Web of Science). In this figure, the network intensity from the core of the author Pringle, J.K. to other researchers is highlighted. Note: This analysis only considers the first author of each citation. This is a limitation of the data exported from the Web of Science.

Kimberly Coutinho Paes Leme de Castro & Luciano Soares da Cunha

Table 2 - Identification of associated researcher clusters to co-authorship.

Cluster	Researcher	Institution	Country
1	Pringle, J. K.	Keele University	United Kingdom
1	Evans, G. T.	Keele University	United Kingdom
1	Martin, M. C.	Universidad Nacional de Colômbia	Colombia
1	Saumet, M.	Universidad Nacional de Colômbia	Colombia
2	Cassela, J. P.	Keele University	United Kingdom
2	Cassidy, N. J.	Keele University	United Kingdom
2	Hansen, J. D.	Keele University	United Kingdom
2	Jervis, J. R.	Keele University	United Kingdom
3	Fernandez-Alvarez, J.	Universidad de Oviedo	Spain
3	Roberts, D.	Universidad de Oviedo	Spain
3	Rubio-Melendi, D.	Universidad de Oviedo	Spain
4	Heaton, V.	Keele University	United Kingdom
4	Wisniewski, K. D.	Staffordshire University	United Kingdom
5	Ruffell, A.	Queen's University, Belfast	United Kingdom
5	Donnelly, C.	Queen's University, Belfast	United Kingdom
6	Dick, H. C.	Keele University	United Kingdom

Controlled Sites

This group represents 62.5% of the total articles extracted in this SLR. The publications in this group occurred between the years 2000 and 2020. The general objectives of the surveys included: comparing different antenna frequencies, evaluating and demonstrating the effectiveness and the best methods and methodologies for grave detection, establishing an initial forensic research methodology, and evaluating the applicability of GPR.

All of the articles had their controlled sites constructed in a natural area having clay soils as the one that appeared the most, at 36.6% (Cavalcanti *et al.*, 2018;

Schoor *et al.*, 2017; Molina *et al.*, 2016a; Molina *et al.*, 2016b; Molina *et al.*, 2015; Hansen & Pringle, 2013; Lowe *et al.*, 2013; Pringle *et al.*, 2008; Freeland *et al.*, 2003; Miller *et al.*, 2002; Freeland *et al.*, 2002) of the controlled sites, in second place the soil type that appeared most was clayey sandy, present in 23.3% (Pringle *et al.*, 2020; Pringle *et al.*, 2016; Booth & Pringle, 2016; Almeida *et al.*, 2014; Lowe *et al.*, 2013; Pringle *et al.*, 2012a; Schultz *et al.*, 2006) of the controlled sites, followed by sandy soil, present in 16.6% (Schultz *et al.*, 2016; Pudova *et al.*, 2016; Pringle *et al.*, 2012b; Schultz & Martin, 2012; Schultz, 2008) of the controlled sites of the selected articles in this group

Controlled Sites

This group represents 37.5% of the total SLR articles. The publications in this thematic group occurred between the years 2007 and 2019. The main objectives included: highlighting the importance of geophysical methods by reporting results of the methods, proposing general requirements for field operations, presenting research results and documenting investigations, assisting in locating human remains, and determining the location of unmarked graves.

Table 3 – Main parameters used in Controlled Sites research. ER= Electroresistivity; MS= Magnetic Susceptibility; MC= Magnetic Conductivity; MG= Magnetic Gradient; MT= Microwave Tomography; LMT= Linear Microwave Tomography; MD= Metal Detector; LS= Laser Scanning; RP= Rectified Photography.

Reference	Goals	Target dimensions (m)	Predominant soil type	Target type	Target depth (m)	Center frequency (MHz)	Complementary techniques	Main results
Pringle et al 2020	Evaluate the response of unmarked graves over ten years.	1,5x0,75x0,6	Clayey sandy	Pig	0,6	110, 225, 450, 900	ER	Target produced low resistivity anomalies for up to four years. GPR (110-900MHz) detected the target and the 225 MHz frequency was the most efficient.
Cavalcanti et al 2018	Observe the geophysical response to different burial scenarios.	1,8x1x1	Clayey	Pig	1	400	ER	Detection due to target contours. The Wenner-Schlumberger arrangement shows a better resolution of the grave boundaries.
Schoor et al 2017	Investigate the changes associated with shallow and clandestine burials.	2,2x1,2x0,75	Clayey	Pig	0,75	250	-	The grave anomalies are discernible as hyperbolic reflections in the unmigrated 2D radargrams and this changes over investigation time to lower resolution.
Schultz et al 2016	Determine the applicability of GPR to detect controlled burials.	1x1x1 / 1x1x0,5	Sandy	Pig	0,5 / 1	250, 500	-	The graves produced a more distinct response with clearer target reflections compared to bare carcasses. The imaging of the dominant 250 MHz frequency antenna was more favorable.

Molina et al 2016a	Evaluate whether the chosen methods can detect the simulated graves.	1,7x0,7x0,5	Clayey	Pig and Human Traces	0,5	250, 500	ER, MC and MS	The 250 MHz and 500 MHz frequencies showed good detection. MS, MC, and ER showed reduced detection of the simulated targets.
Pringle et al 2016	Determine the applicability of GPR to detect controlled graves.	1,5x0,75x0,6	Clayey sandy	Pig	0,6	110, 225, 450, 900	ER	The unwrapped pig shows low resistivity anomalies until the fourth year. The wrapped pig shows high resistivity anomalies. The frequencies (110 and 900 MHz) were good for the wrapped pig and low resolution for the bare pig.
Molina et al 2016b	Evaluate whether the chosen methods can detect the mock graves.	2x2x0,8 / 2x2x1,2	Clayey	Pigs and Human Remains	0,8 / 1,2	250, 500	ER, MC and MS	Good detection of wrapped targets in all periods with 250 MHz. Skeletons and decapitated and burned remains were poorly visualized.
Pudova et al 2016	Propose a protocol for field operations, data processing, and analysis.	6x8	Sandy	Metal and plastic objects, bones, concrete, wood trunk	0,4 to 1,2	400, 1200	-	Metal objects, concrete blocks, a plastic bottle filled with water, and a PVC bag filled with animal bones were picked up easily. Wood logs and empty plastic bottles were unclear.
Booth et al 2016	Develop a method to quantify the evaluation of a time-lapse file.	Not mentioned	Clayey sandy	Pig	0,5	110, 225, 450	-	Lower frequency antennas provided better results although the grave was detectable by all frequencies tested.
Salsarola et al 2015	Evaluate the effectiveness of the technique in two different burial environments.	2x1x0,9	Permeable and loose	Pig	0,8 to 0,9	500	-	GPR was useful in recognizing anomalies at burial depths. With slight anomalies of skeletal remains at 92 weeks from burial.
Almeida et al 2015	Analyze GPR reflections by a LMT approach.	2x1x1,1	Sandy clayey	Pig	1,1	270, 900	LMT	Anomalies are present in the position of the buried pig in both radargrams and tomographic images.
Molina et al 2015	Evaluate the best detection techniques for forensic geophysics.	2x2x0,8 / 2x2x1,2	Clayey	Pig and human remains	0,8 / 1,2	250	-	Anomalies are present in the position of the buried pig in both radargrams and CT images.

Almeida et al 2014	Apply microwave tomography with GPR.	2x1x1,1	Clayey sandy	Pig	1,1	270, 900	MT	GPR showed reasonable detection of the targets. Simulated burials using skeletonized human remains were not identified after 19 weeks.
Hansen et al 2013	Detail geophysical techniques for detecting surface buried objects.	5x5x0,15	Semi-urban; clay	Metal objects, bladed weapons, grenades, guns, ammunition, and bricks	0,15	450, 900	MS, MG, ER, MD and gradiometry Fluxgate	MT in conjunction with the 270 MHz GPR frequency improved target identification.
Lowe et al 2013	Investigate the applicability of GPR for forensic investigations	Not mentioned	Clayey sandy / silty clay / fine sand	Pig	0,76	500	-	MS: optimal for target detection; MD: did not detect all targets. GPR: optimal for target detection in the semi-urban environment. ER: good for target detection in the semi-urban environment.
Pringle et al 2012a	Determine the applicability of GPR to detect controlled graves.	1,5x0,75x0,6	Clayey sandy	Pig	0,6	110, 225, 450, 900	ER	GPR was successful in identifying clandestine graves in clayey loamy and fine sandy loamy soils.
Pringle et al 2012b	Establish methodologies for forensic research in coastal areas.	1x0,4x0,5	Sandy	Mannequin	0,5	225, 450, 900	MD, ER and MS	The unwrapped pig presents low resistivity anomalies. The wrapped pig shows high resistivity anomalies. Frequencies (110 and 900 MHz) are good for identifying the wrapped pig.
Solla et al 2012	Analyze the effectiveness of GPR in forensics.	Not mentioned	Sandy clayey	Pig and objects	0,5 / 1	500	Photogrammetry	450 MHz frequency was successful, but bad data was due to saltwater. ER and MS were successful.
Schultz et al 2012	Monitor empty and filled control graves.	1x1x0,5 / 1x1x1	Sandy	Pig	0,5 / 1	250, 500	-	GPR was successful in identifying buried remains such as mock hideouts, drug caches, weapons, clothing, and personal effects.

González-Jorge et al 2012	Compare terrestrial laser scanning, rectified photographs, and 3D GPR.	2x1,2x0,7 / 2,1x1x0,5	Not mentioned	Pig and human bones	0,5 / 0,7	500	LS and RP	The frequency of 250 MHz was the best for deep grave detection and 500 MHz for shallow grave detection.
Schultz et al 2011	Compare GPR reflection profiles of a control grave.	1x1x1	Spodosol	Pig	1	250, 500	-	The result obtained with terrestrial laser scanning coincides with real data. GPR data detected the target accurately.
Pringle et al 2008	Determine the best forensic geophysical techniques.	2x0,5x0,6	Clayey	Plastic Resin	0,6	225, 450, 900	ER, MC, MG and MS	With the frequencies of 250 and 500 MHz, the grave was detected with the 6-month-old pig target.
Schultz 2008	Test GPR to detect small pig cadavers.	Not mentioned	Sandy	Pig	0,5 to 0,6 / 1 to 1,1	500	-	ER located the grave. MG did not locate the grave. MS did not show the grave. GPR provided varied responses.
Schultz et al 2006	Test GPR to detect large pig carcasses.	Not mentioned	Clayey sandy	Pig	0,5 to 0,6 / 1 to 1,1	500	-	Target produced low resistivity anomalies for up to four years. GPR (110-900MHz) detected the target and the 225 MHz frequency was the most efficient.
Powell 2004	Detect graves in forensic investigations.	1x1x0,5 / 1x1x1	Limestone	Pig, kangaroo, human cadaver	0,5 / 1	200	ER	Detection due to target contours. The Wenner-Schlumberger arrangement shows a better resolution of the grave boundaries.
Freeland et al 2003	Compare raw data operating on buried corpses.	2,4x1,8x0,6	Clayey	Human cadavers	0,6	400, 900	-	The grave anomalies are discernible as hyperbolic reflections in the unmigrated 2D radargrams and this changes over investigation time to lower resolution.
Miller et al 2002	Evaluate GPR integration and anthropological data of decomposition rates.	~2,4x1,8	Clayey	Human cadavers	~0,45	Not mentioned	-	The graves produced a more distinct response with clearer target reflections compared to bare carcasses. The imaging of the dominant 250 MHz frequency antenna was more favorable.

Schultz et al 2002	Test the applicability of GPR to detect buried bodies.	Not mentioned	Sandy	Pig	0,5 to 0,6 / 1 to 1,1	500, 900	-	The 250 MHz and 500 MHz frequencies showed good detection. MS, MC, and ER showed reduced detection of the simulated targets.
Freeland et al 2002	Evaluate the use of GPR over buried corpses.	~2,4x1,8	Clayey	Human cadavers	~0,6	400, 900	-	The unwrapped pig shows low resistivity anomalies until the fourth year. The wrapped pig shows high resistivity anomalies. The frequencies (110 and 900 MHz) were good for the wrapped pig and low resolution for the bare pig.
Hammon III et al 2000	Perform 2.5D finite-difference simulations in the time domain of GPR responses.	Not mentioned	Dry sandy and clay	Human cadavers	0,4 / 0,9	450, 900, 1200	-	Good detection of wrapped targets in all periods with 250 MHz. Skeletons and decapitated and burned remains were poorly visualized.

In 73.3% of the articles in the controlled sites theme group the targets analyzed were pigs (Pringle *et al.*, 2020; Cavalcanti *et al.*, 2018; Schoor *et al.*, 2017; Schultz *et al.*, 2016; Molina *et al.*, 2016a; Pringle *et al.*, 2016; Molina *et al.*, 2016b; Booth & Pringle, 2016; Salsarola *et al.*, 2015; Almeida *et al.*, 2015; Almeida *et al.*, 2014; Lowe *et al.*, 2013; Pringle *et al.*, 2012a; Solla *et al.*, 2012; Schultz & Martin, 2012; González-Jorge *et al.*, 2012; Schultz & Martin, 2011; Schultz, 2008; Schultz *et al.*, 2006; Powell, 2004; Schultz *et al.*, 2002), but the use of kangaroos (Powell, 2004), human remains (Molina *et al.*, 2016a; Molina *et al.*, 2016b; Molina *et al.*, 2015; González-Jorge *et al.*, 2012; Powell, 2004; Freeland *et al.*, 2003; Miller *et al.*, 2002; Freeland *et al.*, 2002; Hammon *et al.*, 2000), objects such as sheet metal, iron pipe, bag with animal bones, concrete block, wooden log, metal barrels (Pudova *et al.*, 2016), water bottles (Pudova *et al.*, 2016), clothing and personal effects (Solla *et al.*, 2012), rifle and pistol simulacrum (Solla *et al.*, 2012), cell phones and bullet casings (Solla *et al.*, 2012), bricks, screws, knives, grenades (Hansen & Pringle, 2013), plastic resin human skeleton (Pringle *et al.*, 2008), and fiberglass mannequins (Pringle *et al.*, 2012b). Depths studied ranged from 0.15 m representing shallow graves to 1.2 m representing deep graves. Targets at only one depth were the option chosen in 60% of the articles.

The center frequencies used ranged from 110 MHz to 1200 MHz. The most commonly used frequencies were 500 MHz (Schultz *et al.*, 2016; Molina *et al.*, 2016a; Molina *et al.*, 2016b; Salsarola *et al.*, 2015; Lowe *et al.*, 2013; Solla *et al.*, 2012; Schultz & Martin, 2012; González-Jorge *et al.*, 2012; Schultz & Martin, 2011; Schultz, 2008; Schultz *et al.*, 2006; Schultz *et al.*, 2002) and 900 MHz (Pringle *et al.*, 2020;

Pringle *et al.*, 2016; Almeida *et al.*, 2015; Almeida *et al.*, 2014; Hansen & Pringle, 2013; Pringle *et al.*, 2012a; Pringle *et al.*, 2012b; Pringle *et al.*, 2008; Freeland *et al.*, 2003; Schultz *et al.*, 2002; Freeland *et al.*, 2002; Hammon *et al.*, 2000), both employed in 40% of the controlled sites. The 500 MHz frequency appears most often associated with sandy soils, while the 900 MHz frequency was most often associated with clay and sandy-clay soils. The 500 MHz frequency provided good results in tracking the evolution of decomposition with a satisfactory resolution to depth ratio.

Of the 30 articles analyzed, in 53.3% the choice was to use only GPR for the target analyses. In the remaining 46.7% the GPR appeared associated with other geophysical techniques such as electroresistivity (Pringle *et al.*, 2020; Cavalcanti *et al.*, 2018; Molina *et al.*, 2016a; Pringle *et al.*, 2016; Molina *et al.*, 2016b; Hansen & Pringle, 2013; Pringle *et al.*, 2012a; Pringle *et al.*, 2012b; Pringle *et al.*, 2008; Powell, 2004), magnetic susceptibility (Molina *et al.*, 2016a; Molina *et al.*, 2016b; Hansen & Pringle, 2013; Pringle *et al.*, 2012b; Pringle *et al.*, 2008), microwave tomography (Almeida *et al.*, 2014), terrestrial laser scanning (González-Jorge *et al.*, 2012), and magnetic gradiometry (Hansen & Pringle, 2013; Pringle *et al.*, 2008).

Uncontrolled Sites

This group represents 37.5% of the total SLR articles and their publications occurred between the years 2007 and 2019. The main objectives included: highlighting the importance of geophysical methods by reporting their results, proposing general requirements for field operations, presenting research results and documenting investigations,

assisting in locating human remains and determining the location of unmarked graves.

The most frequently investigated site type in this thematic group was cemetery (Damiata *et al.*, 2017; Aziz *et al.*, 2016; Barone *et al.*, 2016; Hansen *et al.*, 2014; Büyüksaraç *et al.*, 2013; Doolittle & Bellantoni, 2010; Fiedler *et al.*, 2009) which was present in 38.8% of the reviewed articles, but investigations of clandestine graves were also frequent (Wisniewski *et al.*, 2019; Abate *et al.*, 2019; Novo *et al.*, 2011; Ruffell *et al.*, 2009b) present in 22.2% of the reviewed articles. The soil types that were most present in this group were clay soils (Rubio-Melendi *et al.*, 2018; Aziz *et al.*, 2016; Hansen *et al.*, 2014; Billinger, 2009; Ruffell *et al.*, 2009a; Fiedler *et al.*, 2009; Ruffell *et al.*, 2009b) found in 38.8% of articles and sandy (Wisniewski *et al.*, 2019; Abate *et al.*, 2019; Rubio-Melendi *et al.*, 2018; Aziz *et al.*, 2016; Hansen *et al.*, 2014; Forbes *et al.*, 2013), which appeared in 33.3% of articles.

In 94.4% of the articles in this group the targets sought were human bodies (Wisniewski *et al.*, 2019; Abate *et al.*, 2019; Barone & Di Maggio, 2019; Rubio-Melendi *et al.*, 2018; Damiata *et al.*, 2017; Aziz *et al.*, 2016; Fernández-Álvarez *et al.*, 2016; Barone *et al.*, 2016; Hansen *et al.*, 2014; Büyüksaraç *et al.*, 2013; Novo *et al.*, 2011; Doolittle & Bellantoni, 2010; Billinger, 2009; Ruffell *et al.*, 2009a; Fiedler *et al.*, 2009; Ruffell *et al.*, 2009b; Schultz, 2007), whether in recent crime burials or in cemeteries where bodies have already been buried for years. In 5.5% of articles the searched target was the grave of a buried dog (Forbes *et al.*, 2013).

The center frequencies used in GPR surveys ranged from 100 MHz to 500 MHz. The most commonly used frequencies were 500 MHz (Barone & Di Maggio, 2019; Rubio-Melendi *et al.*, 2018; Damiata *et al.*, 2017; Fernández-Álvarez *et al.*, 2016; Barone *et al.*, 2016; Forbes *et al.*, 2013) employed in 33.3% of target investigations and the 250MHz (Wisniewski *et al.*, 2019; Rubio-Melendi *et al.*, 2018; Aziz *et al.*, 2016; Büyüksaraç *et al.*, 2013; Novo *et al.*, 2011) used in 27.7% of articles. The 500 MHz frequency appears most often associated with sandy soils while the 250 MHz frequency appears most often associated with sandy and clay soils. In 50% of the articles, the choice was to use GPR associated with other complementary techniques which were quite varied and included: conductivity and magnetic susceptibility (Wisniewski *et al.*, 2019), metal detector (Wisniewski *et al.*, 2019; Ruffell *et al.*, 2009a; Ruffellet *et al.*, 2009b), aerial photography (Abate *et al.*, 2019; Ruffell *et al.*, 2009a), unmanned aerial vehicles (Abate *et al.*, 2019), time-domain reflectometry (Damiata *et al.*, 2017), terrestrial laser scanning (Aziz *et al.*, 2016), electroresistivity (Hansen *et al.*, 2014), victim recovery dogs (Ruffell *et al.*, 2009b) and geographic profiling (Ruffel *et al.*, 2009b) while in the other 50% of the articles only the GPR method was used for the target analysis.

Uncontrolled Sites

This group represents 37.5% of the total SLR articles and their publications occurred between the years 2007 and 2019. The main objectives included: highlighting the importance of geophysical methods by reporting their results, proposing general requirements for field operations, presenting research results and documenting investigations, assisting in locating human remains and determining the location of unmarked graves.

Table 4 – Main parameters used in the Uncontrolled Site surveys. ER= Electroresistivity; ERT= Electrical Tomography; MS= Magnetic Susceptibility; MC= Magnetic Conductivity; TDR= Time Domain Reflectometry; MD= Metal Detector; TLS= Terrestrial Laser Scanning; UAV= Unmanned Aerial Vehicle; GIS= Geographic Information System; VRD= Victim Recovery Dogs.

Reference	Goals	Site Type	Predominant soil type	Target type	Center frequency (MHz)	Complementary techniques	Main results
Wisniewski et al 2019	Document investigations and discuss how geoscience can assist law enforcement in future archived searches.	Clandestine grave	Sandy	Murder Victim	250	MS, MC and MD	Geophysical anomalies were identified and the most promising ones were investigated in a detailed manner.
Abate et al 2019	Locate mass graves and mass graves and increase the excavation recovery rate of the Missing Persons Committee in Cyprus.	Unmarked graves	Site 1: sandy; site 2: not mentioned	Missing Persons	400	Continuous aerial photography, UAV and GIS	There was the effectiveness of the techniques in defining the search parameters for potential burial sites.
Barone et al 2019	Highlight non-destructive geophysical techniques to help find missing persons.	Natural cave	Volcanic tuff	Missing person	500	-	The results accurately located and defined the searched target.
Rubio-Melendi et al 2018	Detail a non-invasive study at the El Salvador Cemetery in the city of Oviedo, northern Spain.	Mass grave	Sandy and clayey horizons	Unmarked graves	250, 500	ERT	The results established the boundaries of the mass grave, as well as extending the knowledge about the internal structure of the grave.
Damiata et al 2017	Report results of a survey using GPR on a Viking Age Christian cemetery.	Cemetery	Andosol	25 graves	500	TDR	All the profiles collected on the skeletons have hyperbolae to some degree.

Aziz et al 2016	Use GPR and TLS to locate and characterize unmarked graves in the Mueschke Cemetery in Houston, Texas.	Cemetery	Sandy / clayey Sandy / clayey	Graves	250	TLS	GPR surveys produced anomalies that were consistent with gravestones and cemetery records.
Fernández-Álvarez et al 2016	Detail the geoforensic search for a Spanish Civil War mass grave.	Mass grave	Silty matrix	Human cadavers	500	-	Clear geophysical anomalies in 2D GPR profiles and remains were successfully discovered.
Barone et al 2016	Present partial results of a GPR search conducted at the Non-Catholic Cemetery in Rome (Italy).	Cemetery	Not mentioned	Gravestones	500	-	The GPR survey was able to discern several anomalies beneath the surface of the Ancient Cemetery.
Hansen et al 2014	To identify the locations of unmarked graves in cemeteries.	Cemetery	Clayey / sandy / alluvium	Unmarked graves	225, 450	ER	The targets were identified effectively using 2D GPR and ER profiles.
Büyüksaraç et al 2013	Determine whether it is possible to use geophysical imaging methods to locate unmarked graves.	Cemetery	Not mentioned	Lost graves	250	ERT and magnetic imaging surveys	The results showed that the methods used are suitable for delineating buried historic sites.
Forbes et al 2013	Use GPR to locate the remains of a dog buried in Canada.	In natural área	Sandy	Buried dog's grave	500	-	The GPR survey was able to accurately identify the location of the investigated grave.
Novo et al 2011	Assisting police investigations.	Clandestine burial	Massive limestone	Murder victim and pickaxe	250	-	The 250 MHz antenna allowed a good fit between target detection, dense acquisition grid, and an extensive survey area.
Billinger 2009	Assist an investigation conducted by the Edmonton Police Service in Alberta, Canada.	The basement of a house	(Clay below basement)	Human cadavers	Not mentioned	-	Positive results were obtained from the GPR analysis, but the excavation was not successful.
Doolittle et al 2010	Identify clandestine and unmarked graves.	Cemeteries	Not mentioned	Unmarked graves	400	-	GPR brought improvements to the identification of unmarked graves in Connecticut.
Ruffell et al 2009a	Confirm the location of a cemetery, assess the number of burials and depth	Mass grave	Clayey	Graves	100, 200, 400	Aerial photography, MD, magnetometric	About 170 anomalies compatible with burials were identified in 200 MHz

	by geophysical survey and measurement.					and electromagnetic survey	GPR data, 84 of which coincided with surface collapses.
Fiedler et al 2009	Determine the location of unmarked graves in cemeteries.	Cemetery	Clayey	95 graves	400	-	GPR proved reliable in determining the exact location of the investigated targets.
Ruffell et al 2009b	Investigate an area of depressed ground with features consistent with a clandestine burial.	Clandestine burial	Clayey	Homicide victim	225	VRD, MD and geographic profiles	GPR showed a hyperbolic anomaly. The investigation showed no evidence of excavation for burial purposes.
Schultz 2007	Provide a discussion of GPR methodology and implementation of this technology by law enforcement agencies.	Burial under a cement slab	Not applicable	Two buried bodies	Not mentioned	-	The results indicated a large disturbance and a skeleton was located in the area studied.

DISCUSSION

Thematically the reviewed papers cover a wide range of scenarios encountered in forensic studies. New scopes of investigations include the comparison of GPR image features for multiple burial scenarios and evaluation of the changing geophysical response of simulated mass graves over the years.

Research generally involves the integration of more than one method. While the use of electroresistivity, susceptibility, and magnetic conductivity have been common methods used for locating grave targets and objects, integration with other indirect methods such as metal detectors can be important in initiating searches for metallic objects such as weapons or even belts that are wearing the grave victims. The application of geophysical methods is gaining popularity and GPR has become a common geophysical option for forensic investigations because, besides being effective in locating buried targets, it can be integrated with other methods as part of a protocol for forensic target search. A major advantage of using GPR for buried target searches is the speed with which the method is employed and returns results for interpretation.

A common goal raised in the articles was the demand to adopt a protocol proposal with requirements for field operations, establishing methodologies for forensic search, processing, and analysis of collected data. Thus determining general requirements such as equipment configuration and how the processing of the data obtained in the field should be managed when searching for forensic targets. Prerequisites for using GPR include analysis of the type of soil being studied, as well as the depth and type of

target.

From the articles reviewed, the timing of this research reflects strong experimentation with new technologies with the potential for integration with GPR, although, in parallel, there is still a search to understand the advantages and disadvantages that these techniques can imprint on forensic research.

One of the advantages of GPR is that it can be used to search for forensic targets under asphalt and concrete without the need for excavation. Thus GPR is used to determine the location of possible burials under concrete and under these conditions, there was discussion about false-positive results through analysis of GPR data in only 2.1% of the articles. The results of GPR analysis can only be properly interpreted by individuals with significant experience. The presence of a signature on radargrams can lead to misinterpretations of targets buried under the concrete which highlights the importance of experienced interpreters and the use of complementary techniques.

CONCLUSIONS

The main objective of this SLR was to analyze the advances in forensic research in the identification of bodies in different burial scenarios with the help of the GPR geophysical method, and this objective was achieved as can be seen in the results. In a complementary way, it was aimed to indicate the

common characteristics of the controlled sites, the limitations in the use of GPR, and which are the real improvements in the use of complementary geophysical methods in this thematic as it was evidenced in the results and discussions mentioned above. Geophysical methods

play an important role in the non-destructive detection of buried or hidden targets. The non-invasive nature of geophysical methods is of particular value in forensic geophysics and can provide quick answers in criminal investigations, for example.

This review article highlights the most promising areas and presents a basis for the scientific development of forensic geophysics. Recommendations for further research should include the nature of the environment, the influence of physical parameters on the identification of human evidence in forensic investigations using GPR, and the determination of gas concentration variations related to the decomposition of organic material from forensic targets, being the current object of the authors' research that will rely on the laboratory analysis of soil samples for moisture monitoring, GPR imaging for analysis of soil moisture variation, evaluation of the influence of clay content on target detection using GPR imaging, and measurement of the variation of CH₄ and CO₂ concentration associated with

decomposition of organic target tissues.

Using all possible techniques and

devices although comprehensive can be expensive and time-consuming a good approach is to use a combination of two methods which can be helpful in a possible ambiguity in data interpretation. Surveys with the integration of GPR with magnetic susceptibility are indicated when the targets include small metal objects. Electroresistivity is another complementary technique with potential as it has a fast collection time, good detection rates, and simpler data processing than GPR. The 500MHz frequency, one of the most widely used, brought better results in tracking the evolution of decomposition with a satisfactory resolution to depth ratio. From the analysis of the results, we conclude that the research on the use of GPR in forensic geophysics is seeking to highlight the ability of the method to identify targets in multiple burial scenarios with different sizes and depths and burials in various circumstances. Such as covered bodies by different materials, e.g. rubble, wrapped in plastic, with and without clothing, and to understand its limitations.

REFERENCES

- ABATE D, COLLS SC, MOYSSI N, KARSILI D, FAKA M, ANILIR A & MANOLIS S. 2019. Optimizing search strategies in mass grave location through the combination of digital technologies. *Forensic Science International* 1: 95–107. DOI: 10.1016/j.fsisyn.2019.05.002
- ALMEIDA ER, PORSANI JL, CATAPANO I, GENNARELLI G & SOLDOVIERI F. 2014. GPR data analysis enhanced by microwave tomography for forensic archaeology. *Proceedings of the 15th International Conference on*

- Ground Penetrating Radar. 474–478. DOI: 10.1109/ICGPR.2014.6970470
- ALMEIDA ER, PORSANI JL, CATAPANO I, GENNARELLI G & SOLDOVIERI F. 2015 Microwave Tomography-Enhanced GPR in Forensic Surveys: The Case Study of a Tropical Environment. *IEEE Journal of Selected Topics in Applied Earth Observations and Remote Sensing* 9:115–124. DOI: 10.1109/jstars.2015.2466556
- AZIZ AS, STEWART R, GREEN S & FLORES J. 2016 Locating and characterizing burials using 3D ground-penetrating radar (GPR) and terrestrial laser scanning (TLS) at the historic Mueschke Cemetery, Houston, Texas. *Journal of Archaeological Science: Reports* 8: 392–405. DOI: 10.1016/j.jasrep.2016.06.035
- BARONE PM, SWANGER KJ, STANLEY-PRICE N & THURSFIELD A. 2016. Finding graves in a cemetery: Preliminary forensic GPR investigations in the Non-Catholic Cemetery in Rome (Italy). *Measurement* 80: 53–57. DOI: 10.1016/j.measurement.2015.11.023
- BARONE PM & DI MAGGIO RM. 2019. Forensic geophysics: ground penetrating radar (GPR) techniques and missing persons investigations. *Forensic Sciences Research* 4: 337–340. DOI: 10.1080/20961790.2019.1675353
- BENEFIELD LE. 2003. Implementing Evidence-Based Practice in Home Care. *Home Healthcare Nurse: The Journal for the Home Care and Hospice Professional* 21: 804–809. DOI: 10.1097/00004045-200312000-00005
- BEVAN BW. 1991. The search for graves. *Geophysics* 56: 1310–1319. DOI: 10.1190/1.1443152
- BILLINGER MS. 2009. Utilizing Ground Penetrating Radar for the Location of a Potential Human Burial under Concrete. *Canadian Society of Forensic Science Journal* 42: 200–209. DOI: 10.1080/00085030.2009.1075760
- BOOTH AD & PRINGLE JK. 2016. Semblance analysis to assess GPR data from a five-year forensic study of simulated clandestine graves. *Journal of Applied Geophysics* 125: 37–44. DOI: 10.1016/j.jappgeo.2015.11.016
- BÜYÜKSARAÇ A, YALÇINER CC, EKİNCİ YL, DEMIRCI A & YÜCEL AM. 2013. Geophysical investigations at Agadere Cemetery, Gallipoli Peninsular, NW Turkey. *Australian Journal of Forensic Sciences* 46: 111–123. DOI: 10.1080/00450618.2013.804948
- CAVALCANTI MM, ROCHA MP, BLUM MLB & BORGES WR. 2018. The forensic geophysical controlled research site of the University of Brasilia, Brazil: Results from methods GPR and electrical resistivity tomography. *Forensic Science International* 293: e1–101.e21. DOI: 10.1016/j.forsciint.2018.09.033
- CHEETHAM P. 2005. Forensic geophysical survey. In J. Hunter and M. Cox (eds.). *Forensic Archaeology: Advances in Theory and Practice*: 62–95.
- DAMIATA BN, STEINBERG JM,

- BOLENDER DJ, ZOËGA G & SCHOENFELDER JW. 2017. Subsurface imaging a Viking-Age churchyard using GPR with TDR: Direct comparison to the archaeological record from an excavated site in northern Iceland. *Journal of Archaeological Science: Reports* 12: 244–256. DOI: 10.1016/j.jasrep.2017.01.004
- DAVENPORT GC. 2001. Remote sensing applications in forensic investigations. *Hist Arch* 35: 87–100. DOI: 10.1007/BF03374530
- DICK HC & PRINGLE JK. 2018. Inorganic elemental analysis of decomposition fluids of an in situ animal burial. *Forensic Science International* 289: 130–139. DOI: 10.1016/j.forsciint.2018.05.034
- DOOLITTLE JA & BELLANTONI NF. 2010. The search for graves with ground-penetrating radar in Connecticut. *Journal of Archaeological Science* 37: 941–949. DOI: 10.1016/j.jas.2009.11.027
- FERNÁNDEZ-ÁLVAREZ JP, RUBIO-MELENDI D, MARTÍNEZ-VELASCO A, PRINGLE JK & AGUILERA HD. 2016. Discovery of a mass grave from the Spanish Civil War using Ground Penetrating Radar and forensic archaeology. *Forensic Science International* 267: e10–e17. DOI: 10.1016/j.forsciint.2016.05.040
- FIEDLER S, ILLICH B, BERGER J & GRAW M. 2009. The effectiveness of ground-penetrating radar surveys in the location of unmarked burial sites in modern cemeteries. *Journal of Applied Geophysics* 68: 380–385. DOI: 10.1016/j.jappgeo.2009.03.003
- FORBES SL, HULSMAN S & DOLDERMAN M. 2013.
- Locating Buried Canine Remains Using Ground Penetrating Radar. *Canadian Society of Forensic Science Journal* 46: 51–58. DOI: 10.1080/00085030.2013.1075719
6
- FRANCE DL, GRIFFIN TJ, SWANBURG JG, LINDEMANN JW, DAVENPORT GC, TRAMMEL V, ARMBRUST CT, KONDRAEFF B, NELSON A, CASTELLANO K & HOPKINS D. 1992. A Multidisciplinary Approach to the Detection of Clandestine Graves. *Journal of Forensic Science* 37: 1445–1458.
- FREELAND RS, YODER RE, MILLER ML & KOPPENJAN S. 2002. Forensic application of sweep-frequency and impulse GPR. *Ninth International Conference on Ground Penetrating Radar* 4758: 533–538. DOI: 10.1117/12.462241
- FREELAND RS, MILLER ML, YODER RE & KOPPENJAN S. 2003. Forensic Application of FM-CW and Pulse Radar. *Journal of Environmental and Engineering Geophysics* 8: 97–103. DOI: 10.4133/jegg8.2.97
- GALVÃO TF, PANSANI TSA & HARRAD D.. 2015. Principais itens para relatar Revisões sistemáticas e Meta-análises: A recomendação PRISMA. *Epidemiologia e Serviços de Saúde* 24: 335–342. DOI: 10.5123/s1679-49742015000200017
- GONZÁLEZ-JORGE H, SOLLA M, MARTÍNEZ-SÁNCHEZ J & ARIAS P. 2012. Comparison between laser scanning, single-image

- rectification and ground-penetrating radar technologies in forensic science. *Measurement* 45: 836–843. DOI: 10.1016/j.measurement.2012.02.013
- HAMMON WS, MCMECHAN GA & ZENG X. 2000. Forensic GPR: finite-difference simulations of responses from buried human remains. *Journal of Applied Geophysics* 45: 171–186. DOI: 10.1016/s0926-9851(00)00027-6
- HANSEN JD & PRINGLE JK. 2013. Comparison of magnetic, electrical and ground penetrating radar surveys to detect buried forensic objects in semi-urban and domestic patio environments. Geological Society, London, Special Publications 384: 229–251. DOI: 10.1144/sp384.13
- HANSEN JD, PRINGLE JK & GOODWIN J. 2014. GPR and bulk ground resistivity surveys in graveyards: Locating unmarked burials in contrasting soil types. *Forensic Science International* 237: e14–e29. DOI: 10.1016/j.forsciint.2014.01.009
- LOWE A, BERESFORD D, CARTER D, GASPARI F, O'BRIEN R & FORBES S. 2013. Ground penetrating radar use in three contrasting soil textures in southern Ontario. Geological Society, London, Special Publications 384: 221–228. DOI: 10.1144/sp384.12
- MILLER ML, FREELAND RS & KOPPENJAN S. 2002. Searching for concealed human remains using GPR imaging of decomposition. Ninth International Conference on Ground Penetrating Radar 4758. DOI: 10.1117/12.462240
- MOLINA CM, PRINGLE JK, SAUMET M & HERNÁNDEZ O. 2015. Preliminary results of sequential monitoring of simulated clandestine graves in Colombia, South America, using ground penetrating radar and botany. *Forensic Science International* 248: 61–70. DOI: 10.1016/j.forsciint.2014.12.011
- MOLINA CM, PRINGLE JK, SAUMET M & EVANS GT. 2016a. Geophysical and botanical monitoring of simulated graves in a tropical rainforest, Colombia, South America. *Journal of Applied Geophysics* 135: 232–242. DOI: 10.1016/j.jappgeo.2016.10.002
- MOLINA CM, PRINGLE JK, SAUMET M & EVANS GT. 2016b. Geophysical monitoring of simulated graves with resistivity, magnetic susceptibility, conductivity and GPR in Colombia, South America. *Forensic Science International* 261: 106–115. DOI: 10.1016/j.forsciint.2016.02.009
- NOBES DC, FERGUSON RJ & BRIERLEY GJ. 2001. Ground-penetration radar and sedimentological analysis of Holocene Floodplains: Insight from the Tuross valley, New South Wales. *Australian Journal of Earth Science* 48: 437–355.
- NOVO A, LORENZO H, RIAL FI & SOLLA M. 2011. 3D GPR in forensics: Finding a clandestine grave in a mountainous environment. *Forensic Science International* 204: 134–138. DOI: 10.1016/j.forsciint.2010.05.019
- OWSLEY DW. 1995. Techniques for

- Locating Burials, With Emphasis on the Probe. *Journal of Forensic Sciences* 40: 735–740.
- PARKER R, RUFFEKK A, HUGHES D & PRINGLE JK. 2010. Geophysics and the search of freshwater bodies: A review. *Science & Justice* 50: 141–149. DOI: 10.1016/j.scijus.2009.09.001
- PORRITT K, GOMERSALL J & LOCKWOOD C. 2014. JBI's Systematic Reviews. *AJN, American Journal of Nursing* 114: 47–52. DOI: 10.1097/01.naj.0000450430.97383.64
- POWELL K. 2004. Detecting buried human remains using near-surface geophysical instruments. *Exploration Geophysics* 35: 88–92. DOI: 10.1071/eg04088
- PRINGLE JK, JERVIS J, CASELLA JP & CASSIDY NJ. 2008. Time-Lapse Geophysical Investigations over a Simulated Urban Clandestine Grave. *Journal of Forensic Sciences* 53. DOI: 10.1111/j.1556-4029.2008.00884.x
- PRINGLE JK, JERVIS JR, HANSEN JD, JONES GM, CASSIDY NJ & CASELLA JP. 2012a. Geophysical Monitoring of Simulated Clandestine Graves Using Electrical and Ground-Penetrating Radar Methods: 0-3 Years After Burial. *Journal of Forensic Sciences* 57: 1467–1486. DOI: 10.1111/j.1556-4029.2012.02151.x
- PRINGLE JK, HOLLAND C, SZKORNÍK K & HARRISON M. 2012b. Establishing forensic search methodologies and geophysical surveying for the detection of clandestine graves in coastal beach environments. *Forensic Science International* 219: e29–e36. DOI: 10.1016/j.forsciint.2012.01.010
- PRINGLE JK, JERVIS JR, ROBERTS D, DICK HC, WISNIEWSKI KC, CASSIDY NJ & CASELLA JP. 2016. Long-term Geophysical Monitoring of Simulated Clandestine Graves using Electrical and Ground Penetrating Radar Methods: 4-6 Years After Burial. *Journal of Forensic Sciences* 61: 309–321. DOI: 10.1111/1556-4029.13009
- PRINGLE JK, STIMPSON IG, WISNIEWSKI KC, HEATON V, DAVENWARD B, MIROSCH N, SPENCER F & JERVIS JR. 2020. Geophysical monitoring of simulated homicide burials for forensic investigations. *Scientific Reports* 10. DOI: 10.1038/s41598-020-64262-3
- PUDOVA N, URUSOVA A, SHIROBOKOV M & MARCHKOV A. 2016. Developing GPR surveys, data processing and interpretation techniques for criminal gravesites location. 16th International Conference on Ground Penetrating Radar (GPR): 1–5. DOI: 10.1109/ICGPR.2016.7572616.
- RUBIO-MELENDI D, GONZALEZ-QUIRÓS A, ROBERTS D, GARCÍA MCG, DOMÍNGUEZ AC, PRINGLE JK & FERNÁNDEZ-ÁLVAREZ JP. 2018. GPR and ERT detection and characterization of a mass burial, Spanish Civil War, Northern Spain. *Forensic Science International* 287: e1–e9. DOI: 10.1016/j.forsciint.2018.03.034

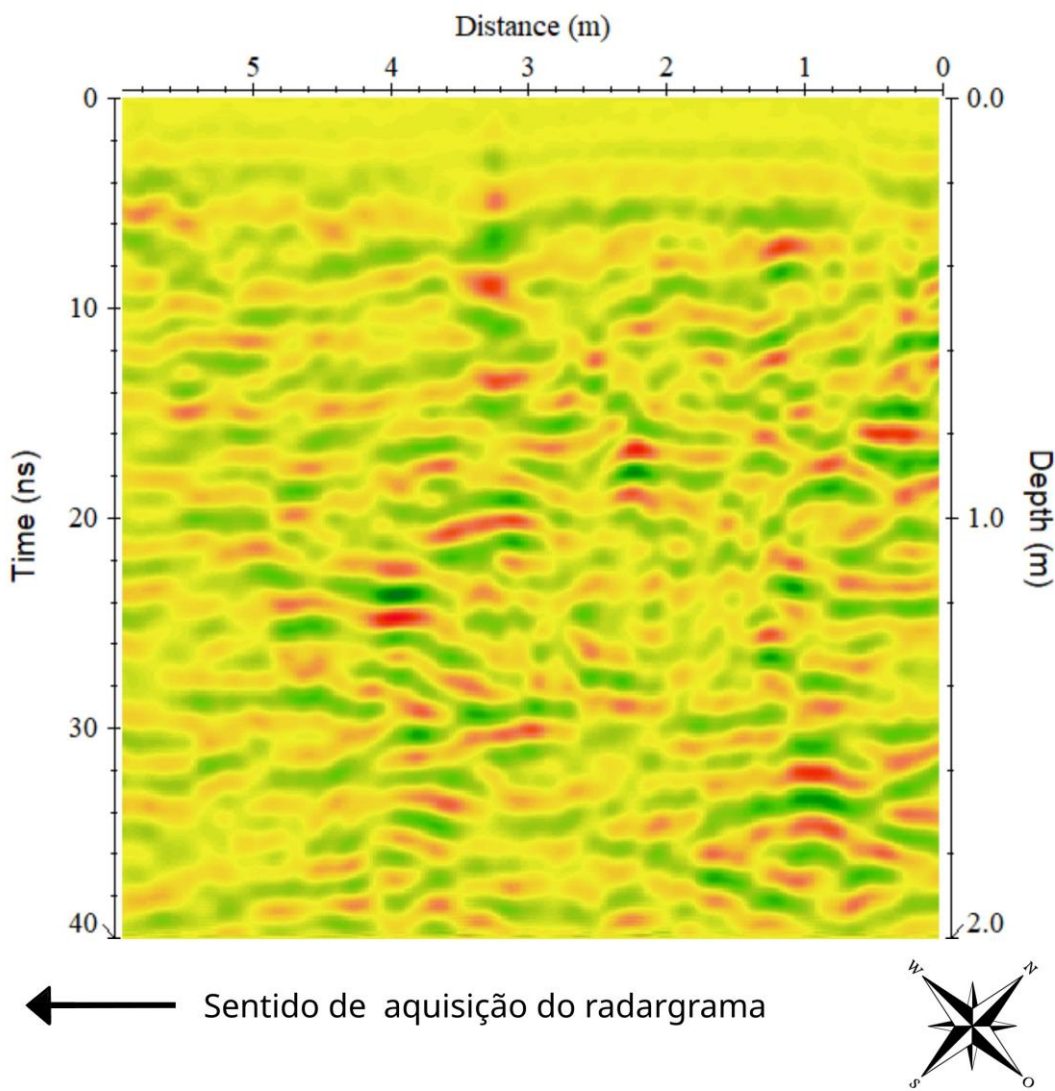
- RUFFELL A & MCKINLEY J. 2005. Forensic geoscience: applications of geology, geomorphology and geophysics to criminal investigations. *Earth-Science Reviews* 69: 235–247. DOI: 10.1016/j.earscirev.2004.08.002
- RUFFELL A, MCCABE A, DONNELLY C & SLOAN B. 2009a. Location and Assessment of an Historic (150-160 Years Old) Mass Grave Using Geographic and Ground Penetrating Radar Investigation, NW Ireland. *Journal of Forensic Sciences* 54: 382–394. DOI: 10.1111/j.1556-4029.2008.00978.x
- RUFFELL A, DONNELLY C, CARVER N, MURPHY E, MURRAY E & MCCAMBRIDGE J. 2009b. Suspect burial excavation procedure: A cautionary tale. *Forensic Science International* 183: e11–e16. DOI: 10.1016/j.forsciint.2008.10.013
- RUFFELL A, PRINGLE JK, CASSELLA JP, MORGAN RM, FERGUSONM, HEATON V, HOPE C & MCKINLEY JM. 2017. The use of geoscience methods for aquatic forensic searches. *Earth-Science Reviews* 171:323–337. DOI: 10.1016/j.earscirev.2017.04.012
- SALSAROLA D, POPPA P, AMADAS A, MAZZARELLI D, GIBELLI D, ZANOTTI E, PORTA D & CATTANEO C. 2015. The utility of ground-penetrating radar and its time-dependence in the discovery of clandestine burials. *Forensic Science International* 253: 119–124. DOI: 10.1016/j.forsciint.2015.06.006
- SCHULTZ JJ, FALSETTI AB, COLLINS M, KOPPENJAN S & WARREN MW.. 2002. Detection of forensic burials in Florida using GPR. Ninth International Conference on Ground Penetrating Radar 4758. DOI: 10.1117/12.462239
- SCHULTZ JJ, COLLINS ME & FALSETTI AB. 2006. Sequential Monitoring of Burials Containing Large Pig Cadavers Using Ground-Penetrating Radar. *Journal of Forensic Sciences* 51: 607–616. DOI: 10.1111/j.1556-4029.2006.00129.x
- SCHULTZ JJ. 2007. Using Ground-Penetrating Radar to Locate Clandestine Graves of Homicide Victims. *Homicide Studies* 11: 15–29. DOI: 10.1177/1088767906296234
- SCHULTZ JJ. 2008. Sequential Monitoring of Burials Containing Small Pig Cadavers Using Ground Penetrating Radar. *Journal of Forensic Sciences* 53: 279–287. DOI: 10.1111/j.1556-4029.2008.00665.x
- SCHULTZ JJ & MARTIN MM. 2011. Controlled GPR grave research: Comparison of reflection profiles between 500 and 250MHz antenna. *Forensic Science International* 209: 64–69. DOI: 10.1016/j.forsciint.2010.12.012
- SCHULTZ JJ & MARTIN MM. 2012. Monitoring controlled graves representing common burial scenarios with ground penetrating radar. *Journal of Applied Geophysics* 83: 74–89. DOI: 10.1016/j.jappgeo.2012.05.006
- SCHULTZ JJ, HEALY CA, PARKER K & LOWERS B. 2013. Detecting submerged objects: The application of side scan sonar to forensic contexts. *Forensic*

- Science International 231: 306–316. DOI: 10.1016/j.forsciint.2013.05.032
- SCHULTZ JJ, WALTER BS & HEALY C. 2016. Long-term sequential monitoring of controlled graves representing common burial scenarios with ground penetrating radar: Years 2 and 3. Journal of Applied Geophysics 132: 60–74. DOI: 10.1016/j.jappgeo.2016.06.015
- SOLLA M, RIVEIRO B, ÁLVAREZ MX & ARIAS P. 2012. Experimental forensic scenes for the characterization of ground-penetrating radar wave response. Forensic Science International 220: 50–58. DOI: 10.1016/j.forsciint.2012.01.025
- SCHOOR M, NIENABER WC & MARAIS-WERNER A. 2017. A controlled monitoring study of simulated clandestine graves using 3D ground penetrating radar. Near Surface Geophysics 15: 274–284. DOI: 10.3997/1873-0604.2017007
- Systematic Reviews: CRD's guidance for undertaking reviews in health care. [s.l.: s.n.]. Disponível em: <https://www.york.ac.uk/media/crd/Systematic_Reviews.pdf>.
- WISNIEWSKI K, COOPER N, HEATON V, HOPE C, PIRRIE D, MITTEN AJ & PRINGLE JK. 2019. The Search for “Fred”: An Unusual Vertical Burial Case. J Forensic Sci 64: 1530–1539. DOI: 10.1111/1556-4029.14035
- Websites:**
- CAPES/MEC - Coordenação de Aperfeiçoamento de Pessoal de Nível Superior/Ministério da Educação. Portal de Periódicos, 2021. Comunidade Acadêmica Federada (CAFé). Available online: <http://periodicos.capes.gov.br/> (accessed on 16 June 2021).
- StArt – LaPES – Laboratório de Pesquisa em Engenharia de Software. Software State of the Art through Systematic Review. Versão 3.3 Beta 03 Ufscar.br. Available online: http://lapes.dc.ufscar.br/tools/start_tool (accessed on 26 October 2020).

C – RADARGRAMAS OBTIDOS NO PERÍODO DE SECA**C1 – RADARGRAMAS 2D OBTIDOS PARALELAMENTE NO PERÍODO DE SECA**

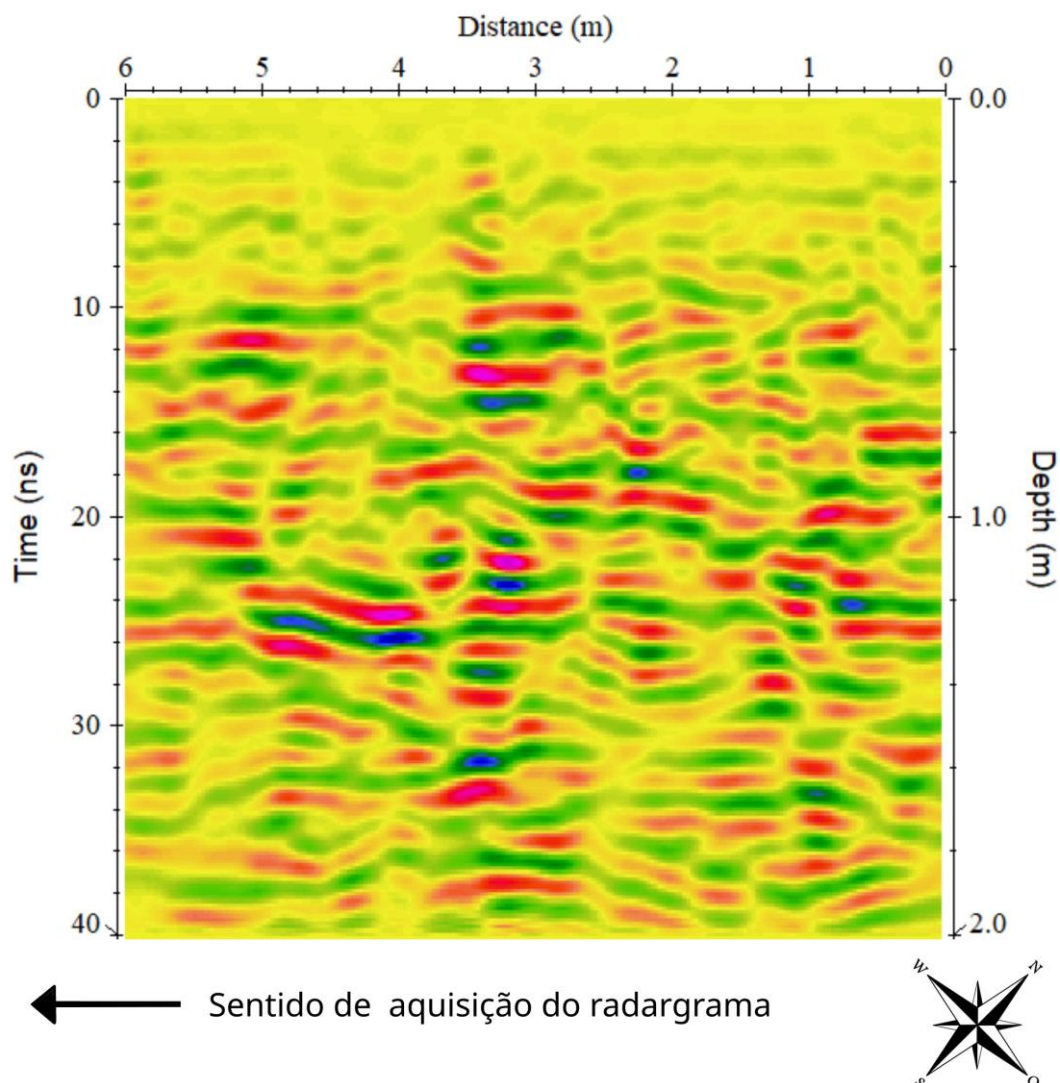
Radargrama obtido fora das SEP's 01 e 02

Frequência de 400 MHZ.



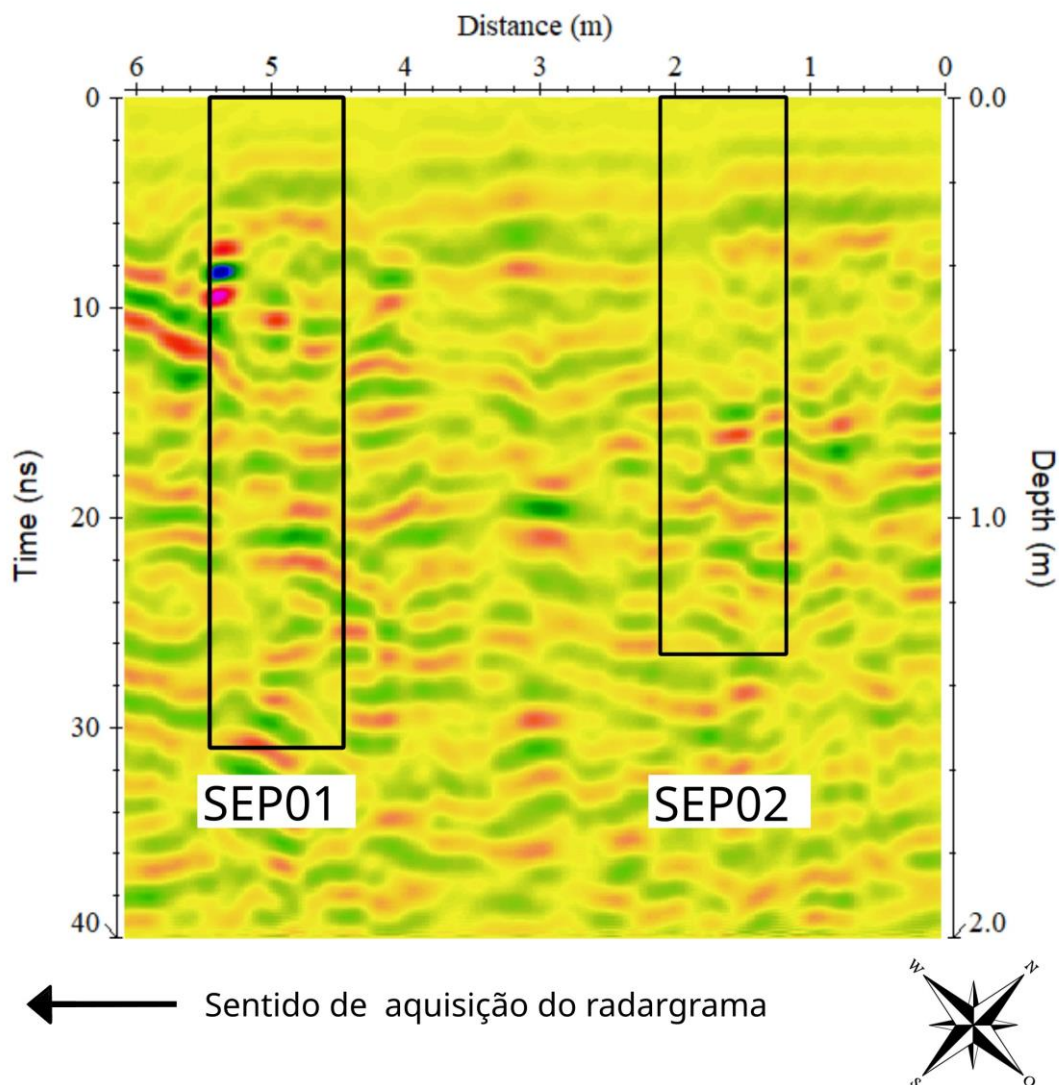
Radargrama obtido fora das SEP's 01 e 02

Frequência de 900 MHZ.



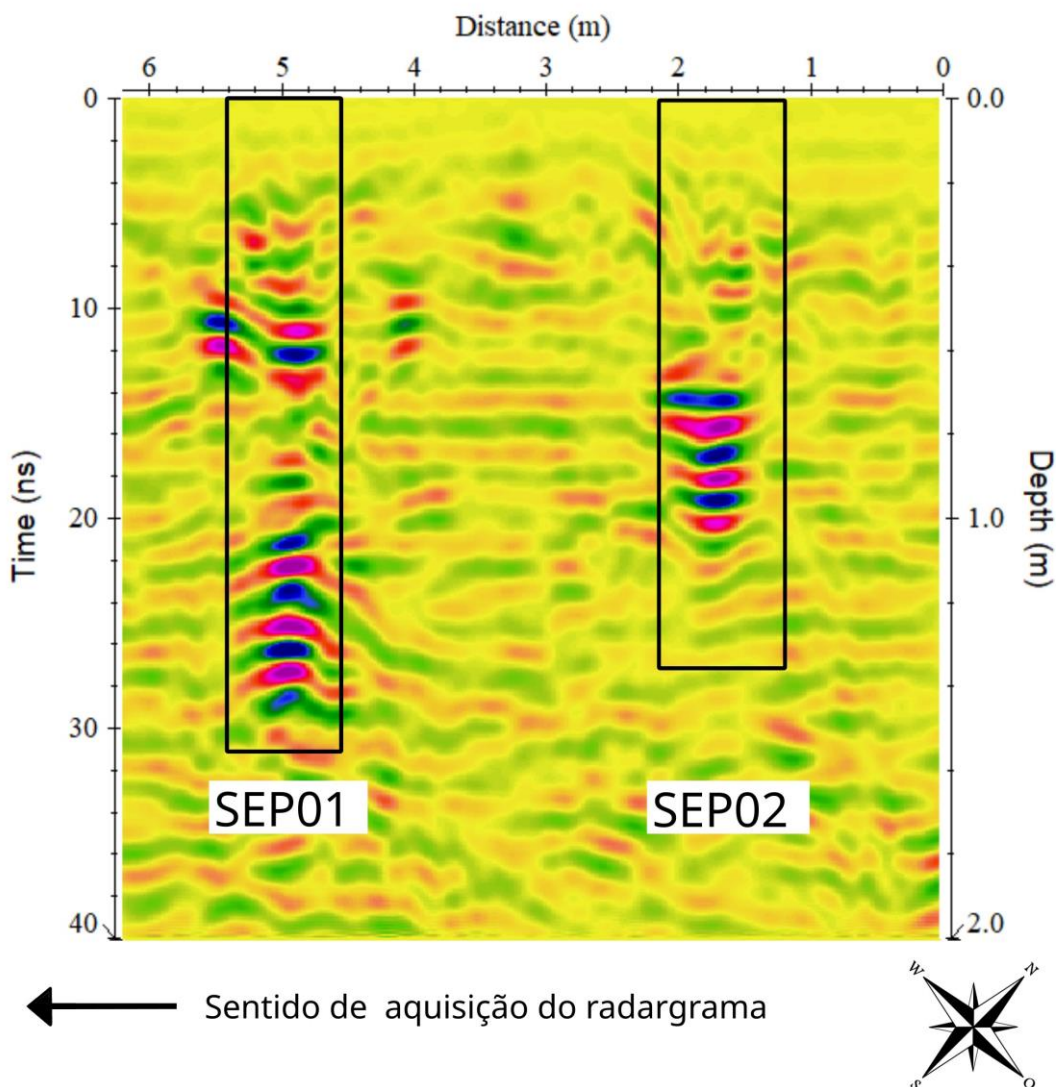
Radargrama obtido dentro das SEP's 01 e 02

Frequência de 400 MHZ.



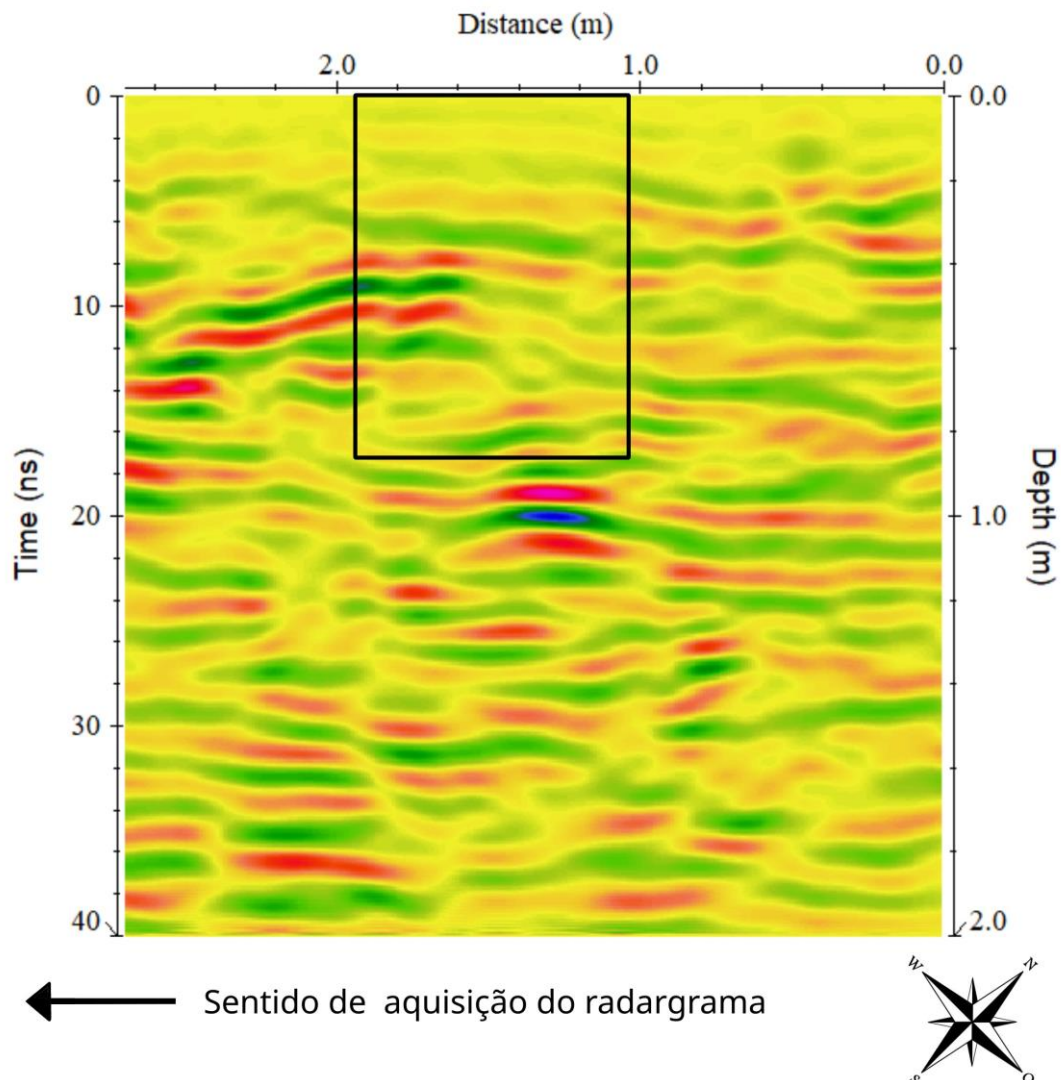
Radargrama obtido sobre o alvo nas SEP's 01 e 02

Frequência de 400 MHZ.



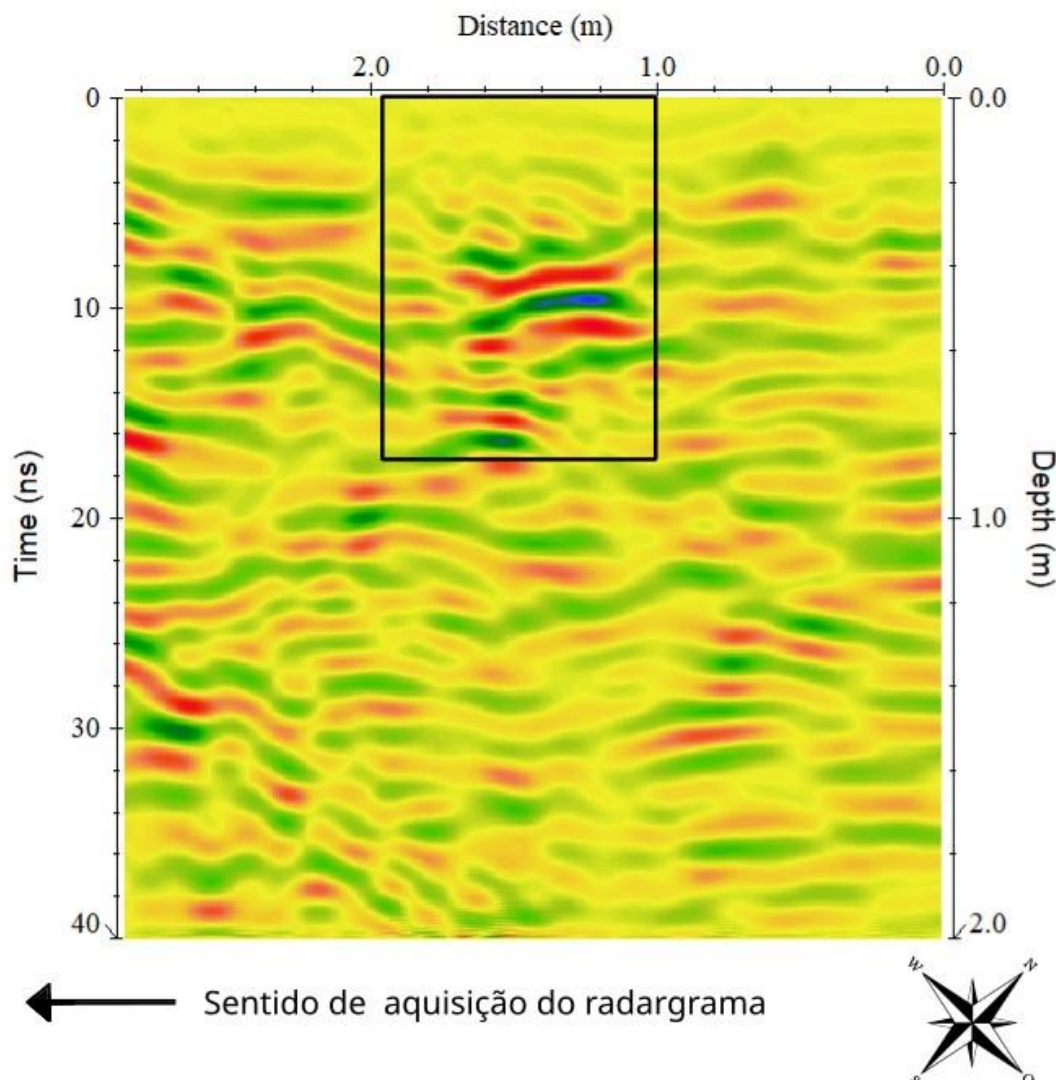
Radargrama obtido dentro da SEP03

Frequência de 400 MHZ.



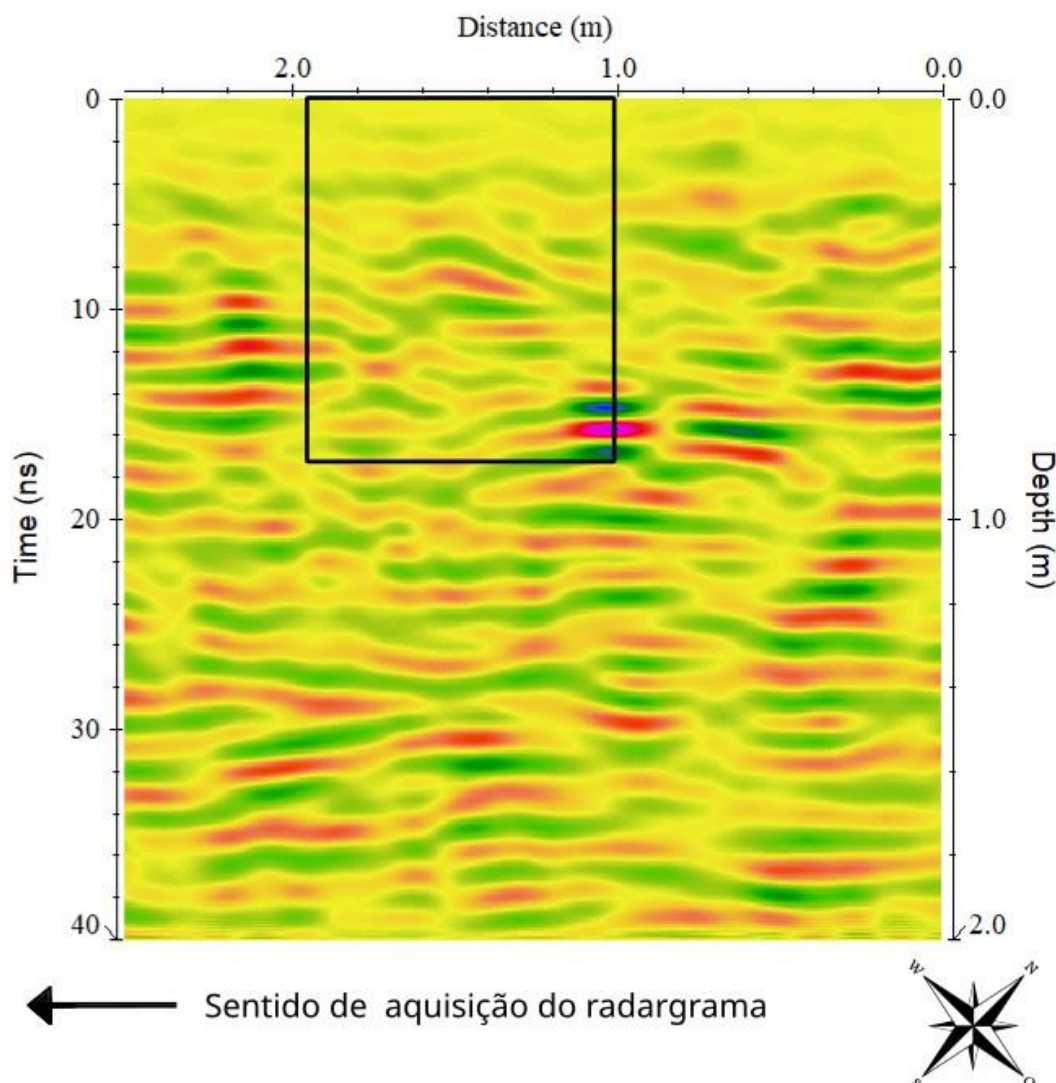
Radargrama obtido sobre o alvo na SEP03

Frequência de 400 MHZ.



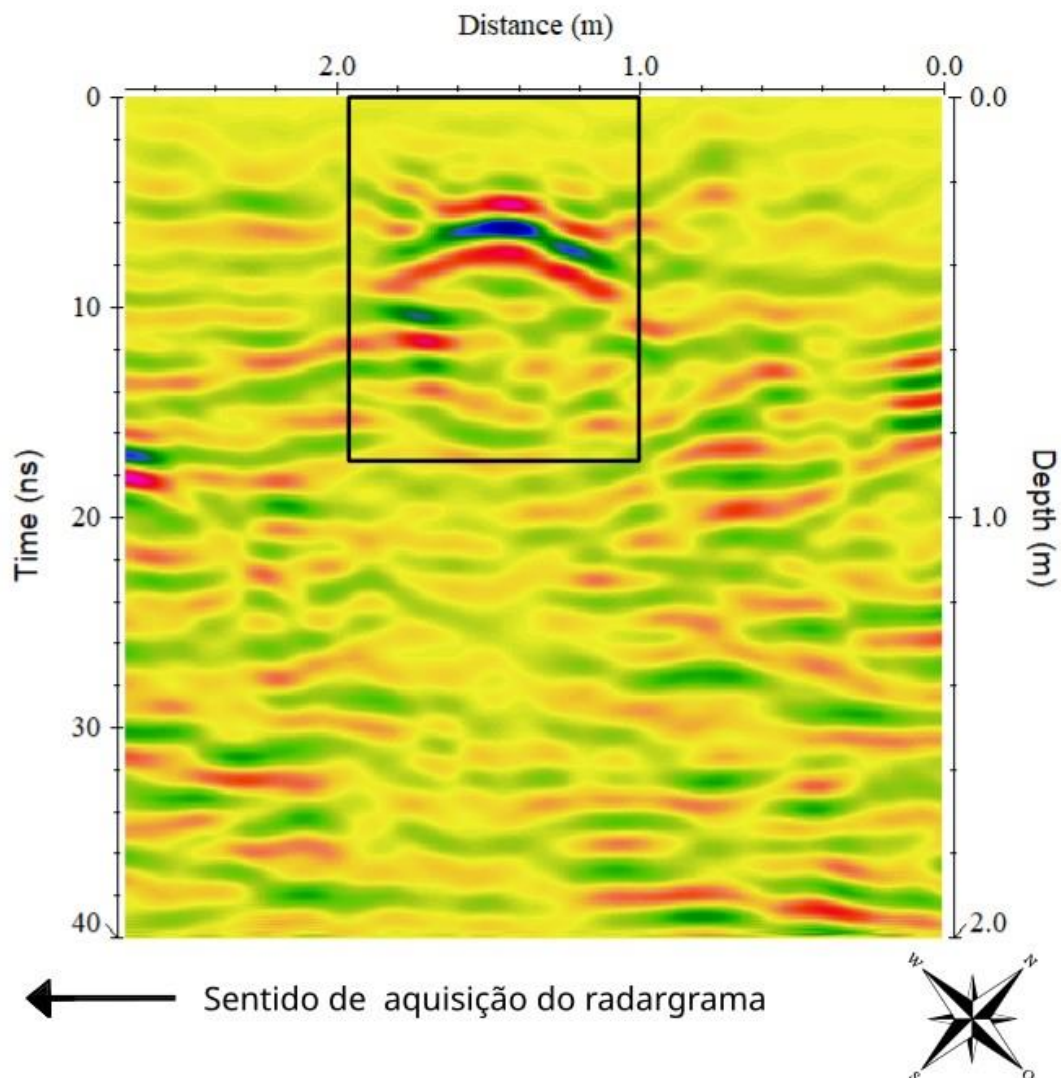
Radargrama obtido dentro da SEP04

Frequência de 400 MHZ.



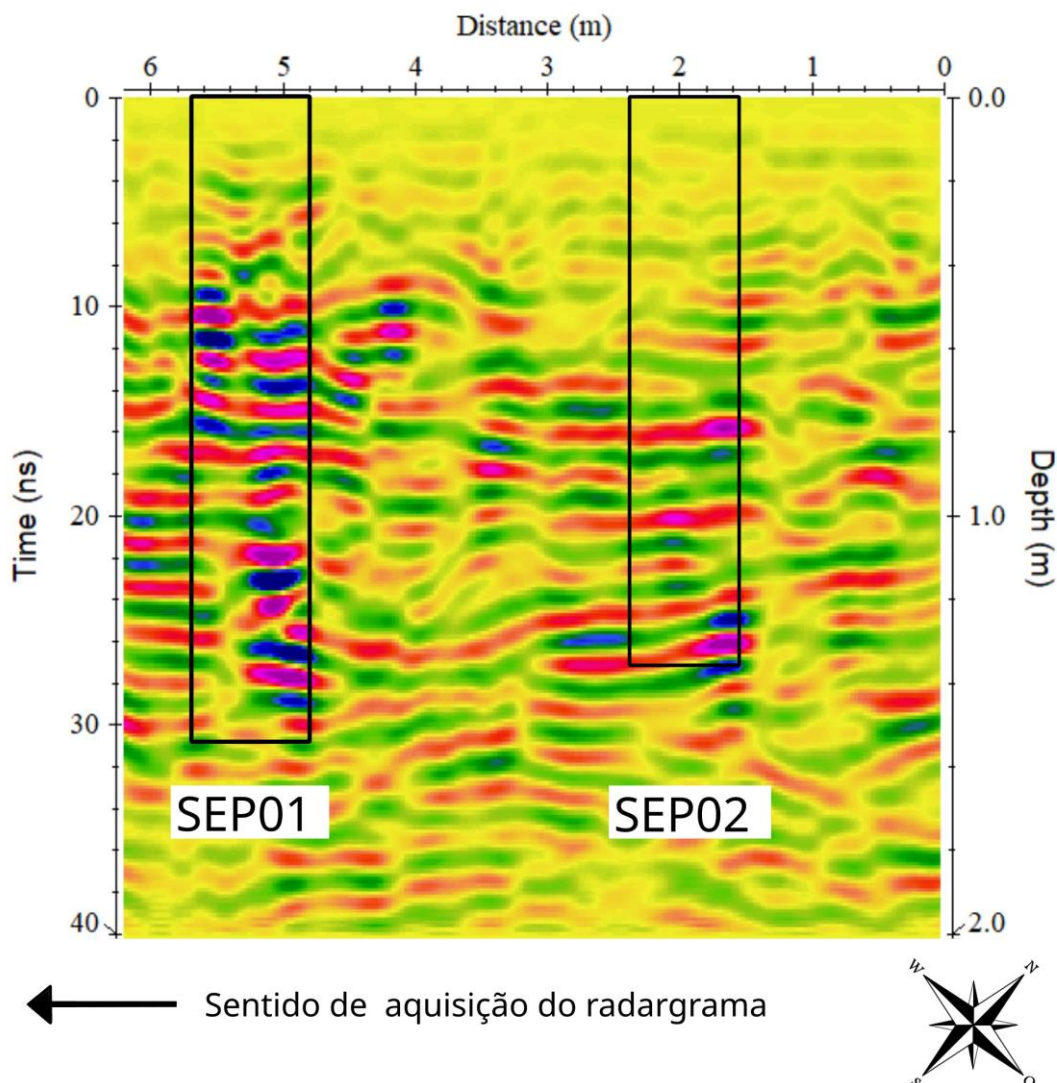
Radargrama obtido sobre o alvo na SEP04

Frequência de 400 MHZ.



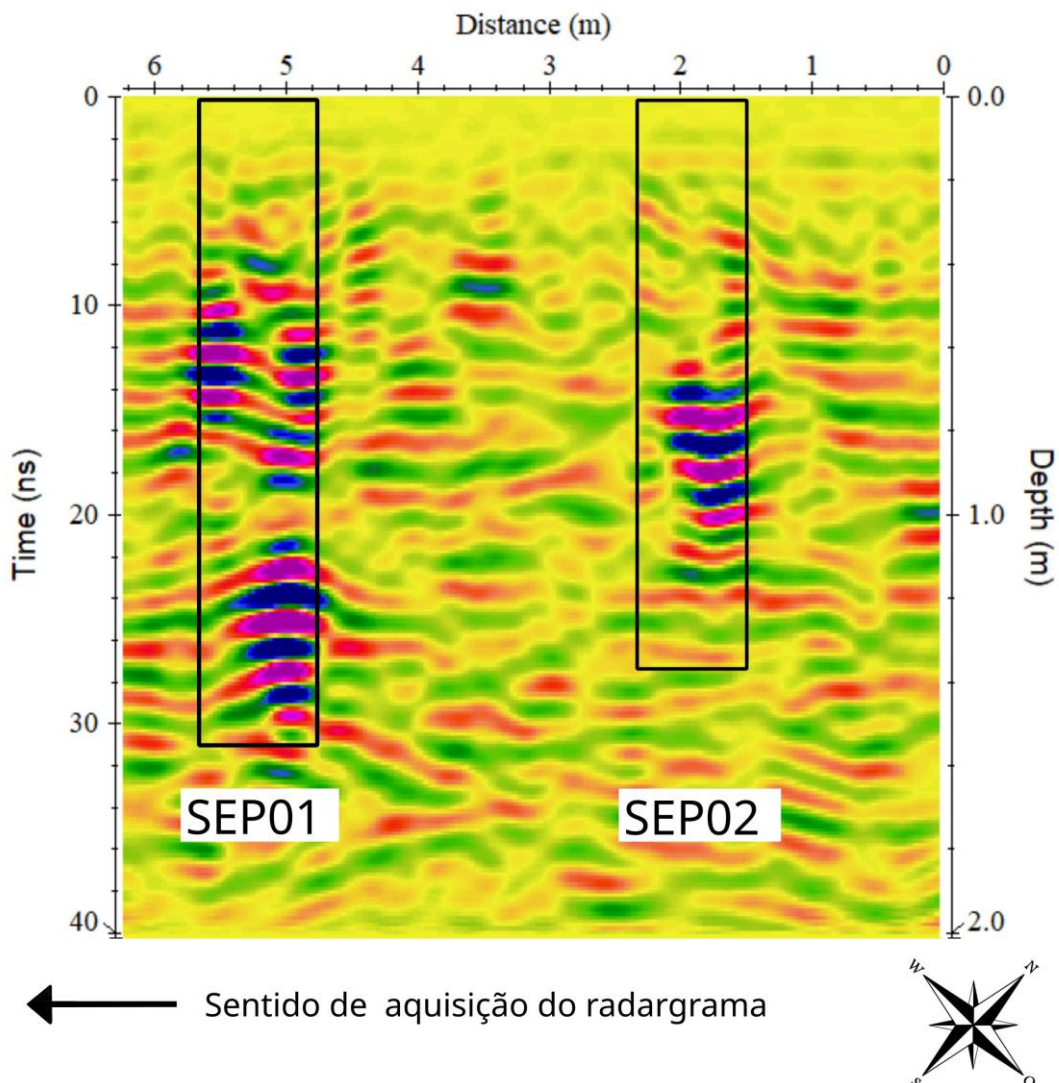
Radargrama obtido dentro das SEP's 01 e 02

Frequência de 900 MHZ.



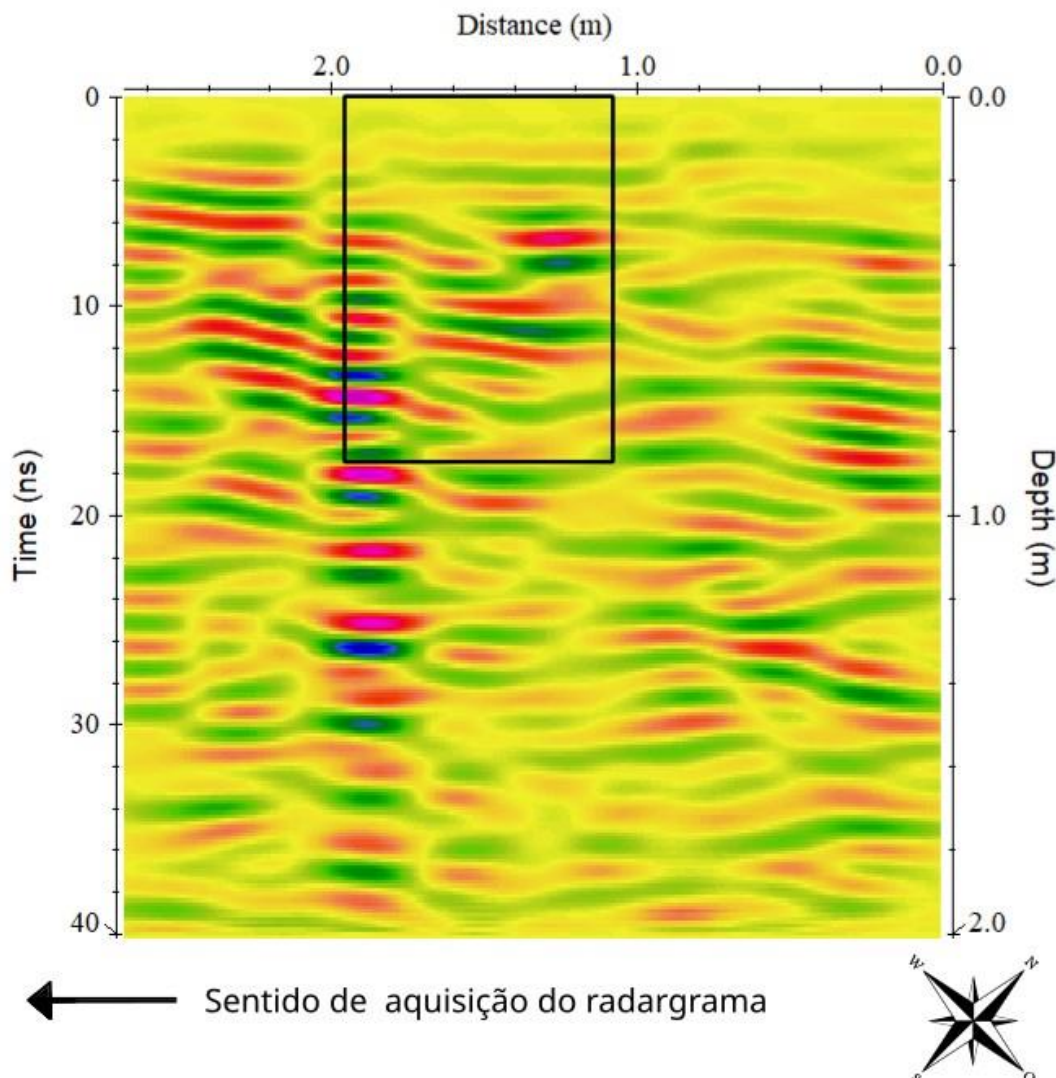
Radargrama obtido sobre o alvo nas SEP's 01 e 02

Frequência de 900 MHZ.



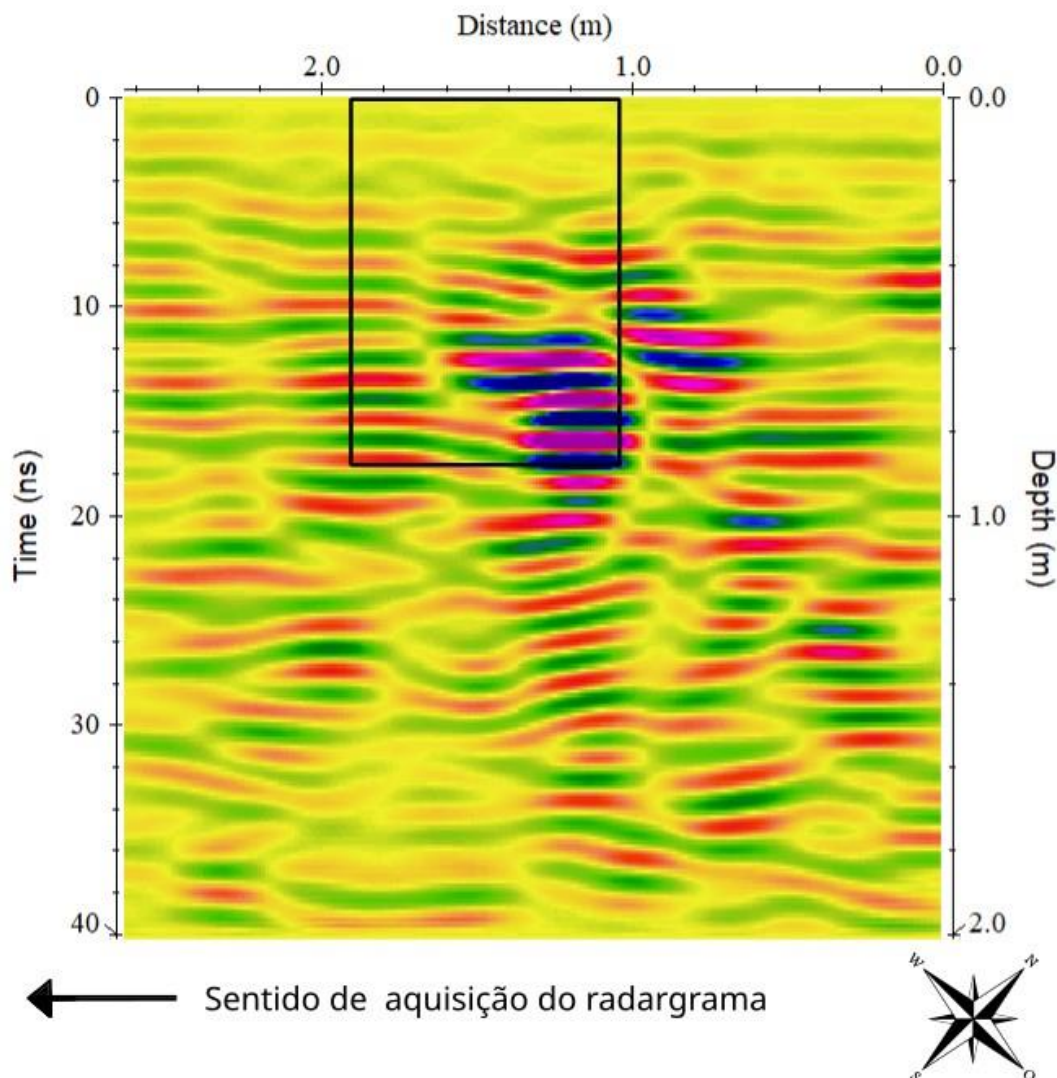
Radargrama obtido dentro da SEP03

Frequência de 900 MHZ.



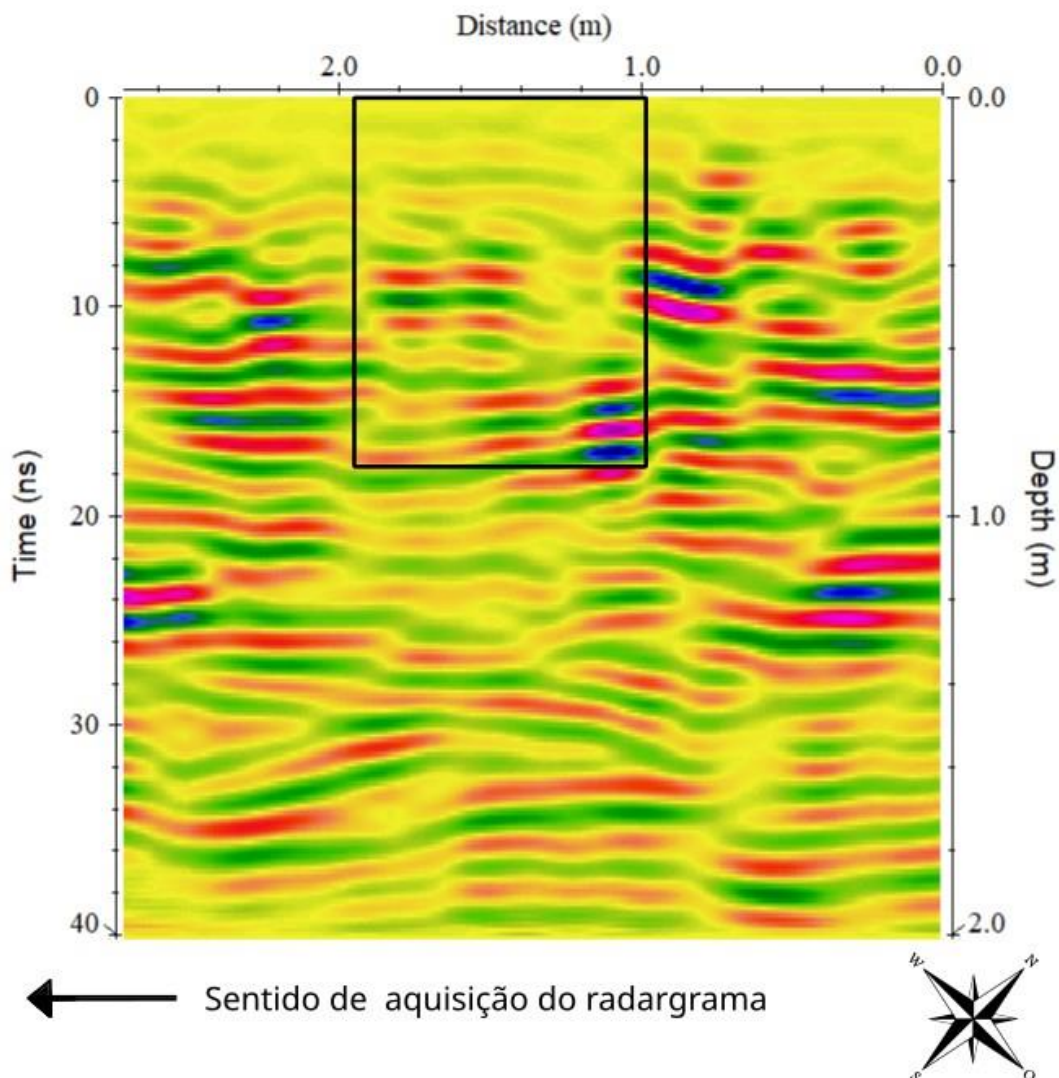
Radargrama obtido sobre o alvo na SEP03

Frequência de 900 MHZ.



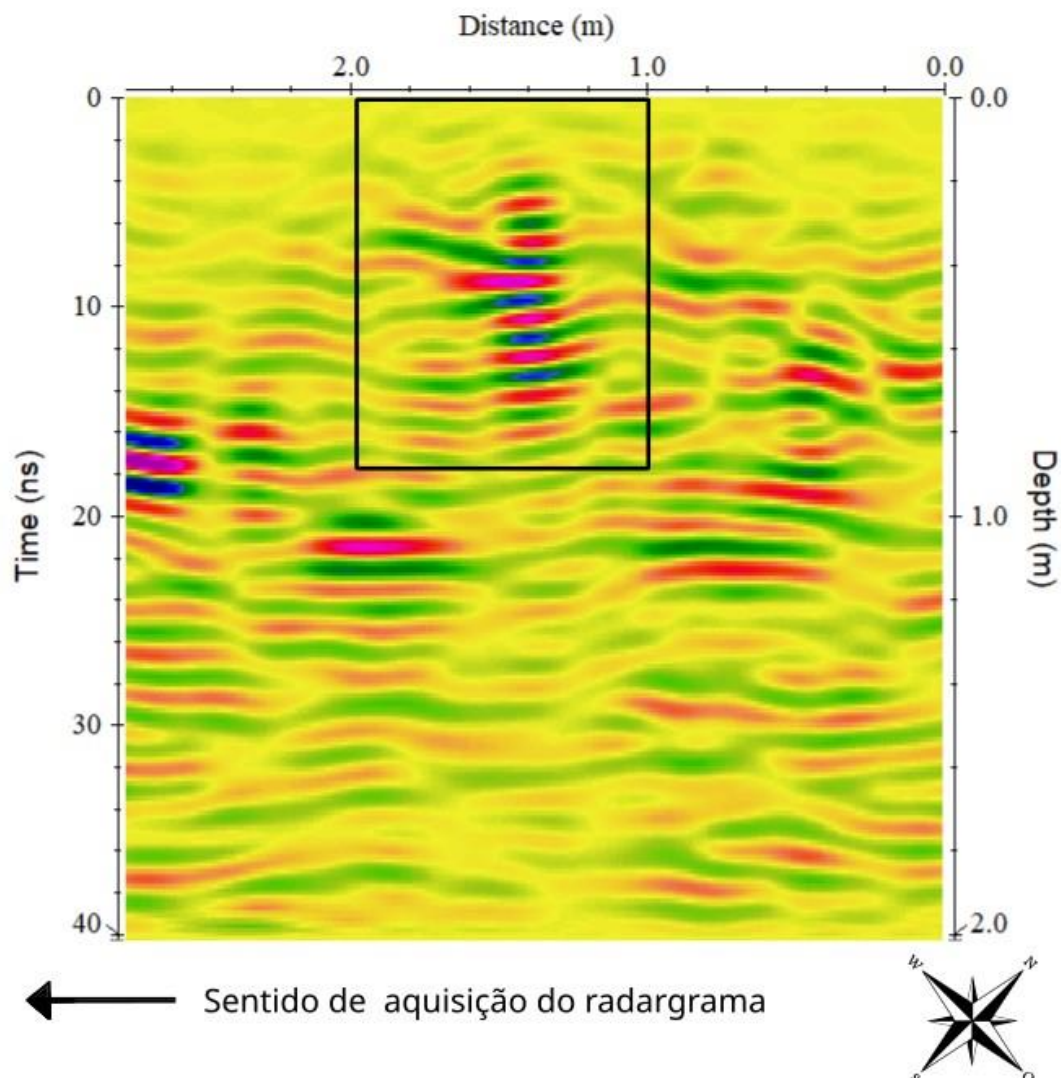
Radargrama obtido dentro da SEP04

Frequência de 900 MHZ.



Radargrama obtido sobre o alvo na SEP04

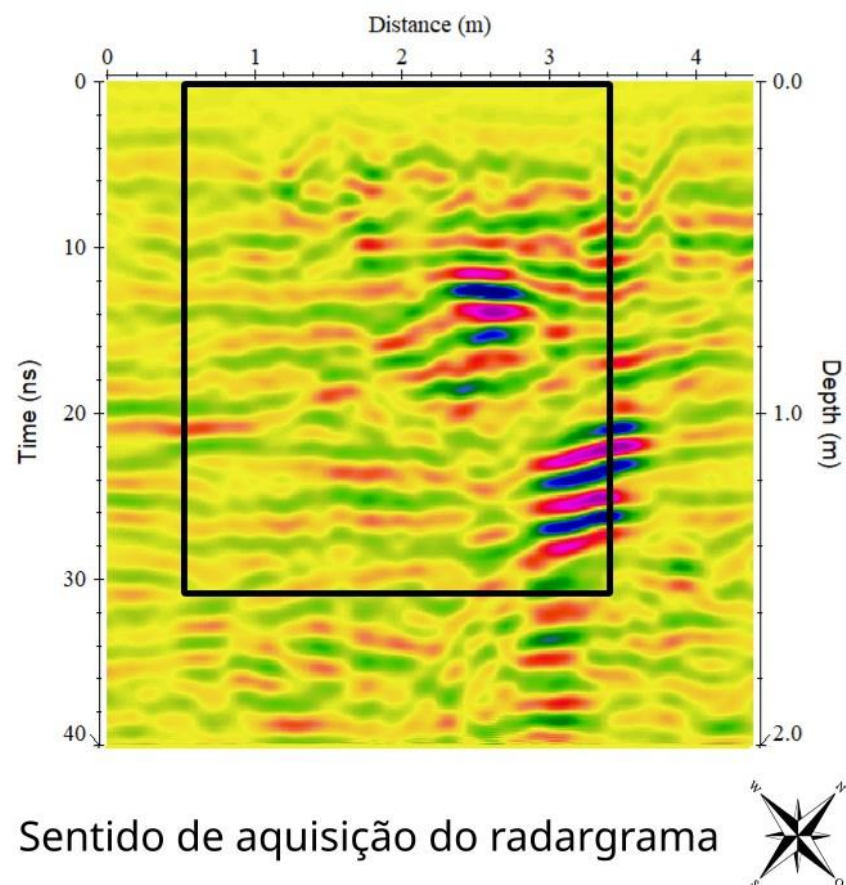
Frequência de 900 MHZ.



C2 – RADARGRAMAS 2D OBTIDOS TRANSVERSALMENTE NO PERÍODO DE SECA

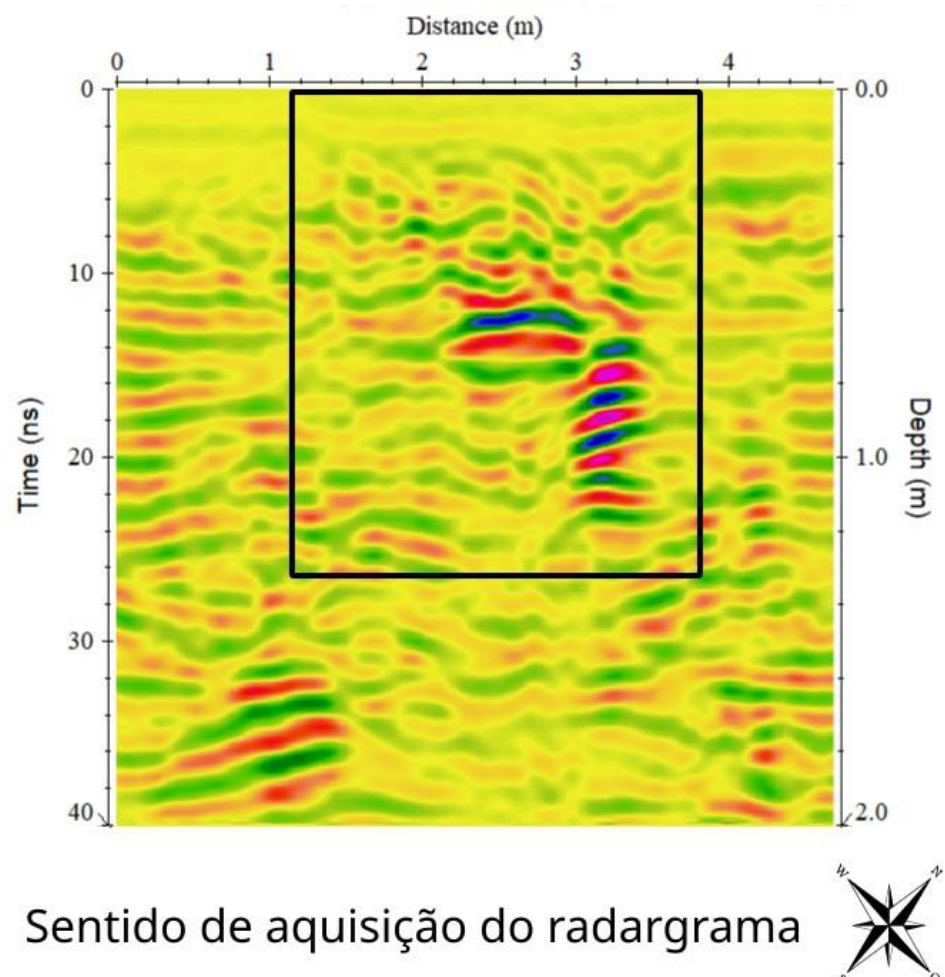
Radargrama obtido sobre o alvo na SEP01

Frequência de 400 MHZ.



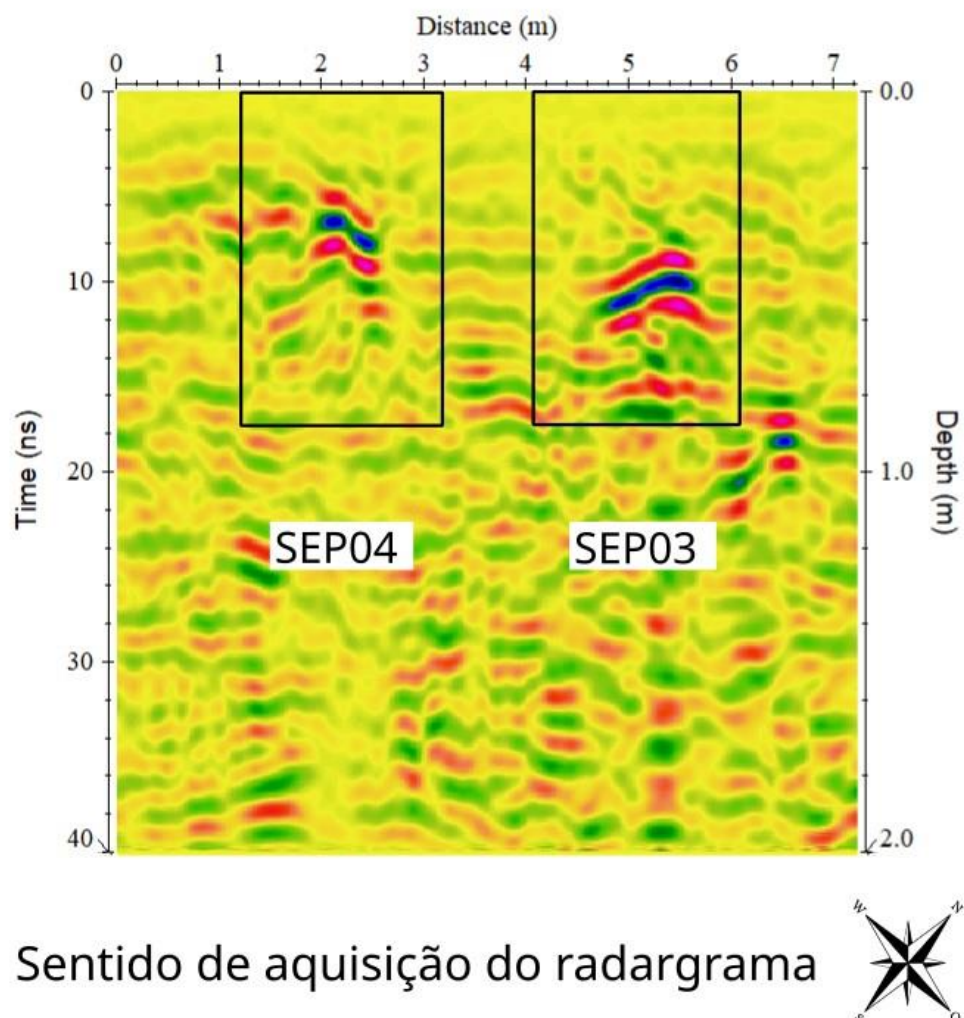
Radargrama obtido sobre o alvo na SEP02

Frequência de 400 MHZ.



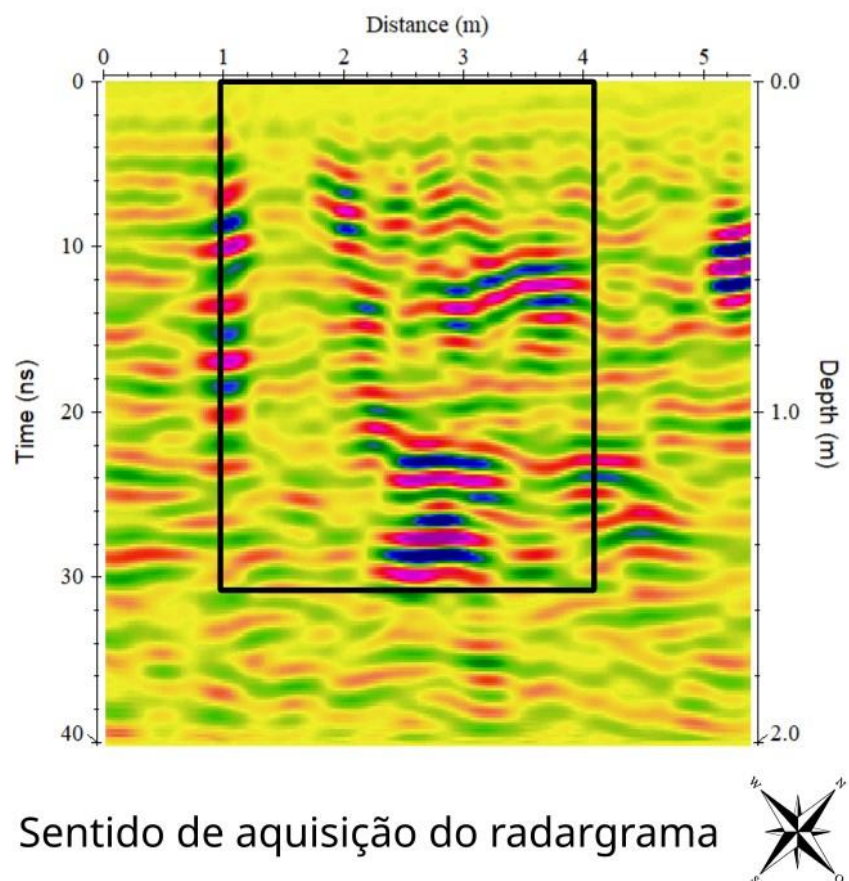
Radargrama obtido sobre o alvo nas SEP's 03 e 04

Frequência de 400 MHZ.



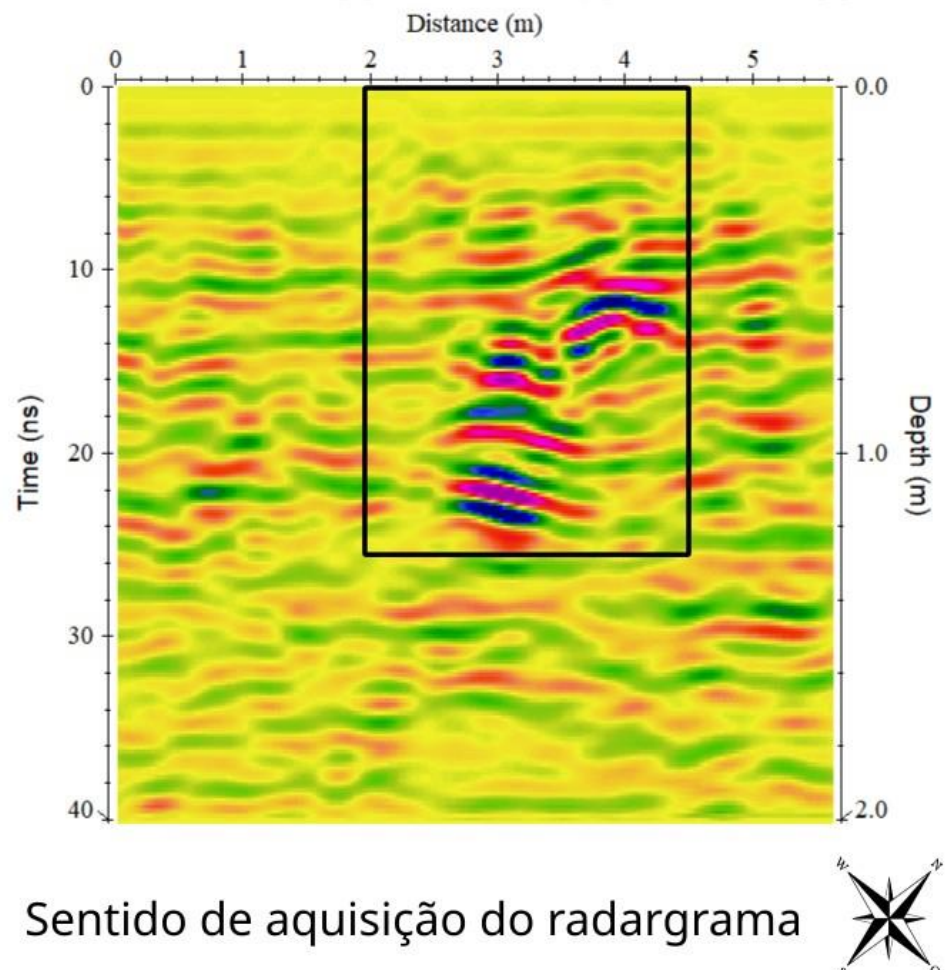
Radargrama obtido sobre o alvo na SEP01

Frequência de 900 MHZ.



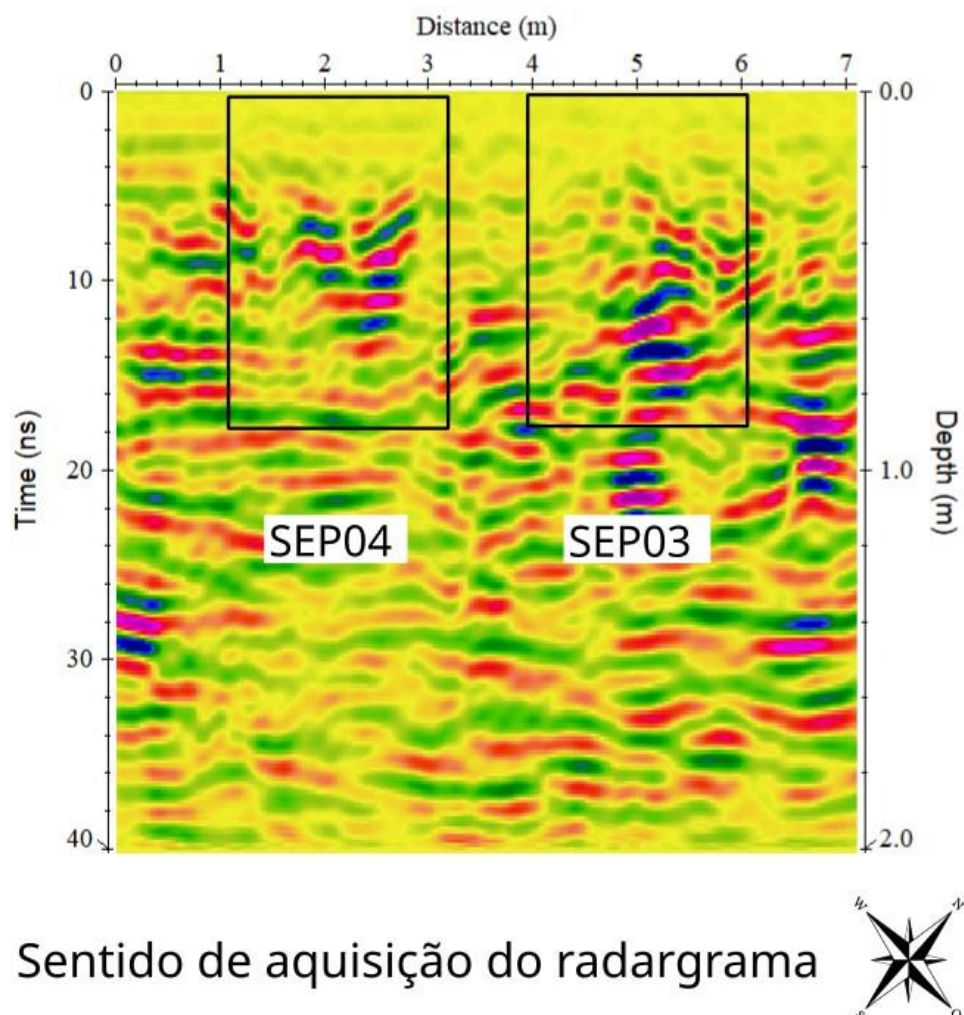
Radargrama obtido sobre o alvo na SEP02

Frequência de 900 MHZ.



Radargrama obtido sobre o alvo nas SEP's 03 e 04

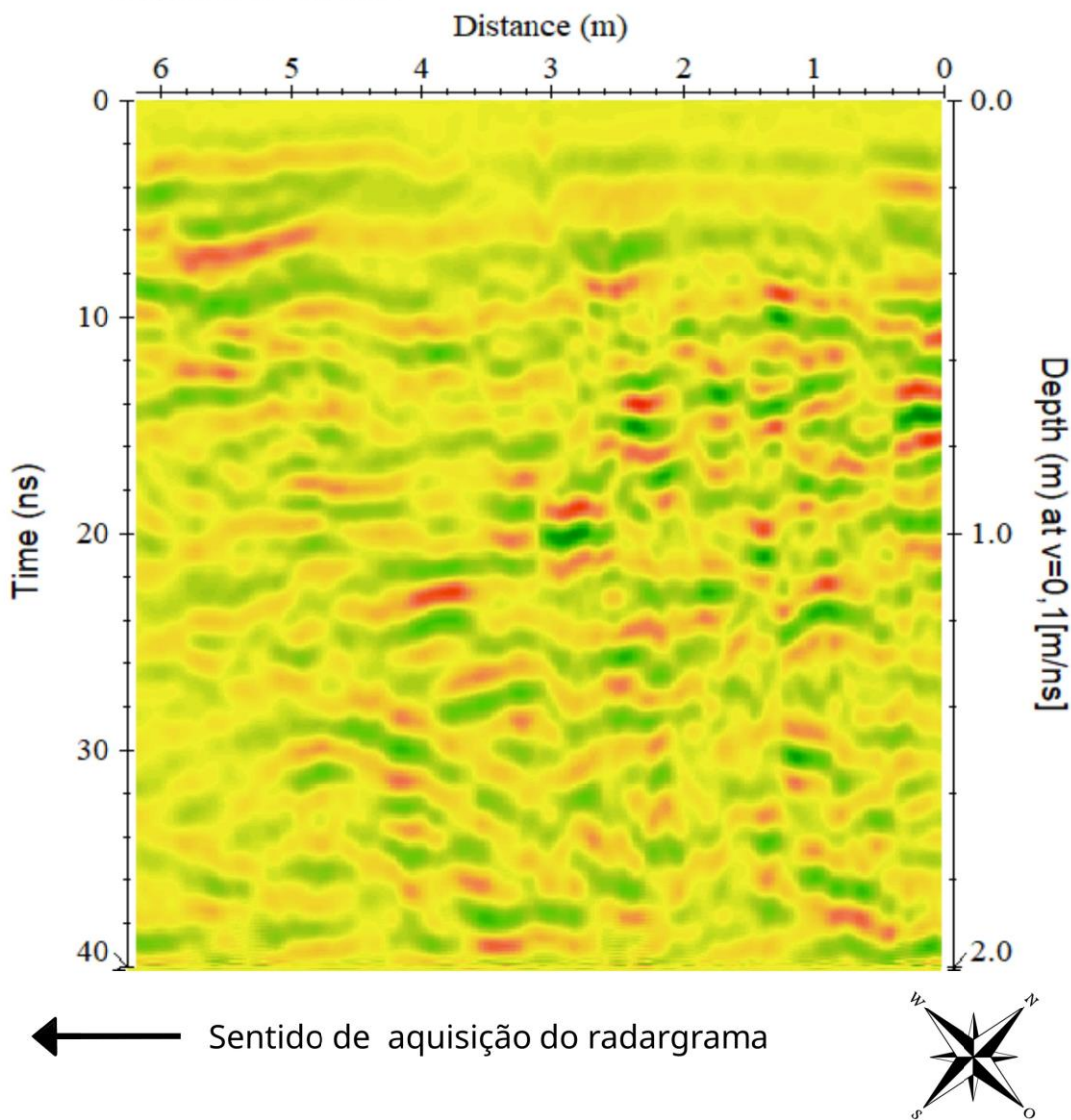
Frequência de 900 MHZ.



D – RADARGRAMAS OBTIDOS NO PERÍODO CHUVOSO**D1 – RADARGRAMAS 2D OBTIDOS PARALELAMENTE NO PERÍODO CHUVOSO**

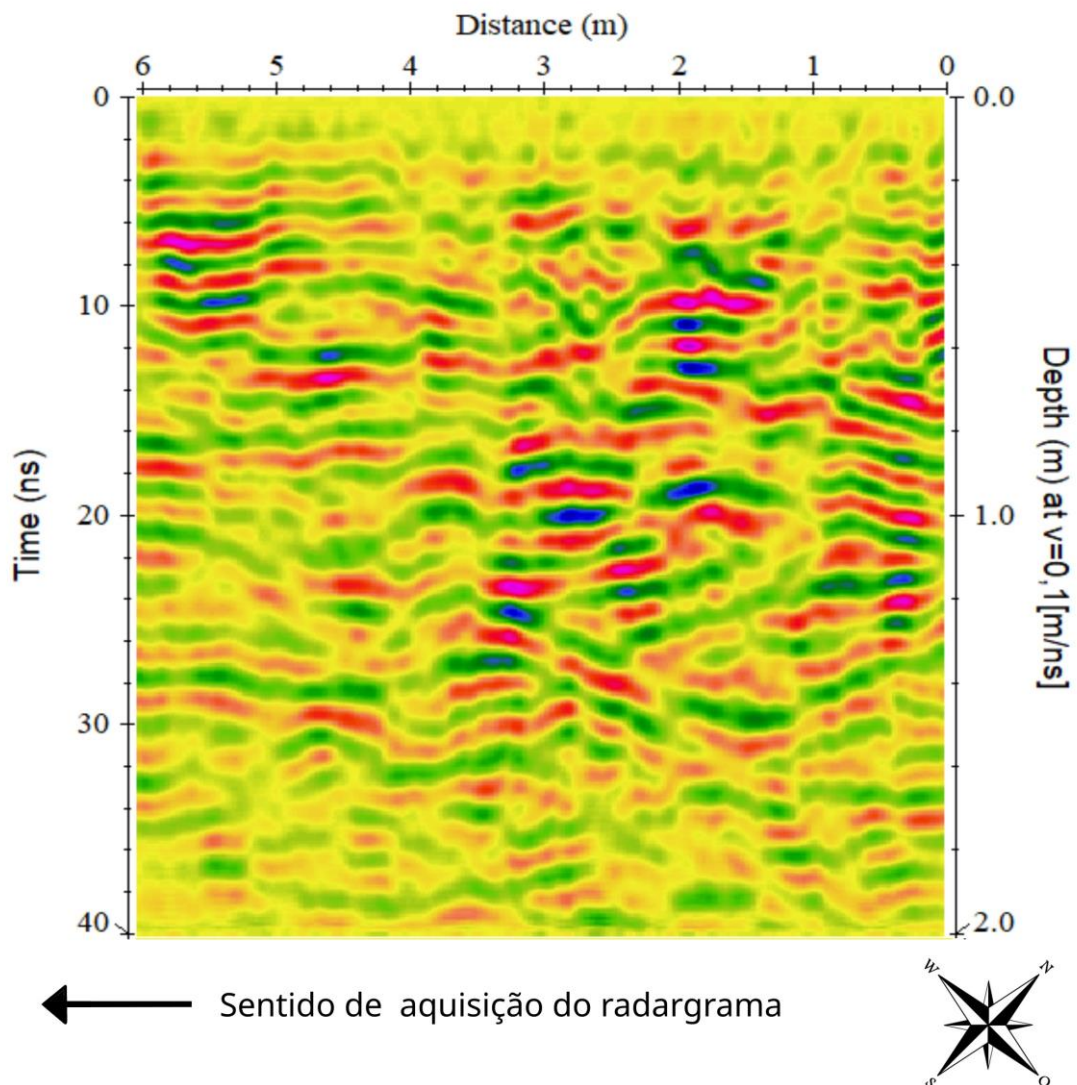
Radargrama obtido fora das SEP's 01 e 02

Frequência de 400 MHZ.



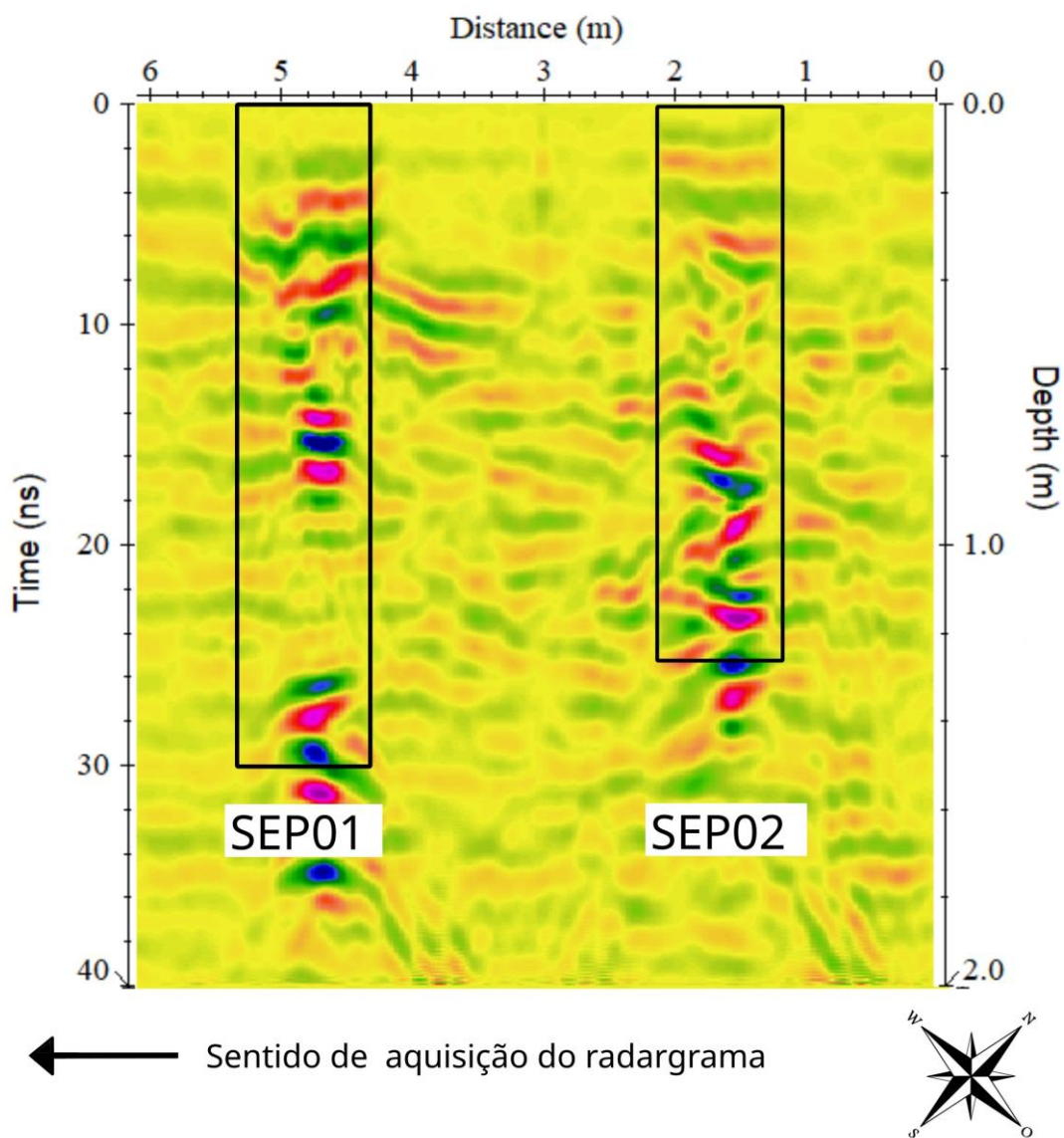
Radargrama obtido fora das SEP's 01 e 02

Frequência de 900 MHZ.



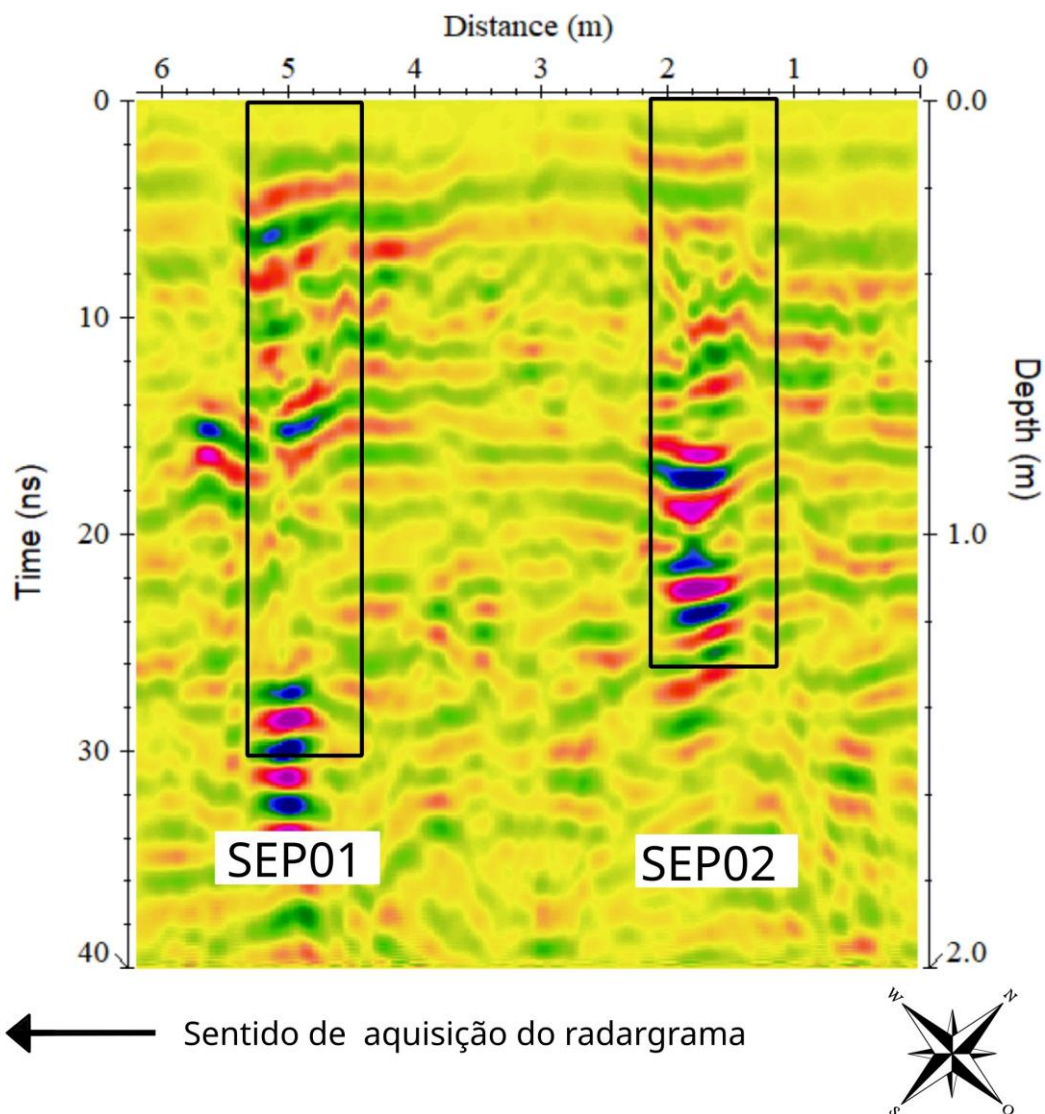
Radargrama obtido dentro das SEP's 01 e 02

Frequência de 400 MHZ.



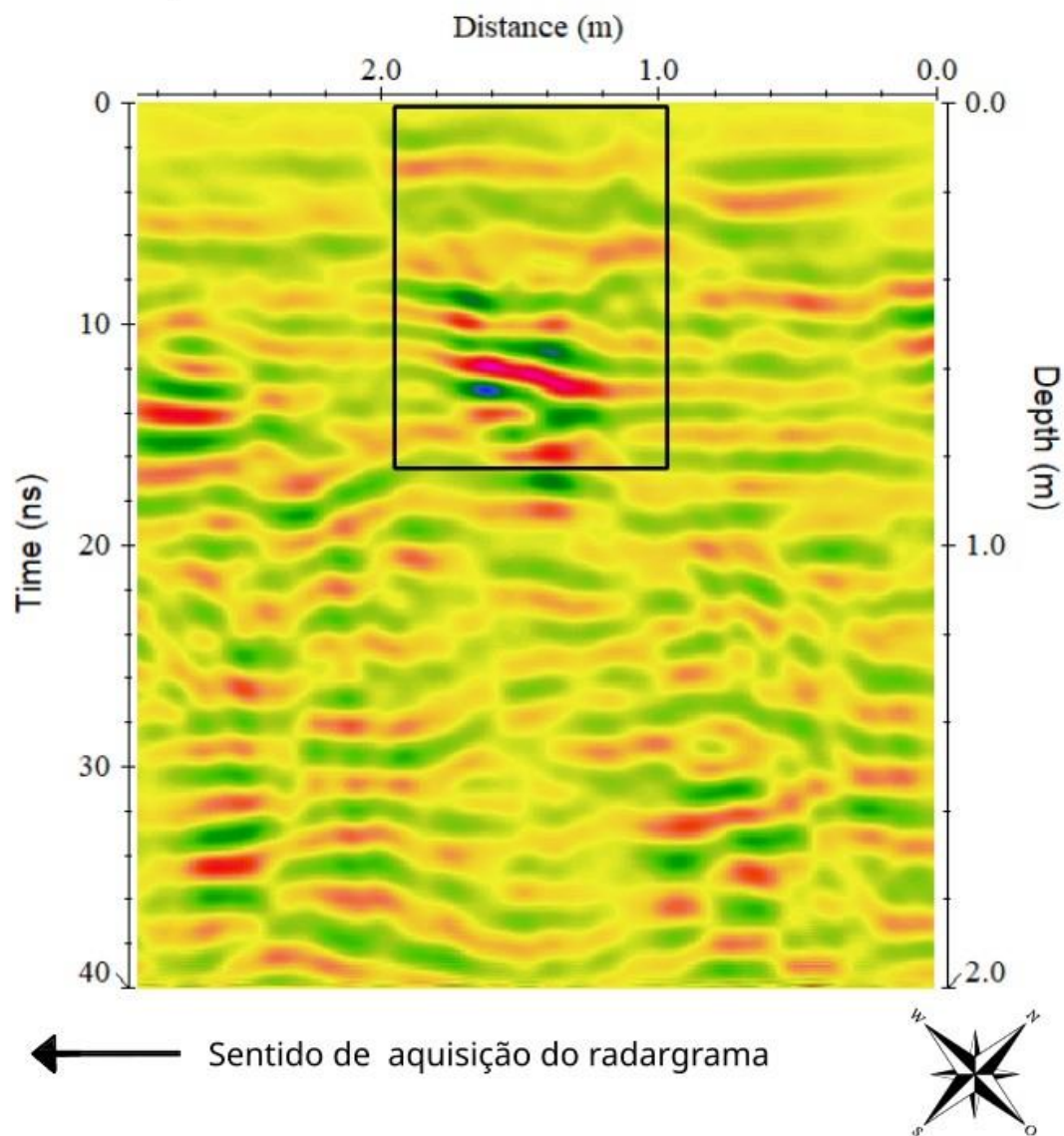
Radargrama obtido sobre o alvo nas SEP's 01 e 02

Frequência de 400 MHZ.



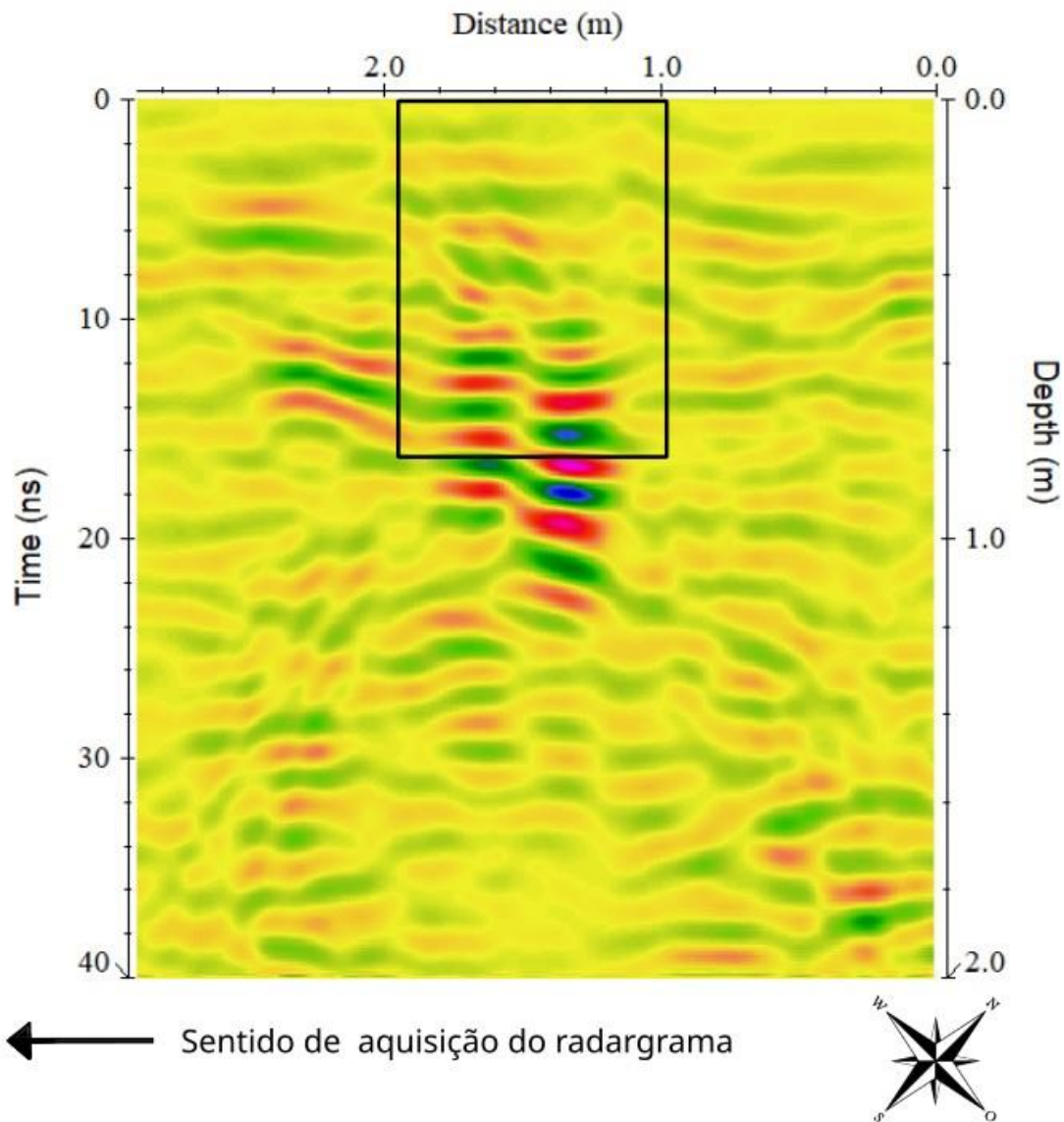
Radargrama obtido dentro da SEP03

Frequência de 400 MHZ.



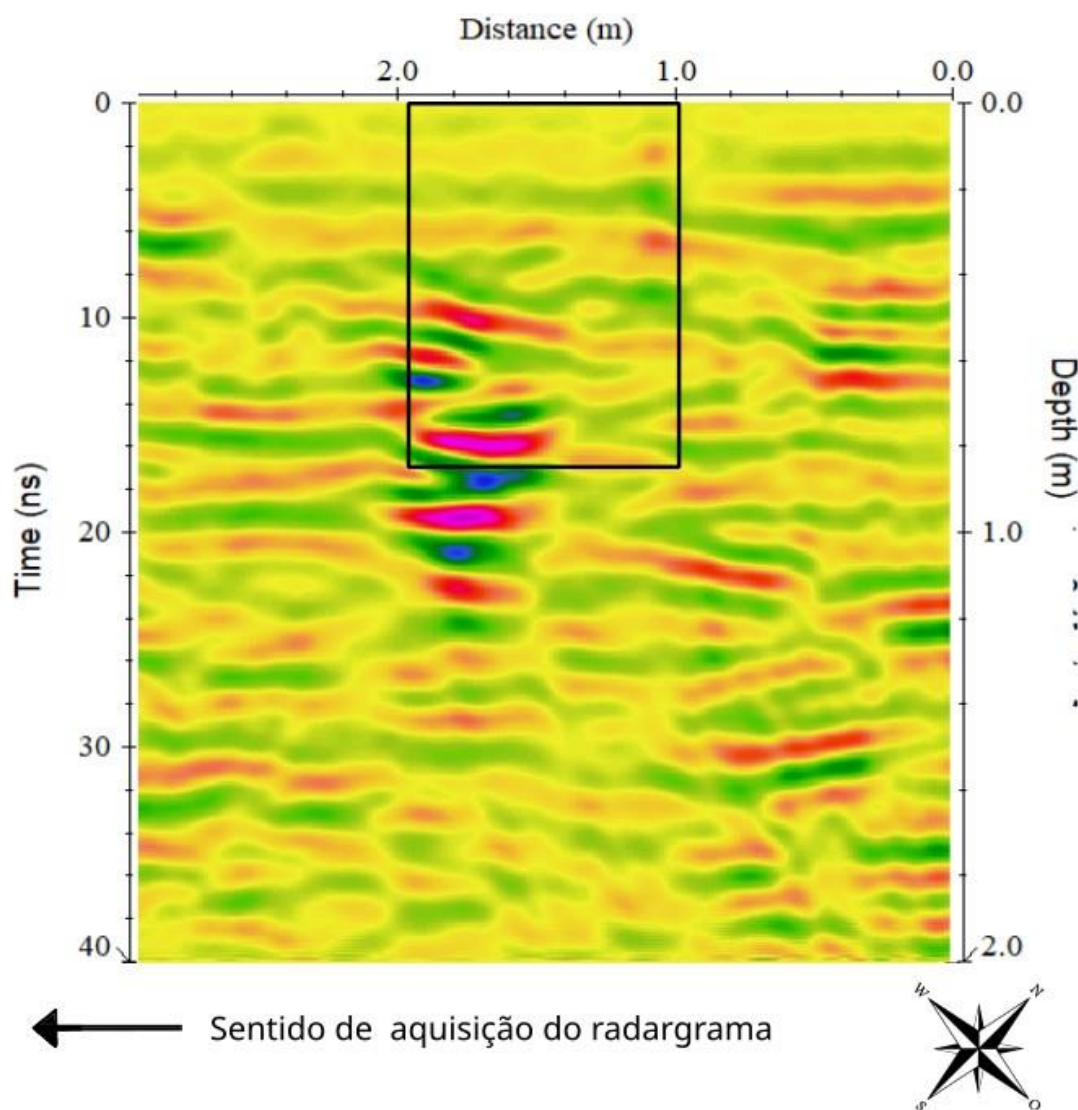
Radargrama obtido sobre o alvo na SEP03

Frequência de 400 MHZ.



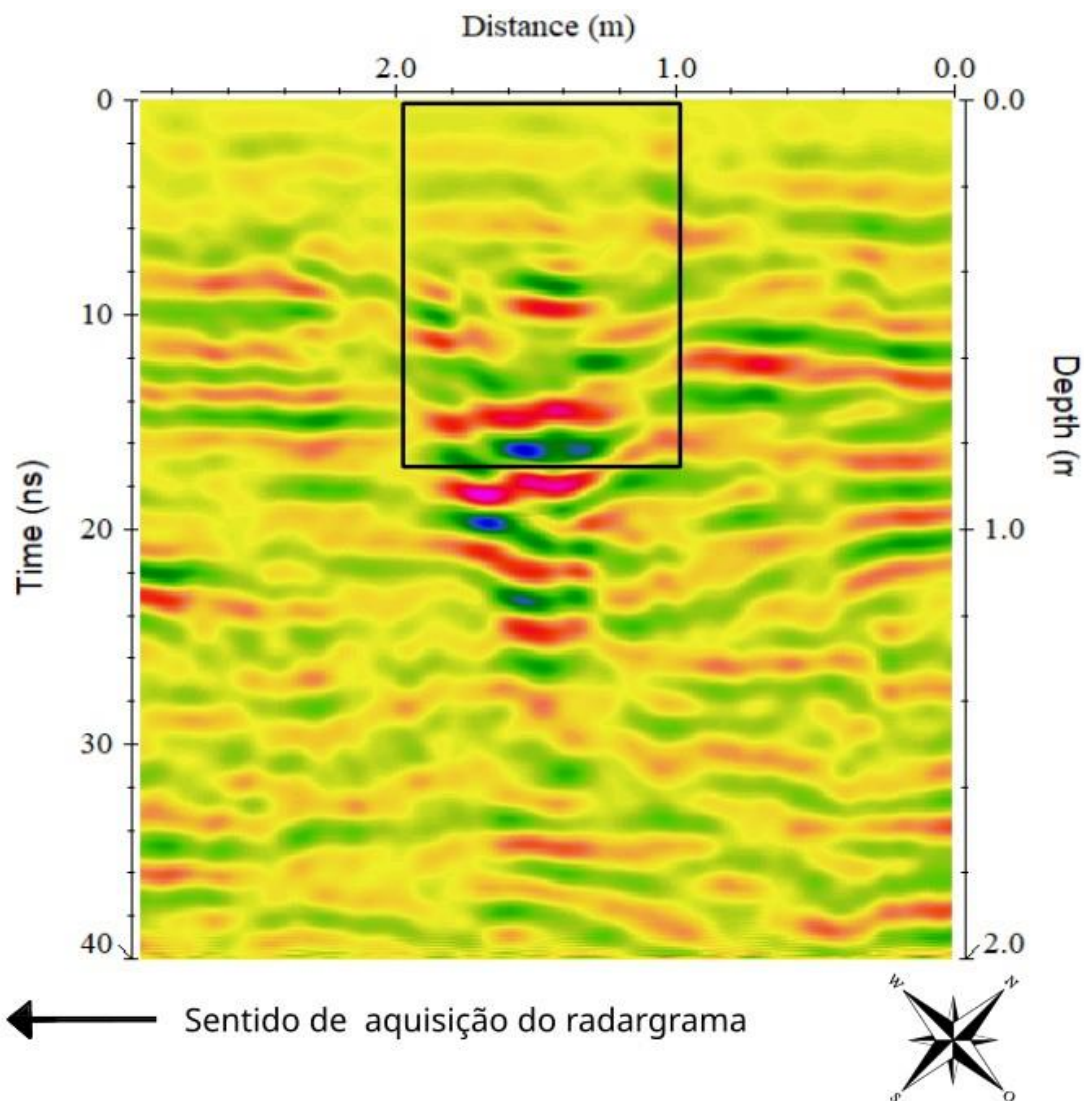
Radargrama obtido dentro da SEP04

Frequência de 400 MHZ.



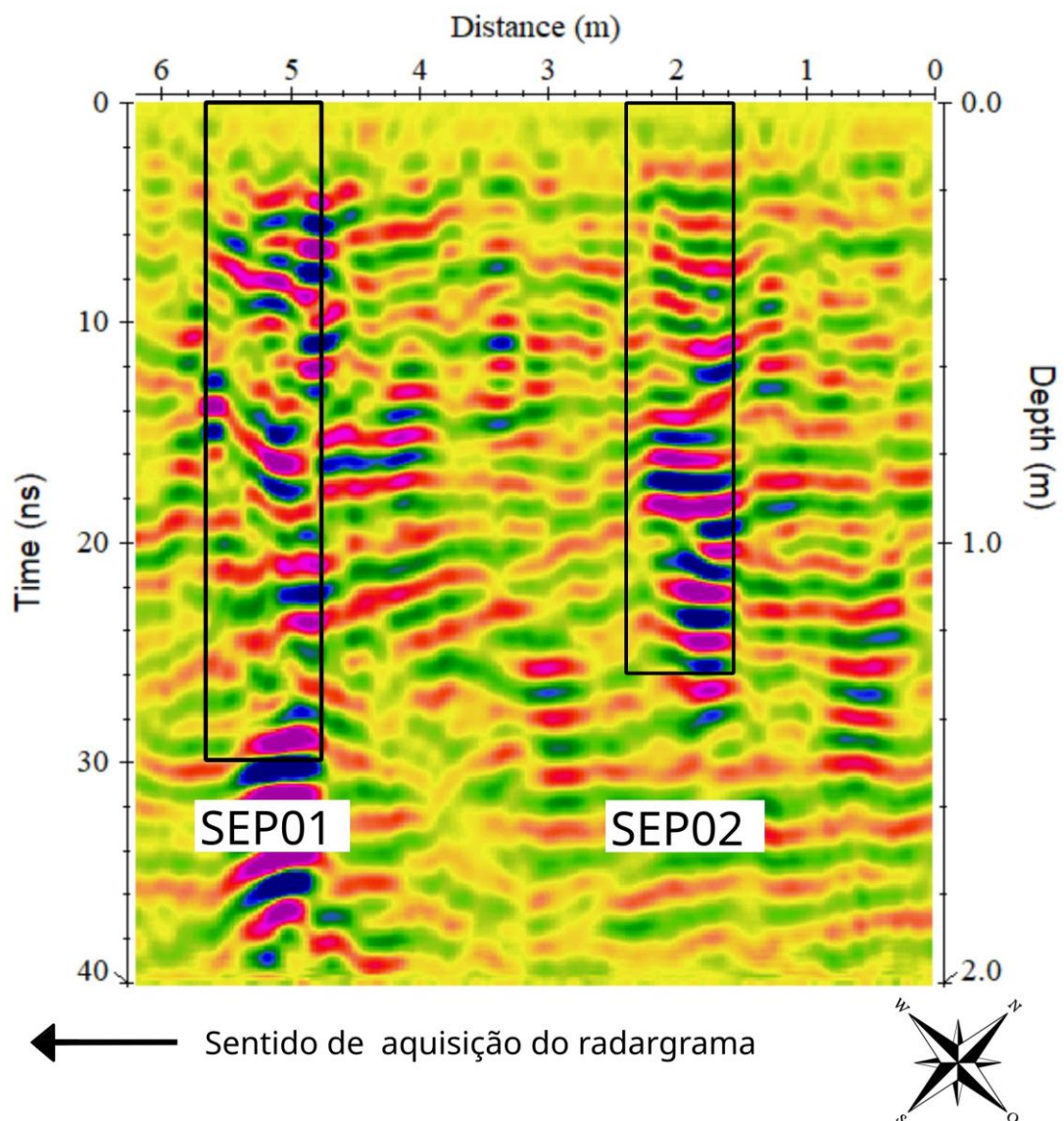
Radargrama obtido sobre o alvo na SEP04

Frequência de 400 MHZ.



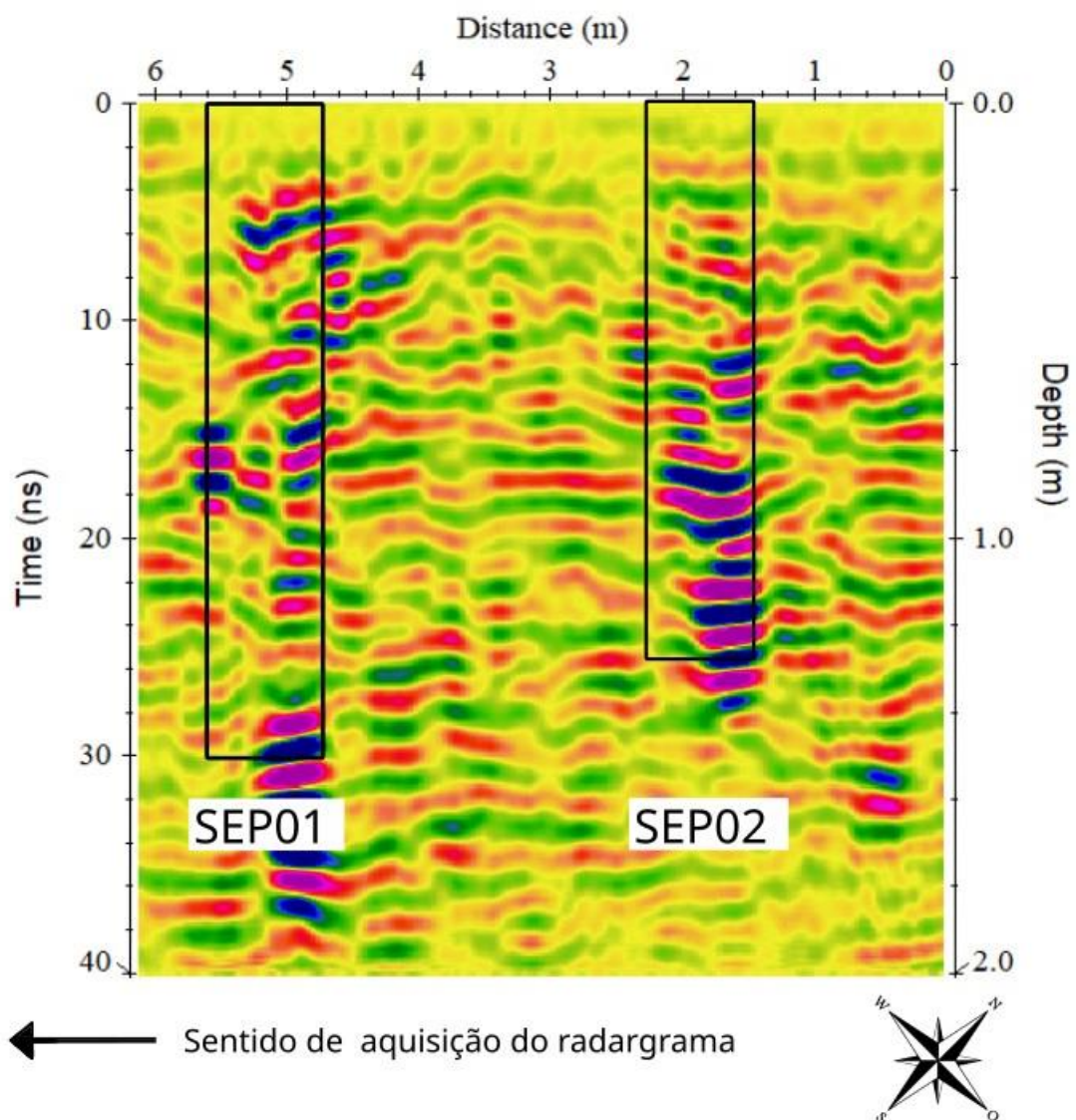
Radargrama obtido dentro das SEP's 01 e 02

Frequência de 900 MHZ.



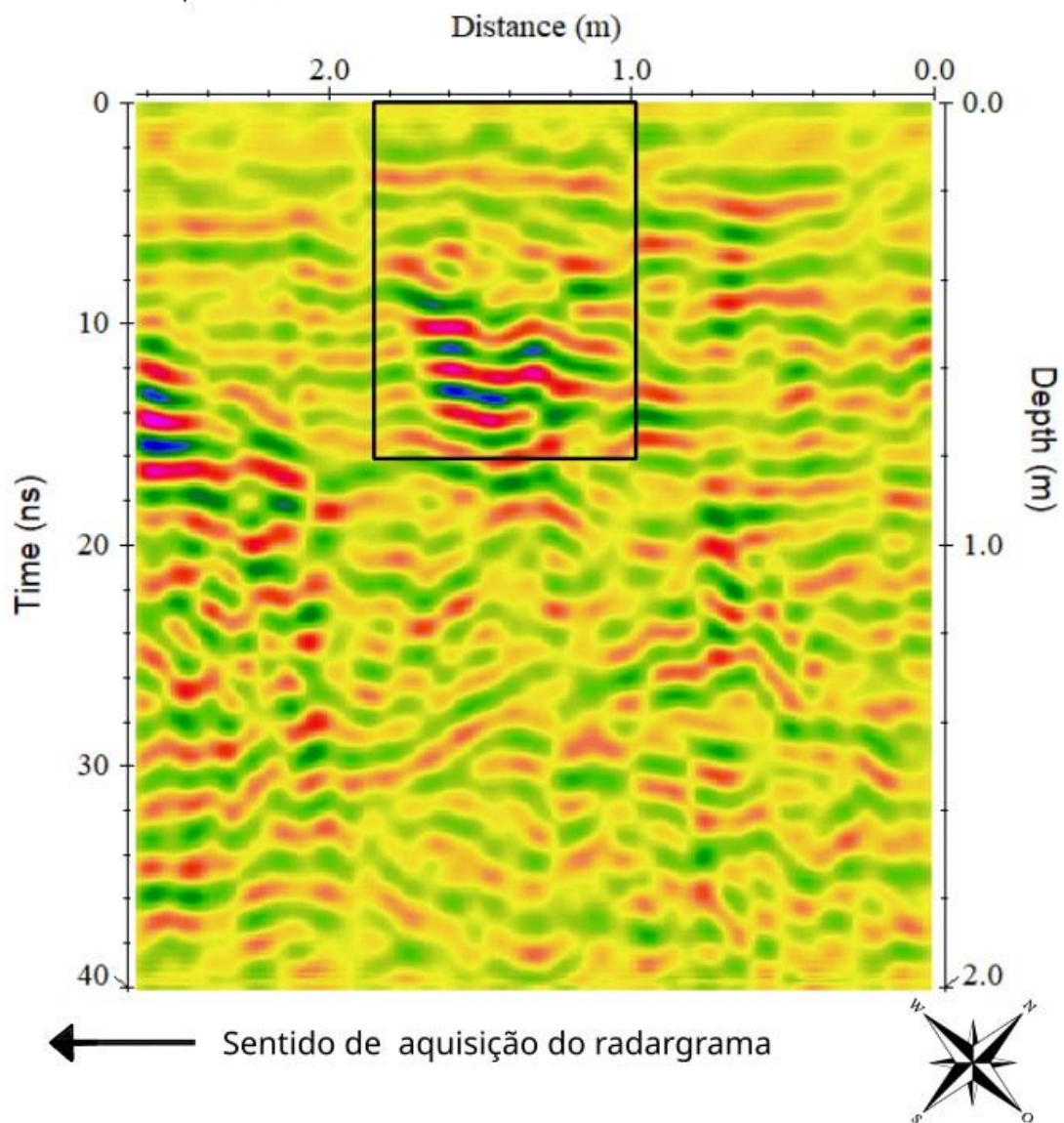
Radargrama obtido sobre o alvo nas SEP's 01 e 02

Frequência de 900 MHZ.



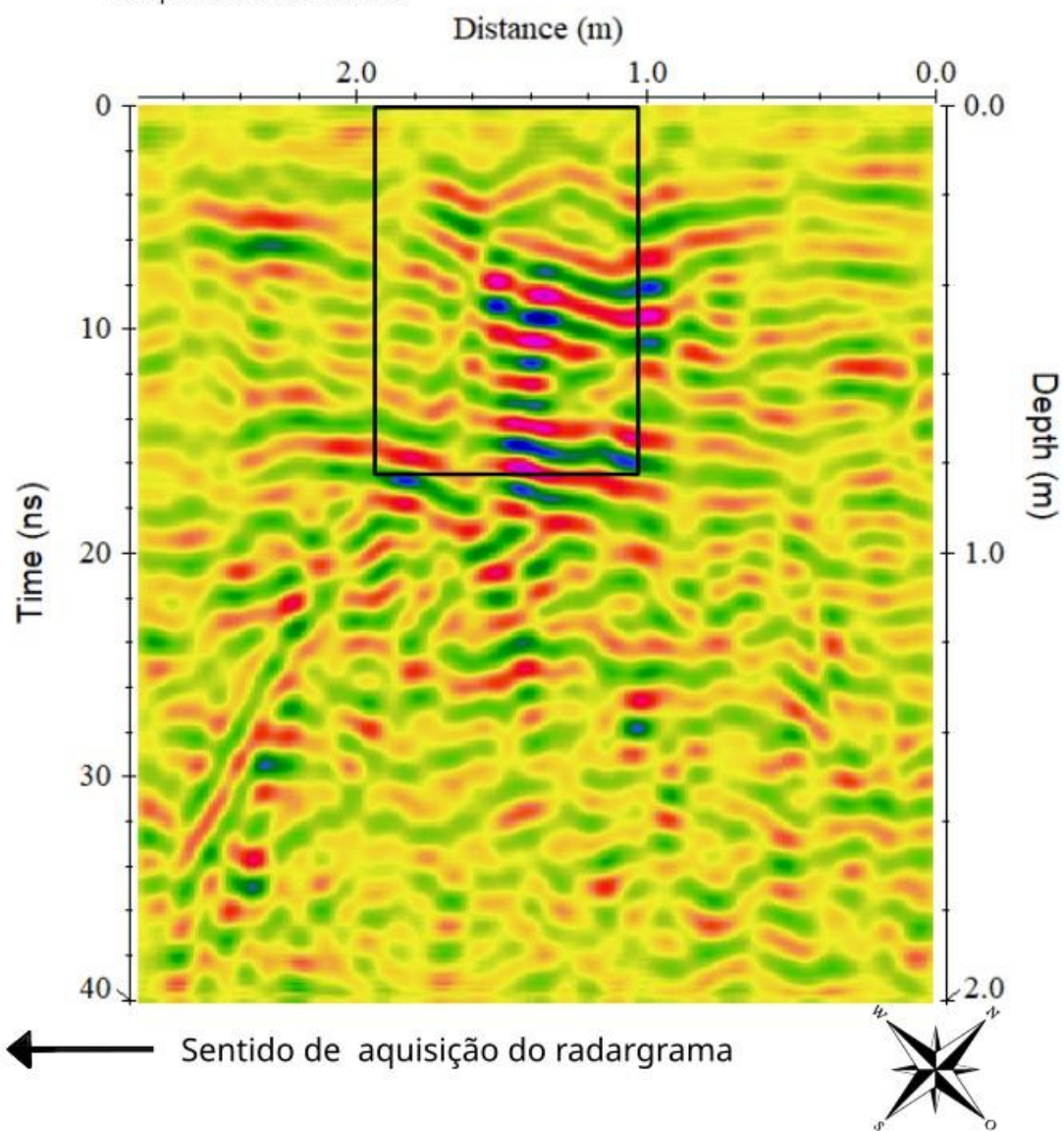
Radargrama obtido dentro da SEP03

Frequência de 900 MHZ.



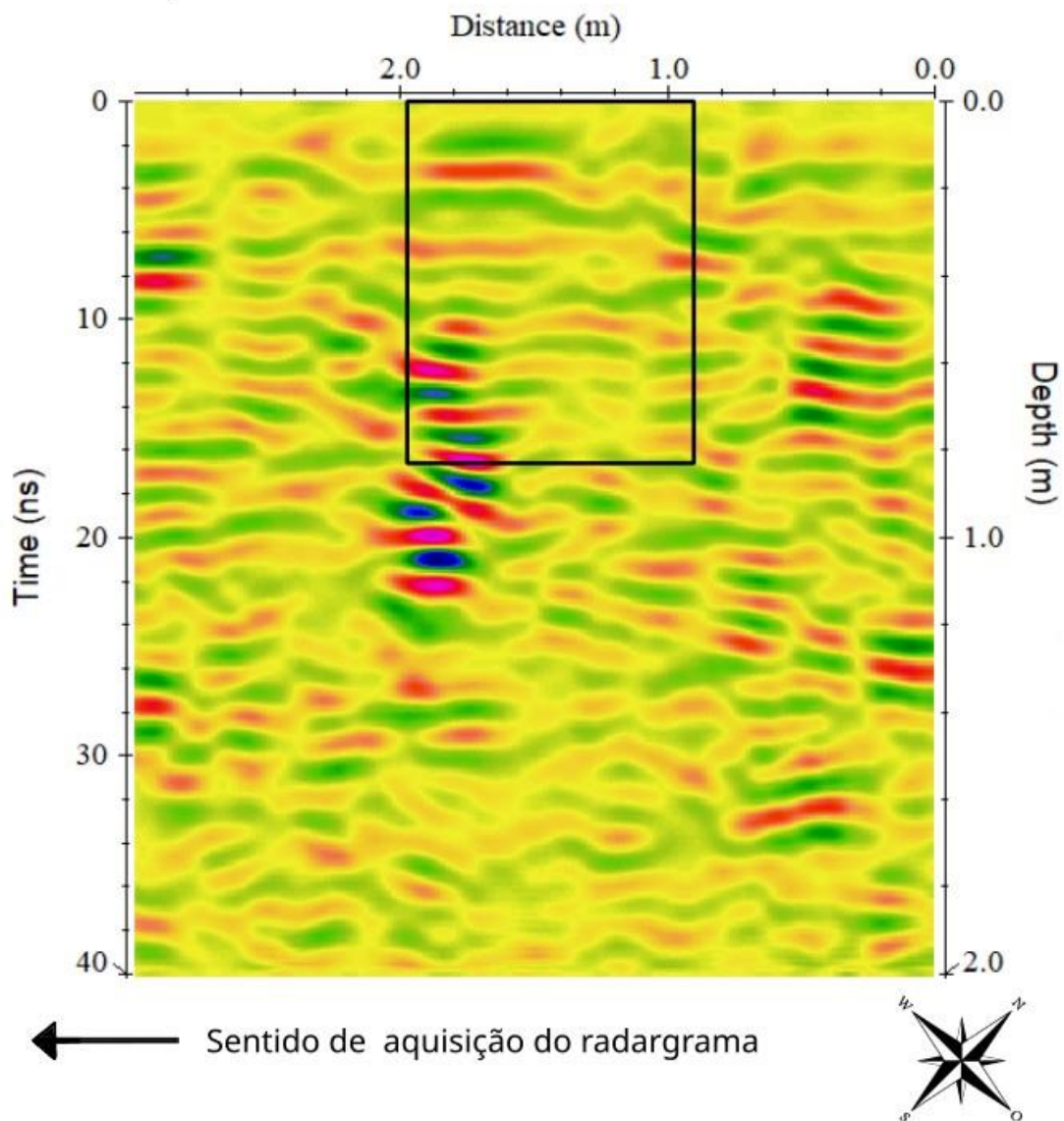
Radargrama obtido sobre o alvo na SEP03

Frequência de 900 MHZ.



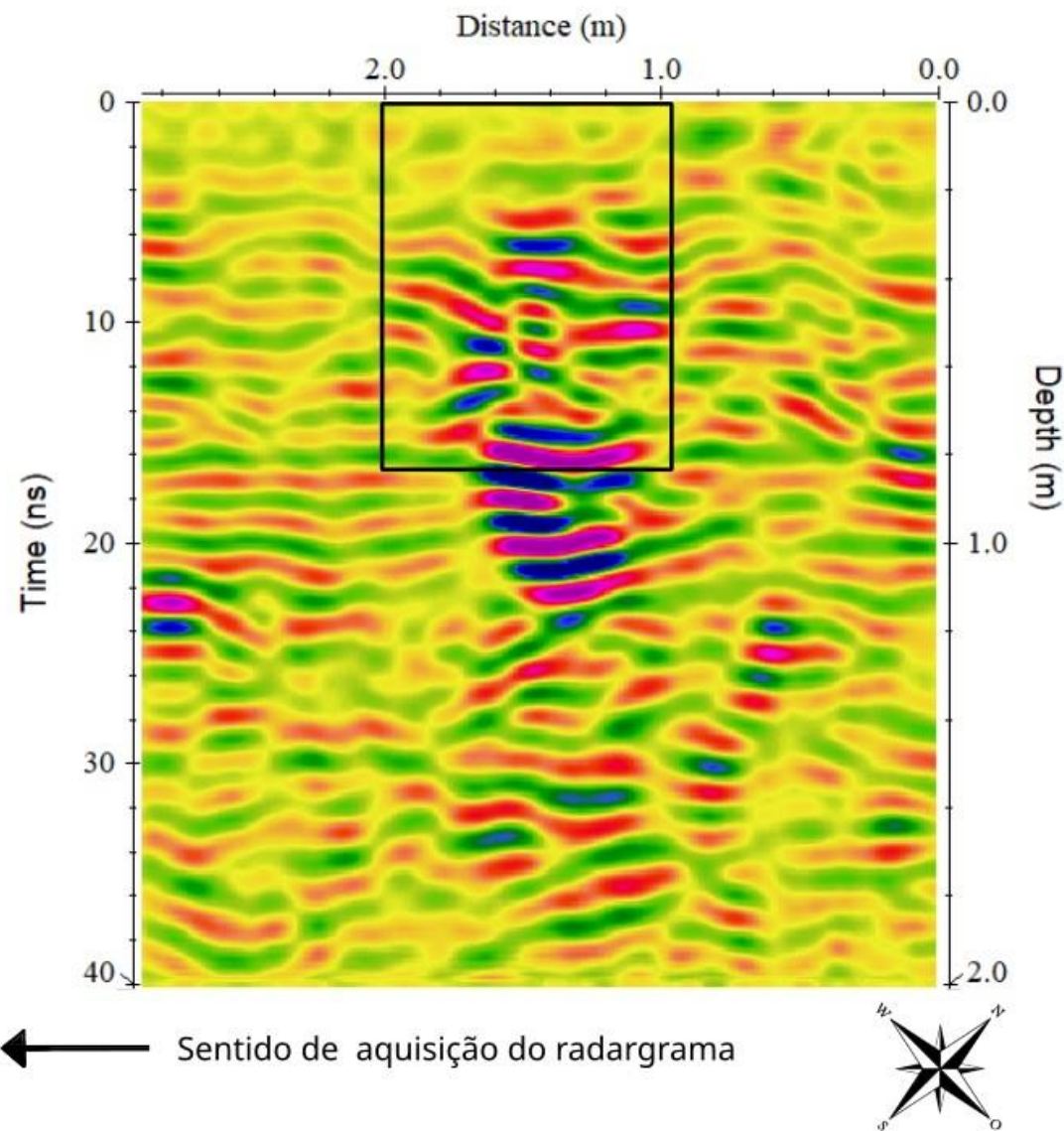
Radargrama obtido dentro da SEP04

Frequência de 900 MHZ.



Radargrama obtido sobre o alvo na SEP04

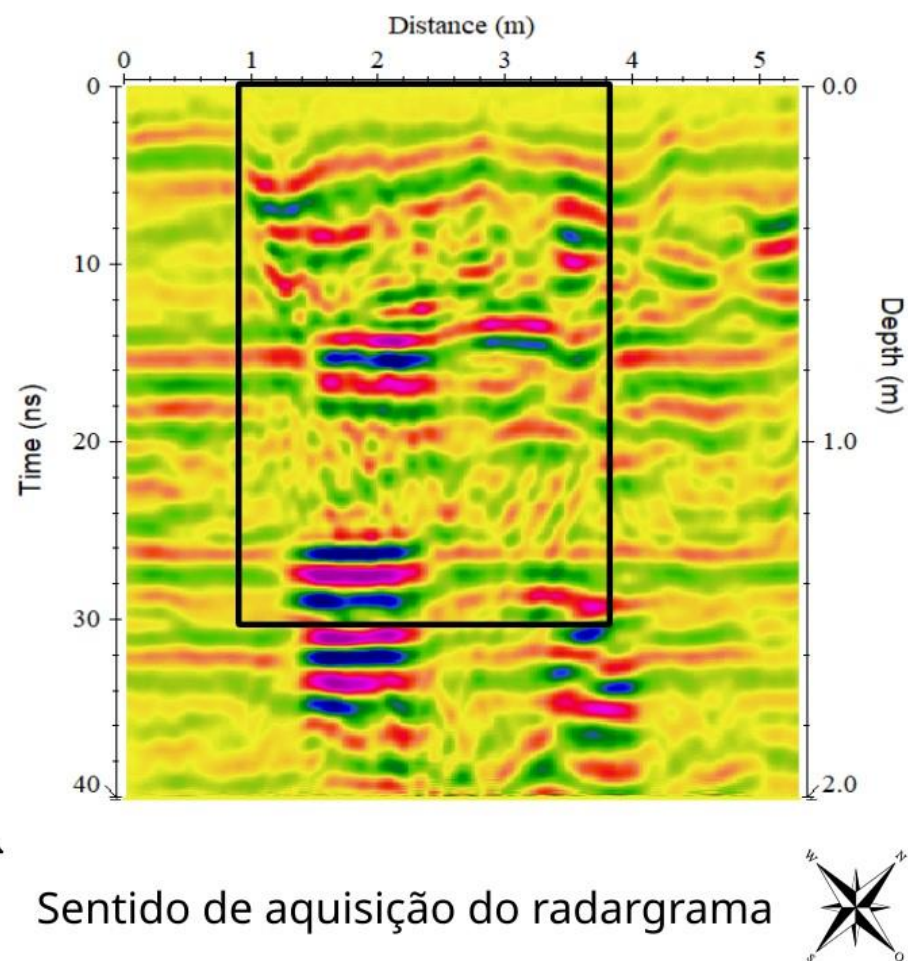
Frequência de 900 MHZ.



D2 – RADARGRAMAS 2D OBTIDOS TRANSVERSALMENTE NO PERÍODO CHUVOSO

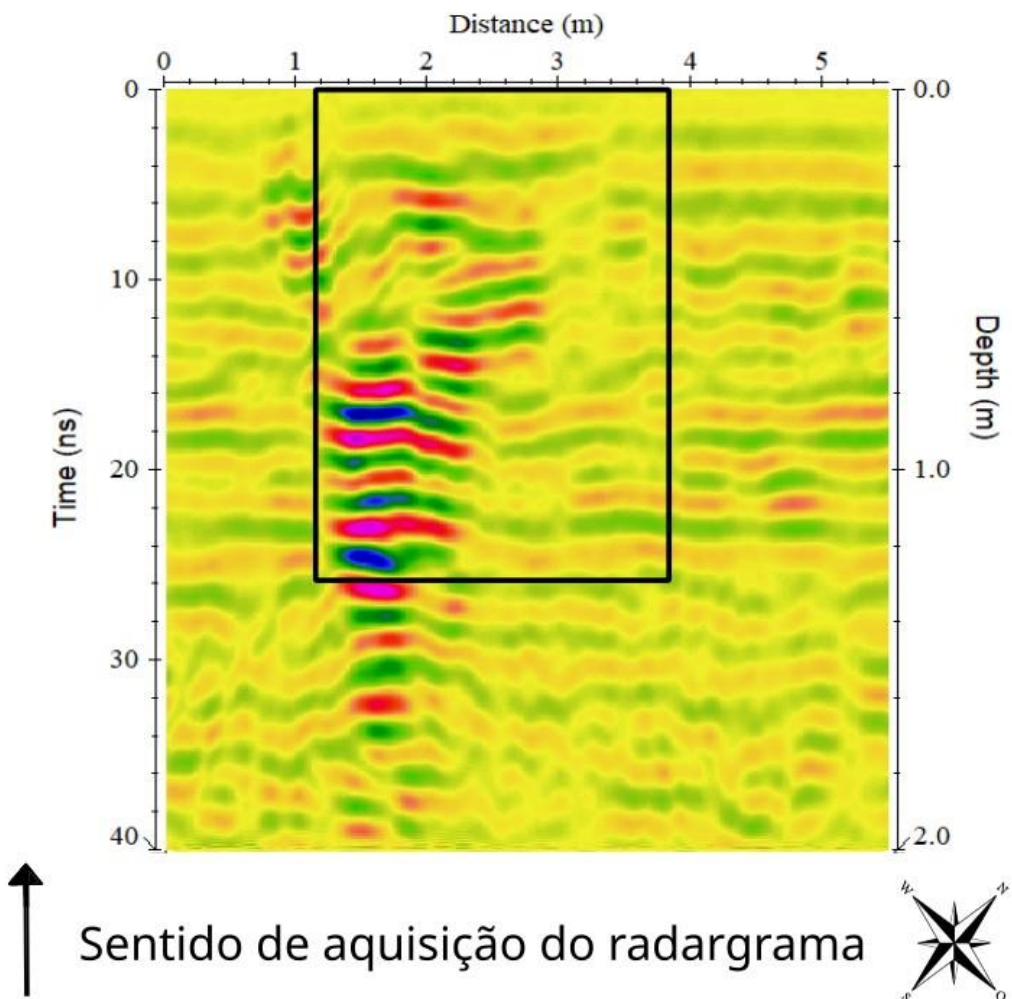
Radargrama obtido sobre o alvo na SEP01

Frequência de 400 MHZ.



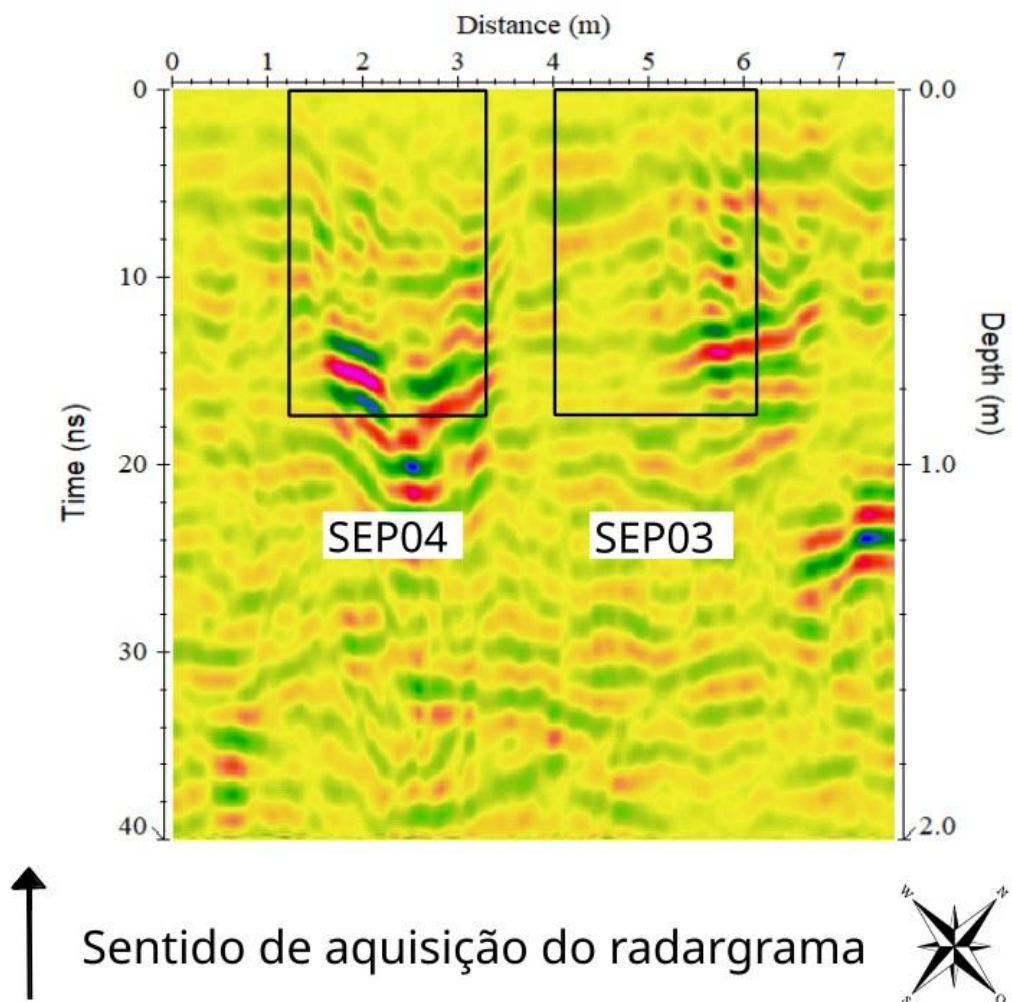
Radargrama obtido sobre o alvo na SEP02

Frequência de 400 MHZ.



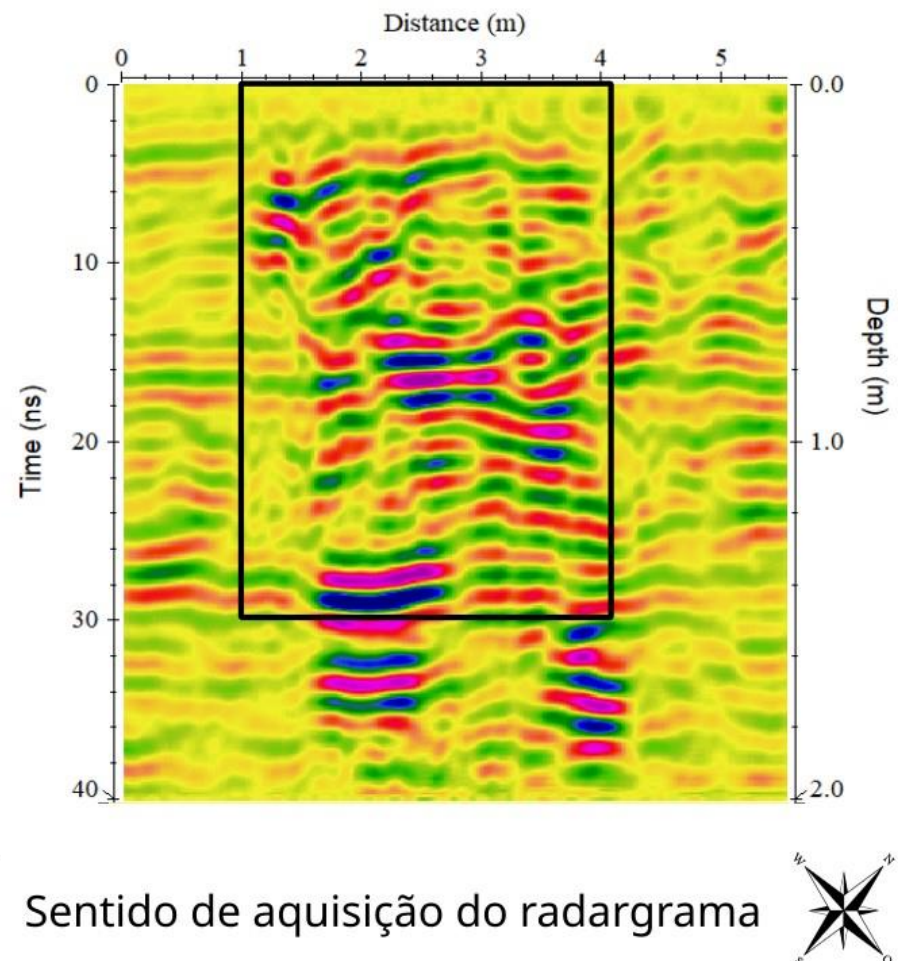
Radargrama obtido sobre o alvo nas SEP's 03 e 04

Frequência de 400 MHZ.



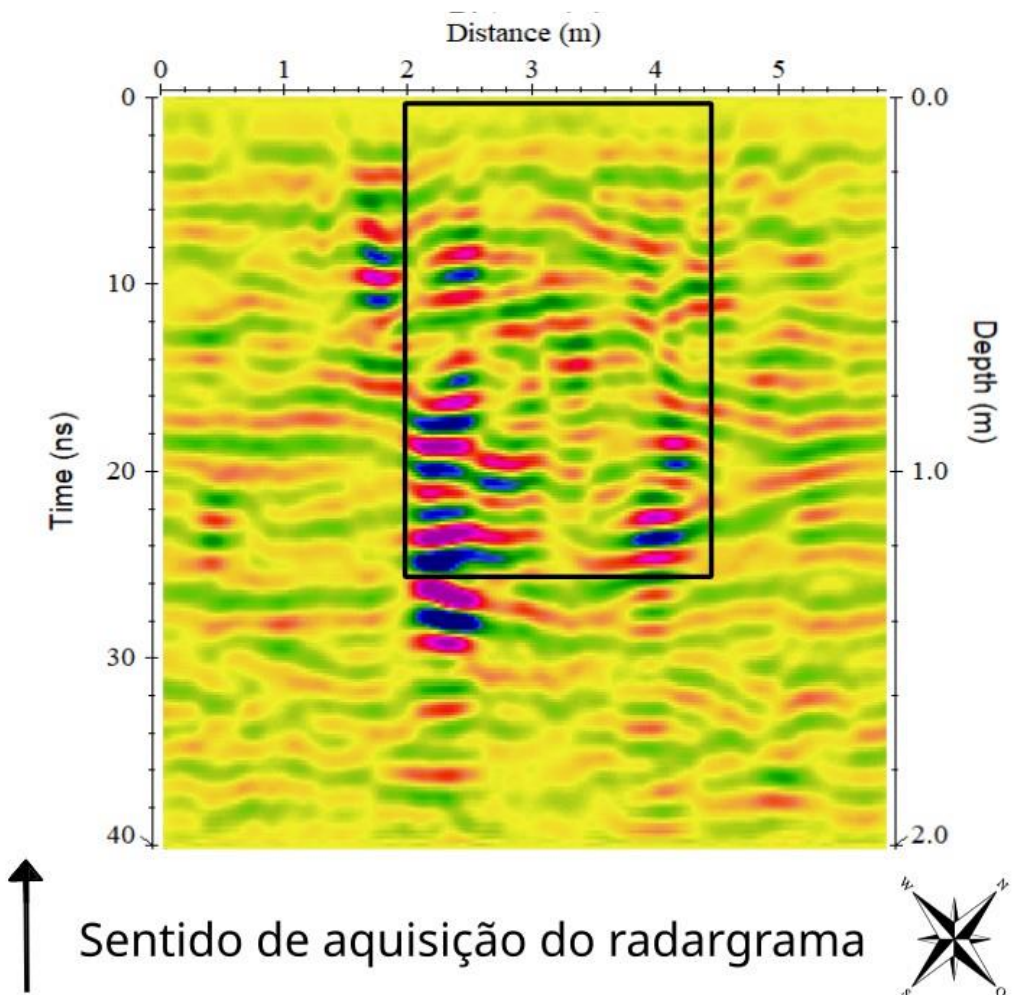
Radargrama obtido sobre o alvo na SEP01

Frequência de 900 MHZ.



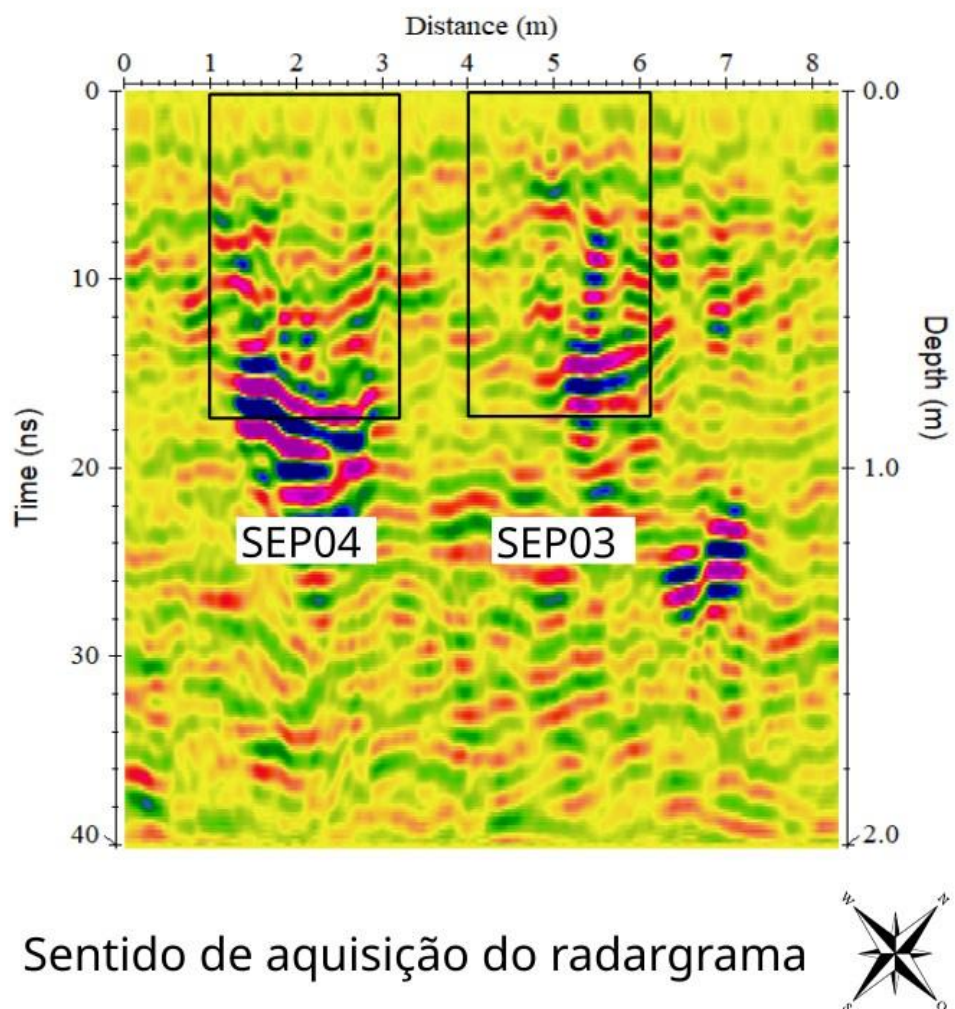
Radargrama obtido sobre o alvo na SEP02

Frequência de 900 MHZ.



Radargrama obtido sobre o alvo nas SEP's 03 e 04

Frequência de 900 MHZ.



E – FOTOGRAFIAS DA ÁREA DO SÍTIO CONTROLADO

Figura 1 - Fotografia tirada após a expansão do FOREN/FAL onde é possível visualizar os canos utilizados para o monitoramento de CH₄ e CO₂.



Figura 2 - Fotografia tirada durante medição de profundidade da SEP01. A esquerda observa-se a retroescavadeira utilizada para escavação das SEP's.



Figura 3 - Fotografia da sepultura experimental após colocação do bidim.



Figura 4 - Fotografia do momento de pesagem do alvo sepultado na SEP02. Para medição do peso dos alvos foi pendurada na pá da retroescavadeira uma balança digital de gancho. Ao fundo na fotografia é possível observar a areia e a brita utilizadas para preenchimento dos horizontes das SEP's.



Figura 5 - Fotografia demonstrando a posição do alvo dentro da SEP. O focinho está orientado para noroeste e a região abdominal orientada para sudoeste.



Figura 6 - Fotografia da área das SEP01 e SEP02 com o arranjo das trenas, corda e cabo de aço devidamente finalizado para aquisição dos dados GPR quasi-3D.



Figura 7 - Fotografia da primeira aquisição dos dados GPR na área do sítio controlado com a antena de 400MHz, no período de seca, logo após a expansão do FOREN/FAL.



Figura 8 - Fotografia da aquisição dos dados GPR na área do sítio controlado com a antena de 900MHz, no período chuvoso.